GEN25

SP-1185

Satellite Radar in Agriculture

Experience with ERS-1

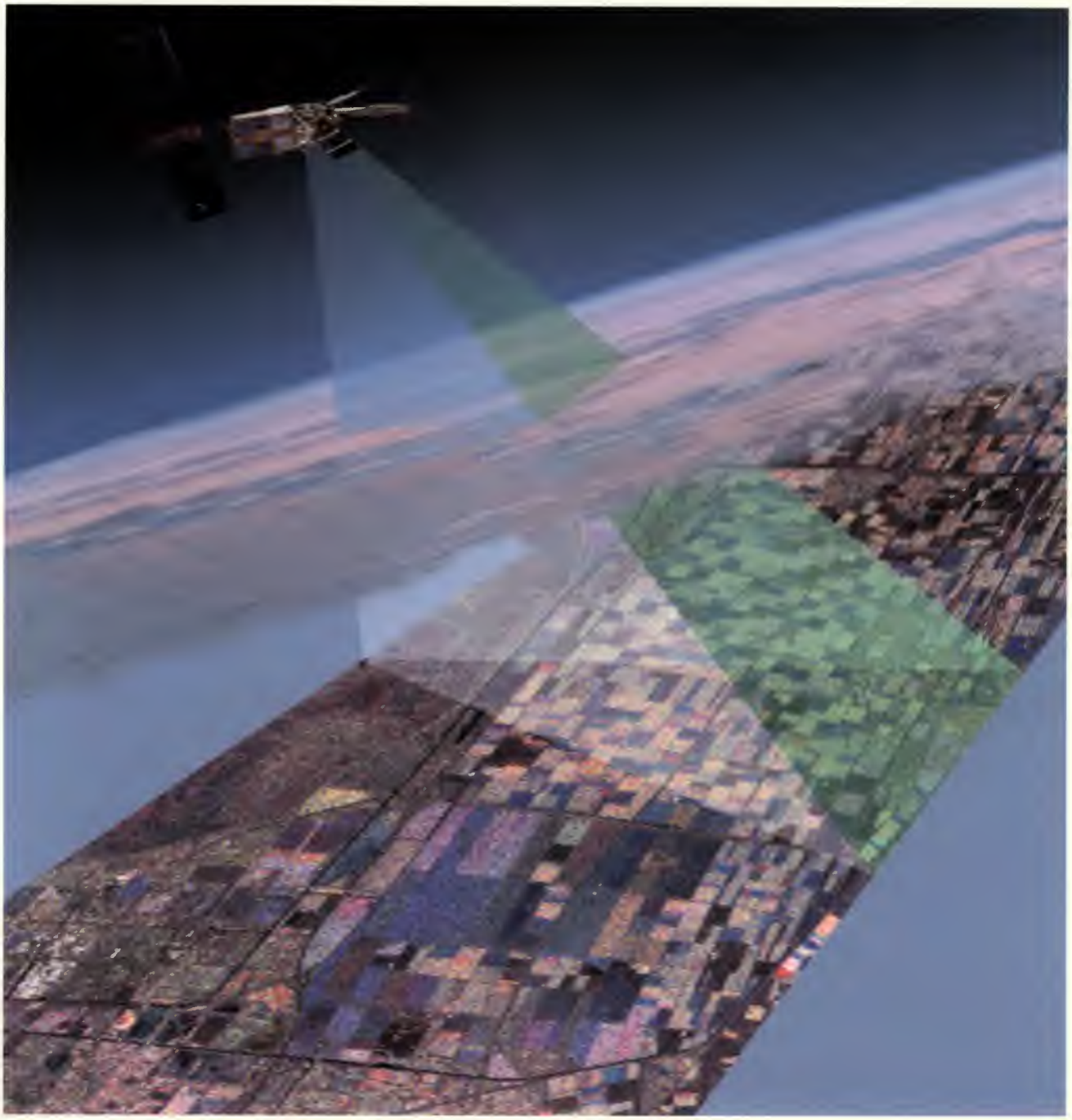

esa
european space agency

SP-1185
ISBN 90-9092-339-3
October 1995

Satellite Radar in Agriculture
Experience with ERS-1

ESA Specialist Panel

M.G. Wooding, *RSAC, UK* (Chairman)
E. Attema, *ESA/ESTEC, The Netherlands*
J. Aschbacher, *JRC Ispra, Italy*
M. Borgeaud, *ESA/ESTEC, The Netherlands*
R.A. Cordey, *MRC, UK*
H. De Groof, *JRC Ispra, Italy*
J. Harms, *Scot Conseil, France*
J. Lichtenegger, *ESA/ESRIN, Italy*
G. Nieuwenhuis, *Staring Centre, The Netherlands*
C. Schmullius, *DLR, Germany*
A.D. Zmuda, *RSAC, UK*

european space agency / agence spatiale européenne

ESA SP-1185

Satellite Radar in Agriculture

Experience with ERS-1

Report prepared by: ESA Specialist Panel

Published by: ESA Publications Division
ESTEC, Noordwijk, The Netherlands

Editor: Tan-Duc Guyenne

ISBN 92-9092-339-3 Price code: E2

Printed in The Netherlands

Contents

1. Introduction

The 1990's have seen major developments in the use of satellite remote sensing for agricultural monitoring and production forecasting. Within Europe the majority of European Union Member States now use satellite remote sensing to control arable and forage areas which benefit from hectare-based subsidies as part of the Common Agricultural Policy (CAP). The 'Monitoring Agriculture by Remote Sensing' (MARS) project of the European Union, is another major initiative using satellite-based techniques for the collection of crop statistical information. At regional and local levels, there is increasing use of remote sensing as a source of information on changes in agricultural cropping and for production forecasting.

Agricultural applications of remote sensing are time critical. The accurate identification of crop types depends on the availability of images acquired within specific time windows through the crop growing season, when there are marked differences in the appearance of particular crop types on remote sensing images. Equally, there is a need for images acquired at particular key times for yield prediction purposes. Despite the progress which has been made towards operational applications, experience shows that high-resolution visible and infrared satellite sensors cannot always provide the desired information due to constraints related to cloud cover and revisit schedules.

Radar satellites like ERS-1 and ERS-2 overcome the problem of cloud cover. Synthetic Aperture Radar (SAR) systems transmit microwave energy down to the Earth's surface and record the variable strength and phase of the 'backscattered' return signal. Images are obtained independently of cloud coverage or daylight conditions *(Figure 1.1)*, and contain information on roughness and dielectric properties of the surface. Radar is sensitive to the structure and moisture content of vegetation canopies, and to soil roughness and moisture content.

When ERS-1 was launched in July 1991 it was intended primarily as an experimental oceanographic satellite, but there have been very significant research efforts directed towards land applications. At first sight the single-channel black-and-white SAR images from ERS-1/2 appear to have limited value for agricultural uses in comparison with the higher resolution

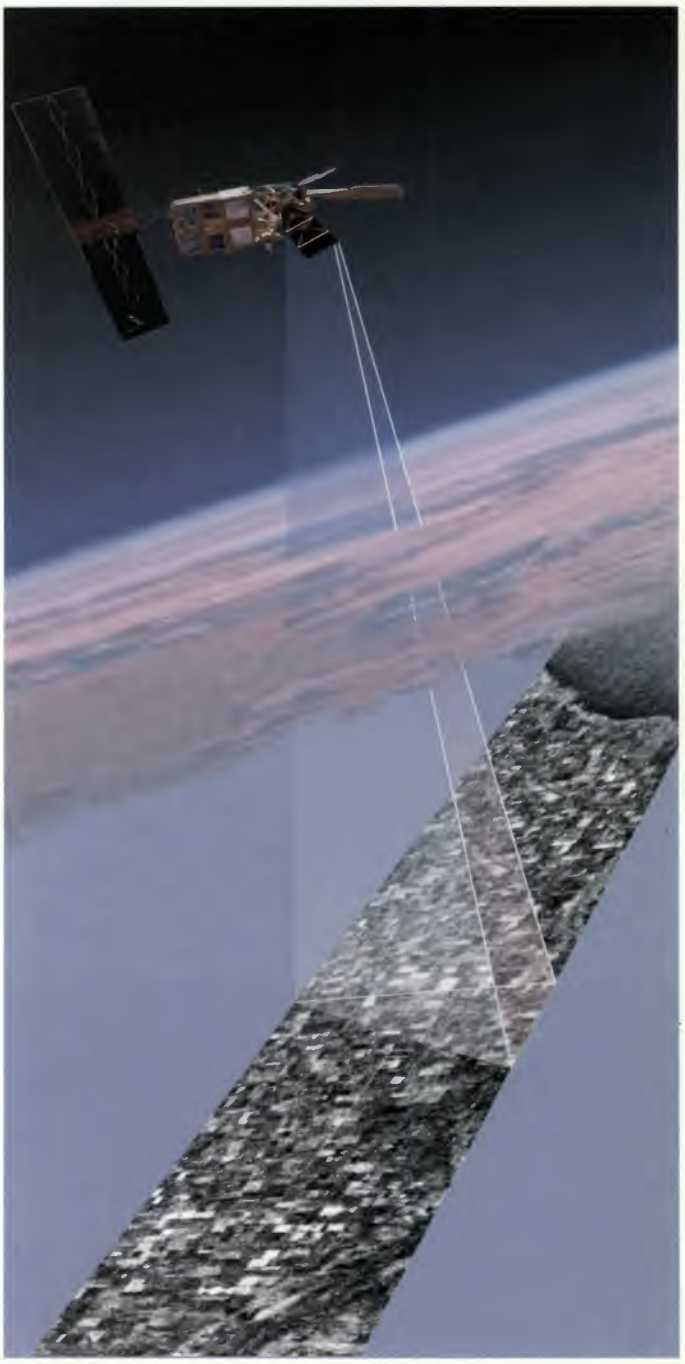

Figure 1.1. Sideways looking imaging geometry of the ERS-1 SAR. The instrument operates at C-band, VV polarisation, with an incidence angle of 23° from the vertical. Image swath width is 100 km.

multispectral visible and infrared images from SPOT and Landsat. However, it is not difficult to become more optimistic once we see colour combinations of images acquired on different dates through the crop growing season, particularly after image filtering techniques are applied to reduce image speckle and improve definition. Further, when we take into account the fact that ERS-1/2 provide stable calibrated measurements of surface conditions which are unaffected by atmospheric effects, one begins to appreciate some of the possible advantages over visible/infrared imaging.

This document (ESA SP-1185) has been prepared by an ESA Specialist Panel charged with the task of reviewing research work and progress so far, and making recommendations for future developments and integration of satellite radar data into operational crop monitoring systems. Chapter 2 of the document provides a general introduction to agricultural information requirements and the potential role of satellite radar. Chapter 3 then develops an understanding of the information content of ERS/SAR images, concentrating on the presentation of results concerning the temporal backscatter signatures of agricultural crops. The different analysis techniques being developed to extract agricultural information from ERS images are then presented in Chapter 4. Chapter 5 contains case study results on temperate crops, including examples of the classification of arable crops, developments aimed specifically at early estimation of crop area, and combined analysis of ERS-1 and optical satellite data. Case studies for tropical crops are presented in Chapter 6, concentrating on developments for rice mapping. Chapter 7 contains information on interesting future developments in analysis techniques, and the potential of new multichannel satellite radar systems. Finally, Chapter 8 provides overall conclusions, and recommendations for future developments and integration into operational systems.

2. Agricultural Information and Remote Sensing

2.1. Application Objectives

Agricultural resources provide mankind with food and have a substantial impact on the economic and environmental welfare of a particular country. The main objectives of the different parties interested in crop production, are the efficient and sustainable management and development of this renewable resource. At European and national levels, knowledge of changes in cropping and crop production is the basic information necessary for the implementation of agricultural policy. The Common Agricultural Policy (CAP) involves a complex arrangement of subsidies and tariffs used to control European agricultural production. At the local level, decisions regarding crop types, varieties, planting dates, irrigation procedures and fertilizers can benefit further from accurate knowledge of production on a field-by-field basis.

The monitoring of agricultural resources is time critical, and encompasses the following:

- Crop condition assessment
- Crop production forecasting
- Mapping of crop area and monitoring changes
- Surveillance of crop declarations for fraud control
- Pollution detection and impact assessment (e.g. erosion risk)

Traditionally, crop production forecasts have been based on crop inventories and yield surveys. Crop inventories involve the identification of crops and measurement of their area. This can be achieved using census and ground survey techniques. However, over very large areas, the application of such techniques becomes costly and unreliable.

The use of satellite data to identify crops and measure their area has now revolutionised crop production forecasting. In the early 1970's, the Large-Area Crop Inventory Experiment (LACIE) in the United States developed the concept of an agricultural information system incorporating satellite remote sensing. Multispectral satellite imagery are used to estimate crop area. Meteorological data from ground stations and NOAA satellites are used to forecast yield and evaluate crop development stage.

2.2. The European MARS Programme

In 1988 the European Community initiated a ten year research programme to build upon the US LACIE experience. *Monitoring Agriculture using Remote Sensing (MARS)* is a major activity aimed at improving European production forecasts by the use of high-resolution remotely sensed imagery. Its main 'actions' include quantitative estimation of crop acreages in a given region or country, vegetation and crop state monitoring, timely crop yield forecasting of the mean crop yields per country, and the rapid and timely estimation of the total production of the most important crops within the EU. Its main users are the Directorate General for Agriculture, and the European Statistical Office (Eurostat).

The first five-year project developed statistical methods to estimate crop acreage and potential yield (called MARS-STAT). The various activities of MARS-STAT, presented in Table 2.1, were conceived, developed and implemented on the basis of inputs from approximately 100 institutions from 17 European countries. These institutions provided data, models, algorithms and software, after having previously validated them for use at the EU scale on the basis of country specific information.

Separate from the MARS-STAT activity, the use of remote sensing for verification and control of the area-based subsidies within the EU has evolved quickly over the last few years and is now used operationally in most countries of the EU. This is known as MARS-PAC (Politique Agricole Commune), and involves the use of computer-assisted photo-interpretation and automatic classification to check farmer's applications for subsidies. Approximately 5% of all farmers' returns within each country are now checked using satellite remote sensing.

In general it can be said that both the LACIE and the MARS programmes were driven by economic motives, which, in a market driven by price, is easily understandable, and which can be seen as a very positive point for the long-term and intensive use of remote sensing data. Taking this into account, as well as the fact that

the major interest in agriculture consists of obtaining as much timely information as possible on the crop area, condition and production, it can be seen that the use of remote sensing can and will be extended to other regions outside Europe within programmes similar to MARS-STAT. Major potential future customers could certainly be the Asian countries which have a requirement to monitor rice resources.

Table 2.1 Different activities within the MARS-STAT programme

Action	Methodology	Geographic location	Input	Comments
A. Main activities				
1. Regional inventories (acreages)	• Regression estimator	• Selected administrative regions	• High-resolution satellite data (SPOT Landsat-TM)	The activity has been stopped at European level
2. Vegetation conditions and yield indicators	• Spatial or temporal comparison of VI and Ts (integrated indices)	• Selected regions and sampling of sites, then all of Europe	• Low- and medium-resolution satellite data (mainly NOAA/AVHRR)	Activity operational
3. Models of yield prediction	• Improvement of existing agro-met. models • Integration of satellite data into agro-met. models • Deriving agronomic parameters (AET) • Direct relationships		• Meteorological data • Agronomic information • Low- and medium-resolution satellite data • High-resolution satellite data	Activity operational
4. European rapid estimates of acreages and potential yield	• Computer assisted photo-interpretation of up to 4 images a year	• Sample over more than 50 sites (40×40 km) throughout Europe (see Figure 2.1)	• High-resolution satellite data (SPOT and Landsat-TM)	Operational activity based upon identification and classification of 12 most important market crops on the images. Information largely obtained before harvest. Integration of results into MARS Bull.
B. Back-up activities				
5. Advanced agricultural information system	• Comparison with previous years		• Integration of all available results	
6. Area frame sampling; associated surveys	• Estimates obtained by integration of the above methods with conventional terrain-based surveys	• Stratification, segmentation, sample survey on the ground in conjunction with farmers		
7. Long-term studies	• Back-up documents and data for other actions		• Using new sensors; Geographical Information Systems	Currently, ERS-1 data are investigated to test their interest for the operational programme

2.3. Potential of Satellite Radar

All-weather acquisition

The capability of satellite radar to provide reliable and frequent imaging, independently of cloud coverage, is a key factor in the context of agricultural applications. Current European operational projects such as MARS-STAT and MARS-PAC, are dependent on the acquisition of multi-date optical satellite imagery acquired over the main crop growing season. Although the SPOT satellite has a variable viewing geometry which can be programmed to increase the opportunities for image acquisition, the ability to collect optical satellite imagery within relatively narrow time windows can still be problematical in Northern Europe, where there are a small number of cloud-free days. At least 17 of the 53 current Action IV test sites lie above 50° North, with new sites in Sweden and Finland being added in 1996. In the 1993 season, for example, only one or two SPOT or Landsat images were obtained for UK sites, which hampered the provision of reliable crop determinations. The capabilities of ERS-1/2 are of even greater importance in tropical regions, where cloud cover is persistent throughout the year.

High revisit frequency

The ERS-1/2 satellites are able to acquire images for any location of the Earth's surface, at a repeat interval of at least every 17 days, with the coverage frequency increasing in middle and high latitudes *(Figure 2.1)*. *Figure 2.2* provides an example of the data coverage of of one of the MARS Action IV test sites; a total of 18 images were acquired during the period 1 April to 31 August 1993 for the Kings Lynn site in the UK. The all-weather day and night imaging capability guarantees good multitemporal coverage over the main growing season.

Early data acquisition

Closely related to the cloud cover penetration capabilities is the potential of the ERS SAR for early crop identification. Cloud cover and low light levels tend to particularly hamper the acquisition of optical satellite images in the spring, and thus during the early part of the crop growing season. The use of radar for classifying soil surfaces being prepared for different crop types in the autumn/winter period is a possible approach to early crop identification.

Sensitivity to surface roughness and moisture

The ERS/SAR is sensitive to the geometrical characteristics of the ground surface, or the 'surface roughness', and the dielectric properties of the surface materials,

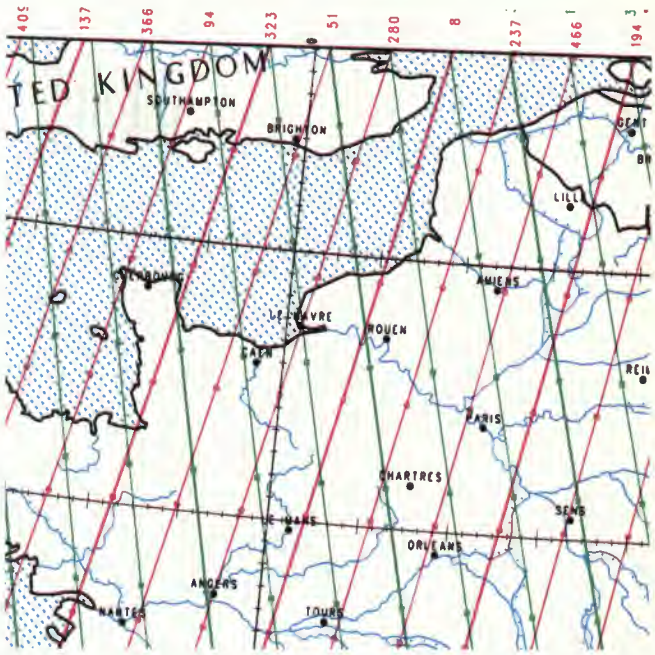

Figure 2.1. Coverage map of ERS-1/SAR for the 35-day repeat cycle (nominal cycle of ERS-2) showing mid-image line and frame centres (dots). Descending orbits (day time passes) are shown in magenta, ascending orbits (night time passes) in green. At these latitudes, a frame (100x100 km) has a large overlap with frames from adjacent passes, allowing more frequent revisits for areas of interest.

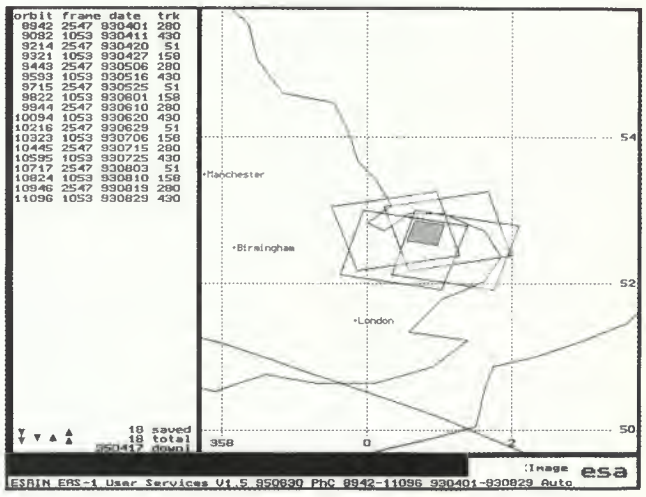

Figure 2.2. Typical print from the off-line catalogue user tool provided by ERS User Services, ESA/ESRIN, Frascati. It shows the ERS frames covering an area of interest (shaded). The frames are for the MARS site Kings Lynn, UK. Between 1 April and 31 August 1993, eighteen images were acquired, three of them during night time passes.

which are strongly correlated with moisture conditions. At the C-band wavelength of ERS there is very limited penetration through surface layers, and radar backscatter of crops is determined by the structure of crop canopy (size, shapes and orientation of leaves, stems and seed heads), crop cover and moisture content. For soil surfaces, there is a strong sensitivity to both the soil surface roughness and surface moisture (see detail in Chapter 3: Scientific Basis). The information content of radar images is thus very different to that of optical satellite data, which record reflectance in visible and infrared wavelengths.

Image geometry

Due to the highly stable orbit of the ERS-1/2 satellites, images taken under the same orbital condition (ascending or descending), can be easily superimposed by a simple shift of the different images in relation to the reference dataset. However, ERS SAR images are subject to geometric terrain distortions related to the sideways looking imaging geometry (see *Figure 1.1*), which can impose some limitations on their use in hilly areas. In flat areas standard polynomial geometric correction techniques, can be used for geometric correction of ERS images to levels of accuracy of about 15 – 30 m. However, in hilly areas it is necessary to use a Digital Terrain Model (DTM) and specialised software to remove the geometric terrain distortions, in order to obtain accurate registration with topographic maps and corrected optical images. Techniques for these types of geometric corrections are commercially available.

Complementary with optical and other radar satellites

Besides the possibilities described above, there is potential for improving crop identification, by taking advantage of the complementary information provided by ERS and optical satellites. For instance, the use of ERS SAR data could concentrate on those crop types, for which SPOT or Landsat data do not provide clear separability. Even with two to three dates of optical images, there can be problems in separating some crop types which have similar visible near- and middle-infrared reflectance, and yet, these crop types may have very different structural characteristics which are able to be distinguished on ERS SAR images. The same potential might become interesting when combining ERS SAR with the Japanese JERS or the Canadian Radarsat imagery. JERS operates at a different wavelength (L-band). Radarsat will acquire imagery with different polarisation (HH) and incidence angles compared to ERS-1.

There may be potential for using ERS SAR data, together with agrometeorological backscatter models, to provide additional quantitative estimates of crop growth. The potential for identifying soil moisture in ERS SAR images might equally become an important information input for future agricultural applications.

Products and costs

The present pricing policy and rapid delivery are both important arguments for developing the use of ERS-1/2 SAR for operational applications. ESA is developing various systems for rapid delivery of ERS data products. The UK ERS-1 ground receiving station, for example, operates a facility for near real-time supply of ERS-1 data using standard telephone lines. Latest information about ERS and available data products is available from:

ERS Help Desk at ESRIN:
via Galiileo Galilei
00044 Frascati, Italy
Tel: +39-6-941 80 600; Fax: +39-6-941 80 510

3. Scientific Basis

3.1 Understanding Radar

The microwave radar carried by the ERS satellites has the potential to provide us with information on agricultural crops and the soil in which they grow. As well as generating images when visible/IR sensors are unavailable because of cloud, the information from radars may be complementary to that from optical systems. The reason for this is the difference in the processes and scale sizes of features, with which radar and optical wavelengths interact in an agricultural field. The response of a field of crops to optical radiation is determined by structures on micron scales and by processes of chemical absorption. Microwave radiation, by contrast, penetrates significant distances into a vegetation canopy and interacts most strongly with structures (leaves, stems etc.) on scales comparable with the radiation's wavelength (a few centimetres to a few tens of centimetres). Thus, microwave radars may be thought of as probing in a very direct manner the structural components of a plant canopy.

Owing to its penetrative power, significant amounts of radar energy can, in certain circumstances, pass completely through a crop canopy to reach the soil below *(Figure 3.1)*. When this happens, the radar image will be influenced by the reflective properties of the soil. Thus, in very broad terms, imaging crops with radar raises the possibility of exploiting differences both in plant structure and in soil properties for the purposes of differentiating crop types, crop condition, or agricultural management practices.

Below, we expand on our understanding of the nature of the interaction between microwaves and plants, and outline some of its complexities. We go on to indicate how computer simulations are helping to develop our understanding from the qualitative to the quantitative.

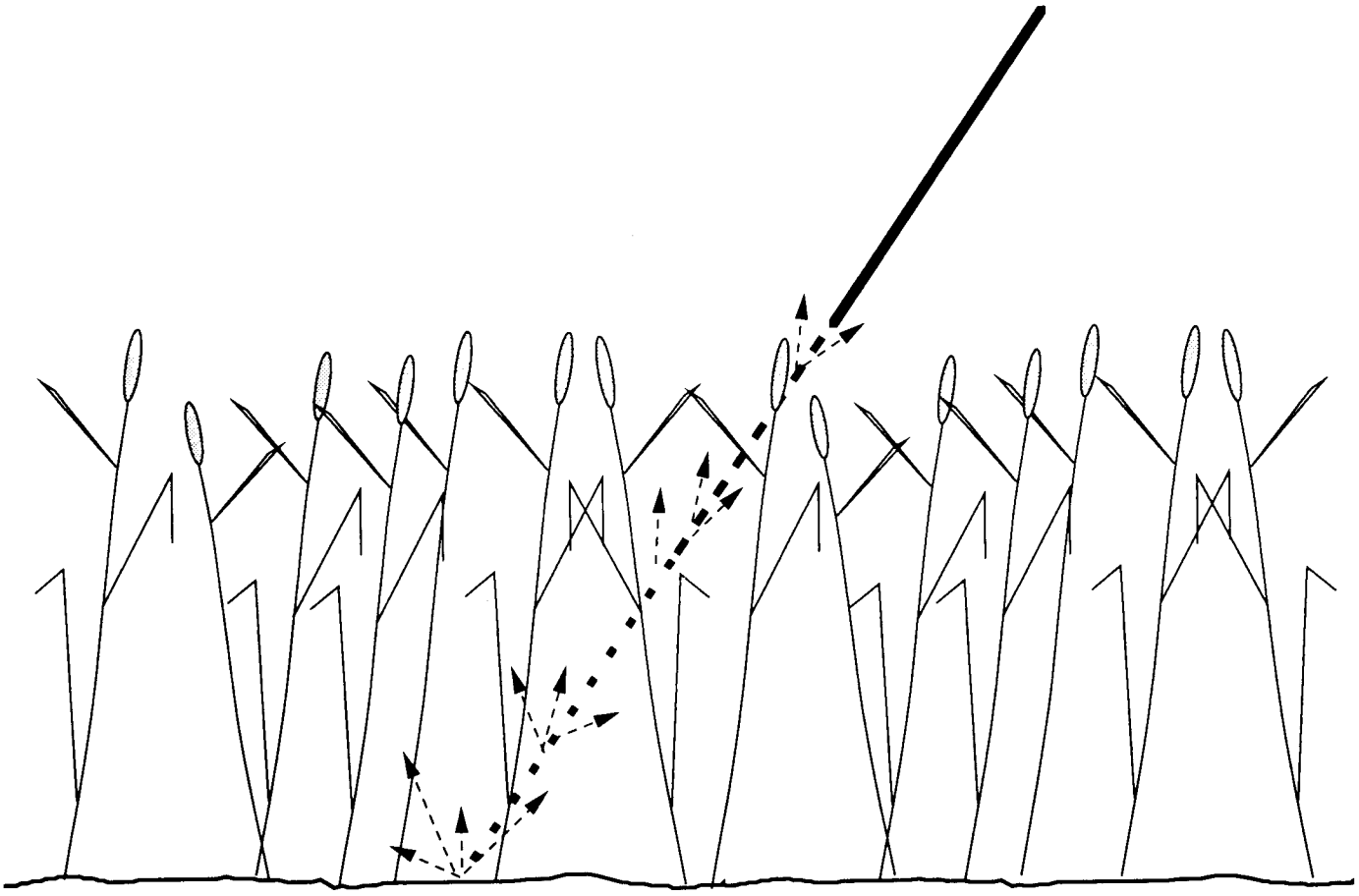

Figure 3.1. Incident microwaves from ERS are attenuated as they pass through the crop canopy. When a canopy is thin or dry, significant energy can interact with the soil.

The basis of interaction between radar and agricultural fields

The properties of vegetation and the soil which influence the amount of microwave power scattered back towards the ERS SAR fall under the two principal headings of *Geometric Structure and Dielectric Constant*. By structure we include the major plant constituents on scales greater than a few millimetres (leaves, stems, flowers, fruits/seed heads). Their sizes, shapes and orientations determine the interaction of individual isolated components with the microwaves. A flattened leaf, for example, scatters microwaves in a different directional pattern to a vertical stem. Below the plant canopy, the soil surface does not act as a simple mirror – rather the scattering from it is influenced by its roughness properties, especially on scales comparable to the radar wavelength. The moisture of the soil influences, through local chemistry, its dielectric constant. For different soil types, there is a different relationship between moisture content and dielectric constant, determined by the soil constituents.

The understanding of the interactions with individual plant components or the soil is relatively straightforward. Electromagnetic modelling has at its disposal a range of techniques and approximations to describe the scattering by at least the more simple shapes which may be encountered in a crop canopy or by a soil surface with a known roughness profile. The real situation, however, is rather more complex than that of microwaves scattering off isolated plant structures or the soil. The relative positions and spatial densities of the plant constituents determine how they respond as an ensemble to the radar, both through multiple scattering events or coherent interactions. Similarly, the soil cannot always be considered separately from the crop above it. Rather, a radar wave may be scattered by a leaf before being reflected off the ground and back to the radar. Furthermore, the relative importance of different interactions, whether single or multiple (some involving reflecting off the ground and others not) is believed to change significantly as a crop develops during the growing season *(Figure 3.2)*.

Radar penetration and probing of crop canopies

Different wavelengths of microwaves have different powers of penetration into vegetation canopies – generally the longer the wavelength the greater the penetration. The degree of penetration sets bounds to the kinds of information which a radar can provide. Discrimination of crops based on their structures will only be realised if the structures which differentiate them occur within the volume probed by the radar. The same comment applies for the use of radars to probe

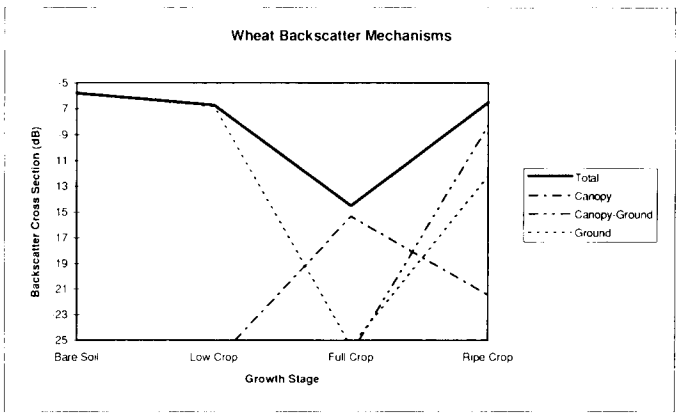

Figure 3.2. The changing contributions to the backscattered radar intensity as a crop develops. Here, the example is a field of wheat where the crop cover is initially nil, then develops to a 10-cm deep canopy, followed in turn by a moist full canopy and then a drier ripening canopy. Initially, simple scattering off the soil dominates the total reflection. As the crop increases in depth, the scattering from the soil becomes weaker, and is largely replaced by volume scattering within the canopy. As the crop ripens and becomes more transparent to ERS's microwaves, the soil becomes visible once again, and contributes to the total, together with more complicated scattering events involving radar waves interacting with both the canopy and the ground. (Source: R. Cordey, MRC).

soil characteristics; only if the radar can actually penetrate to the soil and back will there be any direct information on soil moisture. The C-band radar of the ERS satellites penetrates primarily only into the upper layers of plant canopies when they are dense or moist. This penetration may increase very significantly, however, if the plant canopy becomes more transparent to radar as it dries out. Similarly, with the soil, the depth to which microwaves penetrate increases in drier soils. Thus, the influence of soil moisture on microwave backscatter comes only from that moisture present within the layer which is actually sensed.

Radar polarisation and incidence angle

As well as a radar's wavelength, the polarisation of the microwaves and their angle of incidence relative to nadir, affects the interaction with plants and soils. Polarisation affects the way in which the microwaves respond to different shapes and orientations of scattering elements in a plant canopy. The vertically-polarised electric field of the ERS SAR interacts more strongly with the vertical stalks of a field of grains than would, say, a horizontally-polarised radar. Such interaction leads to differences both in the power scattered

back in those different polarisations and in the degree of penetration through to the soil. Penetration to the soil is also influenced by the incidence angle of the microwaves because that angle determines the path length within a crop canopy through which the radiation must pass. A radar looking at a relatively steep angle, such as ERS's 23°, will tend to see the soil more readily than one looking at a more oblique angle from nadir.

Towards a quantitative understanding

Developments in the modelling of microwave scattering for agriculture have taken advantage of the increasing availability of computing power, to create ever more realistic and explicit models for the structures with which the radiation interacts. The models aim to explain or predict the brightnesses in radar images of different crop types under changing environmental conditions, or different stages of growth during a season. Early developments in the 1970s were based around empirical or semi-empirical models for scattering at particular wavelengths. These did not attempt to represent crops as recognisable structures, but invoked tuneable parameters and were limited in their applicability over the wide range of radar and crop parameters which may be encountered. Widespread recent work has placed greater emphasis on realistic descriptions of plant components, which can be related very directly to measurable parameters (the shapes of leaves, their thicknesses and moisture contents etc.). It is conceivable that significant improvements in the accuracy of predictions will entail even more explicit models of plants 'grown' in the computer, which include descriptions of the spatial interrelationships between leaves, stems and fruits.

So how useful are computer models for understanding and predicting radar backscatter? A limitation on their use for quantitative predictions of image brightness is often the lack of sufficiently detailed information on the crop and soil itself. This has made experiments for the validation of computer models expensive and time consuming. Thus, models are probably of most current use in generating plausible radar images of agricultural areas (e.g. for predicting the relative benefits of radars of different designs) or for investigating the likely sensitivity of image brightness to changes in crop or soil parameters. In that context, they support research towards methods for the retrieval of bulk crop or soil parameters (biomass, soil moisture for example), especially in the context of multi-date imaging when only a sub-set of possible parameters (e.g. moisture) may be changing rapidly.

To summarise then, it is widely believed that a relatively good understanding has been developed of the interactions between microwaves and agricultural fields, which are responsible for the appearances of those fields in a satellite radar image. Although complex, the wide range of interactions which microwaves may undergo with plants and the soil – the sensitivity to detailed structure, moisture and chemistry – encourage us to believe that, given an appropriate set of radar measurements, it will be possible to discriminate effectively between different crops. In the case of the ERS radar, we will see that it is through its sensitivity to changes in crop structures through the growing season that we have a tool for distinguishing different crops.

3.2 Calibration

What kind of calibration?

For applications which demand more from a radar image than just the detection or mapping of features, there is a requirement on the calibration of that radar. We need an understanding of how the radar image brightness relates to the fraction of incident microwave energy which a region reflects back towards the radar antenna. The accuracy with which a radar can be calibrated and the nature of that calibration influence the range of information retrieval purposes to which the radar can be applied. By the nature of the calibration, we mean:

- Has the radar been calibrated on an absolute universal scale (relative ultimately to the signal reflected from a well-understood simple geometrical shape)? This sort of calibration is a pre-requisite for the eventual retrieval of quantitative parameters of crops and soil from individual radar images.
- Is the radar calibration stable in time, albeit on a possibly arbitrary scale? Temporal stability of calibration permits us, in principal, to use multi-date images to quantify changes in crop and soil parameters.
- Is the radar calibration the same at different locations across a single image? Some degree of stability in calibration across an image is needed in order to create stable crop classification algorithms.

ERS-1 has been successfully calibrated over its entire period of operation against a scale defined by ground-based transponders. The units conventionally used are normalised backscatter cross sections (sigma-zero, σ^0), and are usually represented in their logarithmic decibel (dB) form. The dB value of sigma-zero is 10 $\log_{10}$ of the

value in linear units. The intrinsic precision of the transponders is believed to be better than 0.14 dB (i.e. an uncertainty of about 3% in the fraction of incident energy which they reflect). The long-term calibration accuracy of ERS-1 relative to this scale is 0.06 dB with an rms error of 0.22 dB for a given image *(Figure 3.3)*. Across an individual image ($100 \times 100\ km^2$), the estimated uncertainty in calibration is better than 0.2 dB. Compared to previous experience with aircraft and satellite radars, these figures represent very significant improvements, and are achieved without a requirement for local calibration devices to be set out by an operational user. The method by which standard ERS image products can be calibrated by the user is described in the Appendix.

Limitations due to speckle noise

Synthetic-aperture radars suffer from a form of noise in their images called speckle. Speckle is a consequence of the coherent nature of the SAR imaging process (it is closely related to the phenomenon of laser speckle), and can be a significant limitation on the measurability of the mean brightness from an area of land. The problem is that the brightness of a particular resolution cell, depends not just on some form of average of the plant and soil parameters in that area, but on the particular phase relationships between the reflected waves from different parts of that resolution cell. In the most basic of images, speckle typically imposes an uncertainty on the estimate of the brightness from any resolution cell equal to the expected brightness. Only by some form of incoherent averaging can a meaningful measurement of image brightness be made. Routinely, this is done in part by a process known as multi-looking taking not one but two or more (3 in the case of standard ERS scenes) independent images and averaging together the radar brightnesses from each. Speckle can be further reduced by filtering the image, but at the expense of further sacrificing spatial resolution. The purpose of introducing the concept of speckle here is to draw attention to the lack of requirement for very high calibration accuracies for local scales of quantitative analysis. *Figure 3.4* shows how, for ERS-1 imagery, the estimate of the mean brightness improves with the area over which averaging is performed. For an individual field of size 5 hectares, an ERS image can provide at best a speckle-limited accuracy of 6% (or 0.27dB) for the averaged brightness over that field. This is reasonably well-matched to the stability of ERS-1 – a higher accuracy of measurement would be unnecessary for the analysis of fields of this size in individual images.

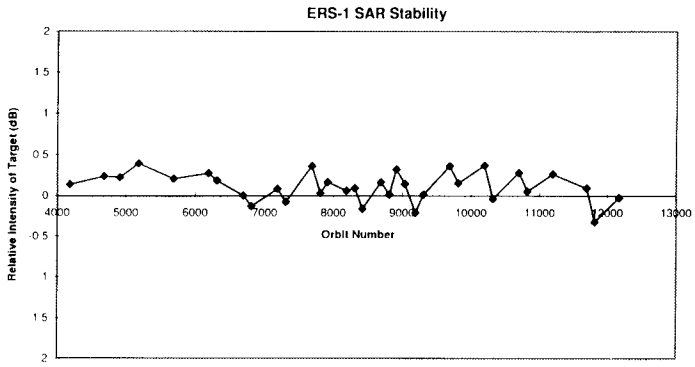

Figure 3.3. The stability of the ERS-1 radar is demonstrated here by the apparent brightness in its images of one of the ESA's transponders sited in Flevoland in The Netherlands. These transponders transmit back to ERS-1 a very precise fraction of the incident microwave energy and allow the radar's calibration to be checked independently. Following the application of the ERS-1 calibration procedure (see Appendix), the brightness of a transponder is plotted for the entire duration of the 'Multidisciplinary Phase' of ERS-1 operation from April 1992 to December 1993. (Source: R. Cordey, MRC).

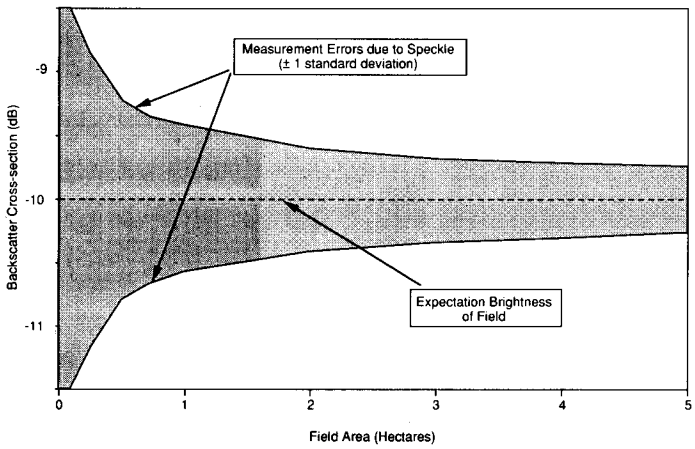

Figure 3.4. ERS-1 intensity estimates as a function of integration area. Due to speckle noise in SAR images, an individual pixel gives a poor estimate of a field's mean brightness. In general the more pixels that are average the better the estimate. The graph shows, for an actual ERS-1 standard 'PRI' image, how the mean brightness changes with the area of image which is averaged. The integration path is taken as a spiral out from a starting pixel, to mimic the averaging over fields of larger and larger sizes, up to a maximum area shown here of 5 ha. For small integration areas, the uncertainty is clearly very significant, but the average settles down for fields of a few hectares to an uncertainty which is a small fraction of a dB. (Source: R. Cordey, MRC).

3.3 Temporal Signatures

The radar backscatter of a crop will vary over the growing season from early crop establishment through to maturity and harvest. For the ERS radar, it is these temporal changes which may hold out the strongest prospect for establishing a routine means of distinguishing one crop from another. While we have confidence that the changes in radar backscatter of a crop during its development can be understood in terms of changes in the moisture and geometry of the crop or soil, the problem facing potential operational users, is to be sure that the profiles are sufficiently characteristic of the crop's development, and not of very localised environmental conditions, to be of use in identifying that crop either regionally or globally.

For this reason, the nature of changes of backscatter with time and the extent to which different crop types have distinctive temporal signatures, have been at the focus of ERS-1 research studies undertaken in the UK, Germany and The Netherlands. In the following sections, some of the principal results of these studies are reviewed, with a view to identifying the extent to which distinctive temporal signatures exist, and can be used as a tool for crop discrimination.

3.3.1 Cereal crops

A study carried out in the UK during the 1992 crop growing season, established that fields of winter wheat have temporal profiles in their ERS-1 backscatter which were distinctive from other crops in the region (*Wooding et al. 1993, Wright et al. 1993*). The profiles showed a clear decline in early-season backscatter, followed by an increase at the time of grain fill and ripening, and then a further major increase following harvest *(Figure 3.5)*.

Repeating the study in 1993, revealed similar trends at four sites across eastern England (*Zmuda et al. 1994*). *Figure 3.6* shows the averaged temporal profiles at

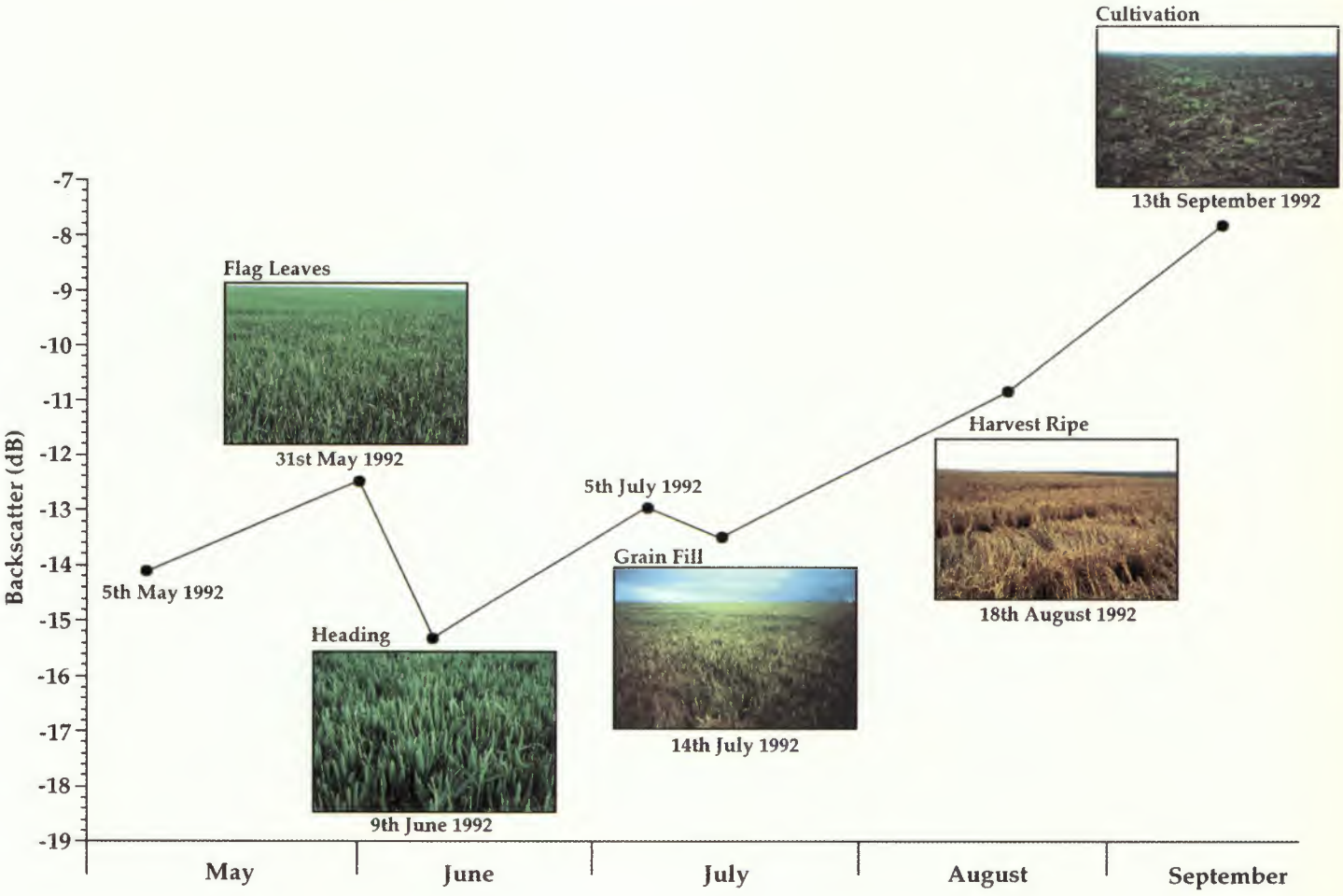

*Figure 3.5. Changes in winter wheat backscatter for a wheat field, development stages are also shown, Boxworth, UK, 1992. (*Source: Wooding et al. 1993*).*

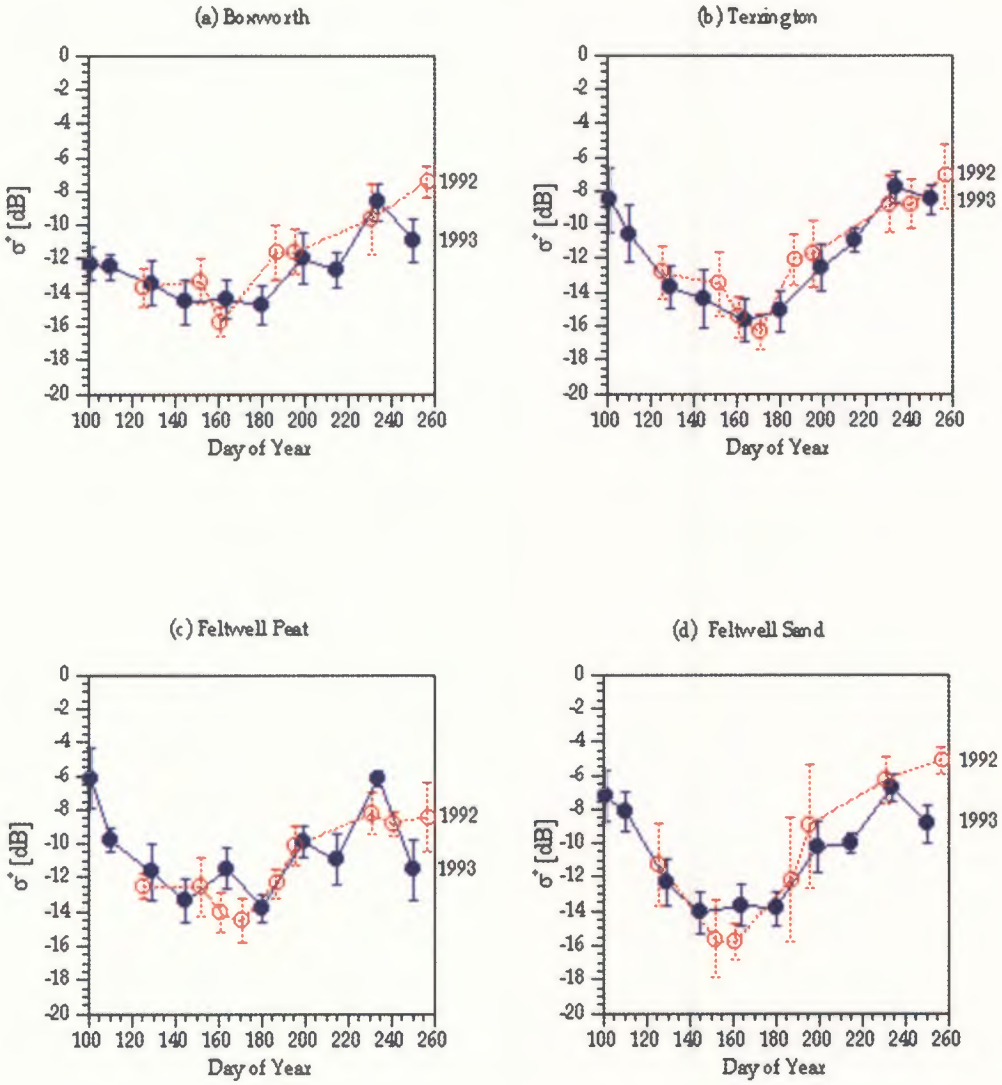

Figure 3.6. Mean ERS-1 backscatter temporal profiles for winter wheat, 1992 and 1993 growing seasons, for four sites in the UK. (Source: Zmuda et al. 1994).

these sites over the two years; as before, we see a set of declining responses in the early season followed by increases through to harvest at around day 220. Despite the overall broad consistency between sites and seasons, however, there are some notable differences between the temporal profiles. The trough and inflexion points are possibly more marked in 1992, while backscatter is higher on day 167 in 1993 for Boxworth and the two Feltwell sites than would have been expected by the annual and inter-annual trends. Such deviations away from the overall trend can most likely be explained as disturbances to the profile caused by meteorological events (see § 3.4).

But how do these profiles from UK wheat fields compare against those from elsewhere in Europe? In *Figure 3.7*, the UK trends are shown alongside profiles of winter wheat from the Dutch and German test sites. All the temporal profiles do indeed show very similar patterns of change.

Changes in wheat backscatter with development stage
Ground data exist which give a clear visual impression of the relationship between phases of the ERS-1 backscatter curves and the development stages of wheat crops. *Figure 3.8* illustrates the crop development stages for one spring-sown and two winter-sown wheat

fields at Boxworth, UK, during 1993. These ground photographs show the crop condition on four dates at the time of ERS-1 SAR acquisitions, and may be used to provide a more detailed interpretation of the processes responsible for the changing response of the ERS-1 radar:

On *19 April (day 109)* the spring crop is only just emerging, in contrast with conditions in the winter wheat fields where tillering is well advanced and there is over 90% crop cover. Crop growth in the two winter wheat fields appears very similar, yet there is a difference of 1.7 dB in their backscatter. The backscatter of the spring wheat field is more than 2dB higher than the highest of the winter wheat fields.

By *24 May (day 144)* the two winter wheat fields have well developed flag leaves, and backscatter has decreased by 1.7 dB in the case of field no. 1.03, and 3.5 dB in the case of field no. 1.05. Comparing the two fields, field no. 1.05 is seen to have a more vertical structure than field no. 1.03 in which the flag leaves are seen to bend over. This structural difference seems to be a possible explanation of the difference in backscatter between the fields. In the spring wheat field, tillering has reached a similar stage to that seen in the winter wheat fields on 19 April, and the backscatter has declined by 3.5 dB to −12.14 dB, which is similar to the values of the winter wheat on 19 April.

On *28 June (day 179)* all three crops were at the heading stage and appear quite similar in terms of structure, which is dominated by vertical components. Backscatter values for all fields reach a minimum at this time (around −14 to −16 dB), with only about 2 dB difference between them.

Finally, on *2 August (day 214)*, grain fill and crop senescence had occurred in all fields, and backscatter values show increases of 1.5 – 2 dB for all fields. In addition to the obvious drying out of the crop by 2 August, one can see that the senescence of the leaf vegetation, with just the stalks and ears remaining, has resulted in a less dense crop canopy.

The observed changes in winter wheat backscatter with crop growth stage might be interpreted as follows. At the early stage of growth, as the crop emerges, backscatter is essentially determined by the condition of bare soil, and in most cases backscatter values are relatively high. As tillering takes place and crop cover develops, a decrease in backscatter is experienced, with volume scattering within the crop reducing the overall return from the soil's surface. This reduction in

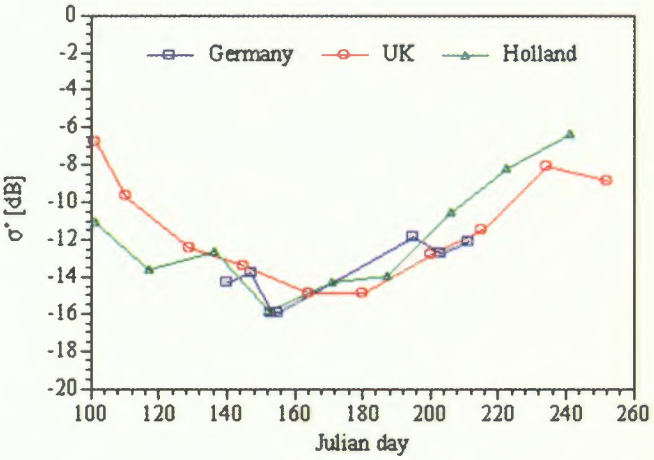

Figure 3.7. Comparison of winter wheat backscatter profiles for the European test sites. (Source: M. Borgeaud, ESA/ESTEC, C. Schmullius, DLR and M. Wooding, RSAC).

backscatter seems to continue until flag leaves develop and start to bend over and produce a more pronounced horizontal structural component to the crop. From the comparison of different fields carried out above, it then seems that a small increase in backscatter may actually occur at this time, related perhaps to surface backscatter from the flag leaves. As heading takes place and the flag leaves become less dominant within the canopy, the crop develops a more open vertical structure which produces very low backscatter returns from within the volume of the crop canopy. Then as the crop begins to ripen, thin and dry out there is an increase in backscatter which seems best explained by radar penetration through the crop to give some backscatter contribution from interaction with the soil surface.

Broadly, then, there is strong evidence to suggest that winter wheat backscatter shows consistent patterns of change as a function of time, namely that:

- high backscatter is associated with the early stages of crop development
- backscatter then declines and reaches a minimum by June (ie the period of maximum crop productivity)
- after anthesis backscatter increases during the grain filling stage.

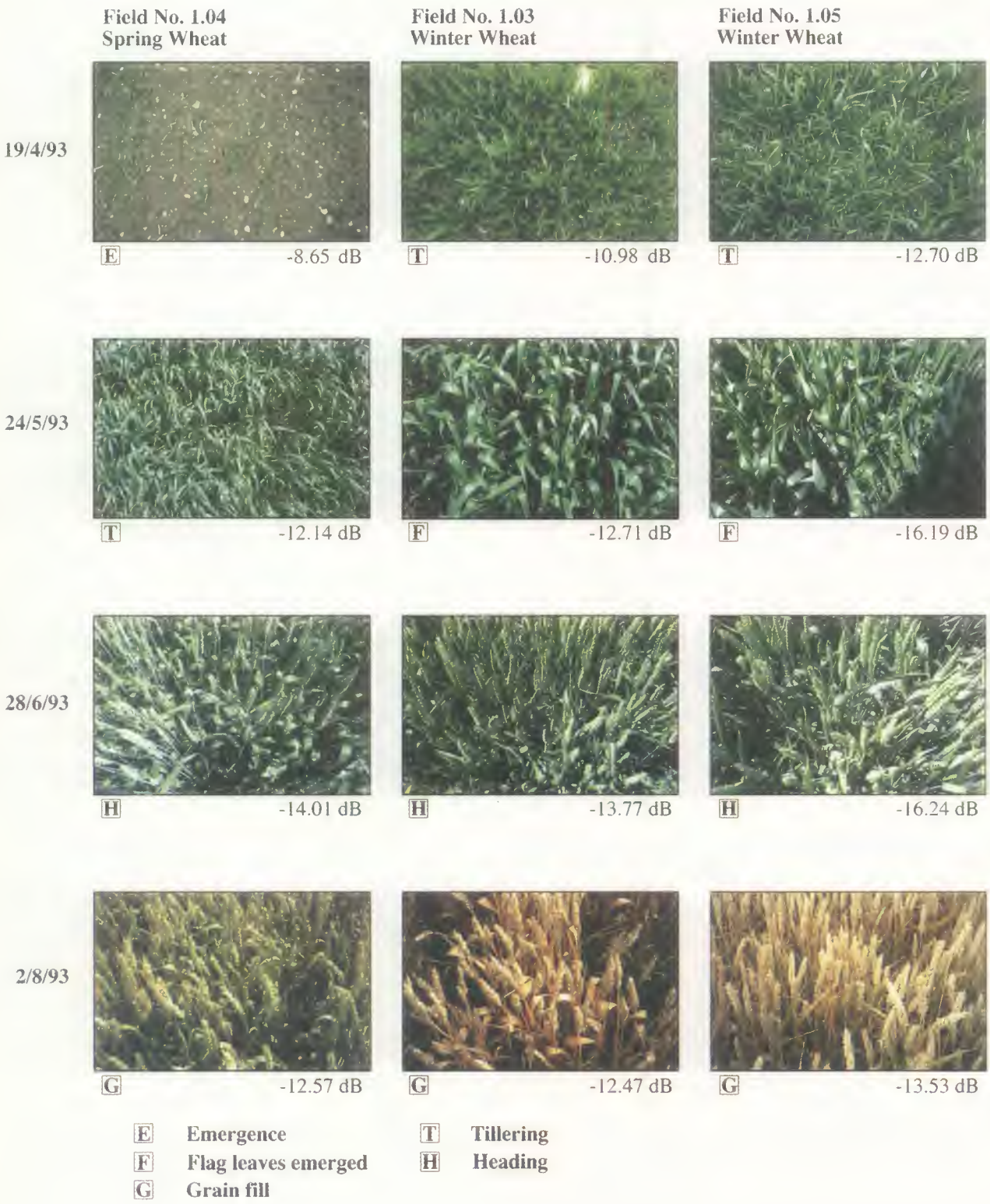

Figure 3.8. Changes in winter wheat backscatter with development stage, Boxworth, UK 1993, growing season. (Source: Zmuda et al. 1994)

Between-field variability
Figure 3.9 shows individual temporal curves for wheat fields imaged by ERS-1 over the Netherlands test site. The profiles show similar trends in backscatter development as a function of time, but there is seen to be a very significant variation in backscatter between fields on each date. This is much greater than can be accounted for in terms of variations in the calibration factor across ERS-1 images. Accounting quantitatively for this variability has proved difficult. In the early stages of development it may be most closely associated with differences in the percentage crop cover. Between-field variability in backscatter at the tillering stage may perhaps be equated with variability in crop growth in different fields at any one time or with field orientation effects. Large variations in backscatter at the end of the season may be attributed to lodging (i.e. flattening of the crop by wind). Lodged fields have been observed to have higher backscatter than unlodged fields (*Wooding et al. 1993*).

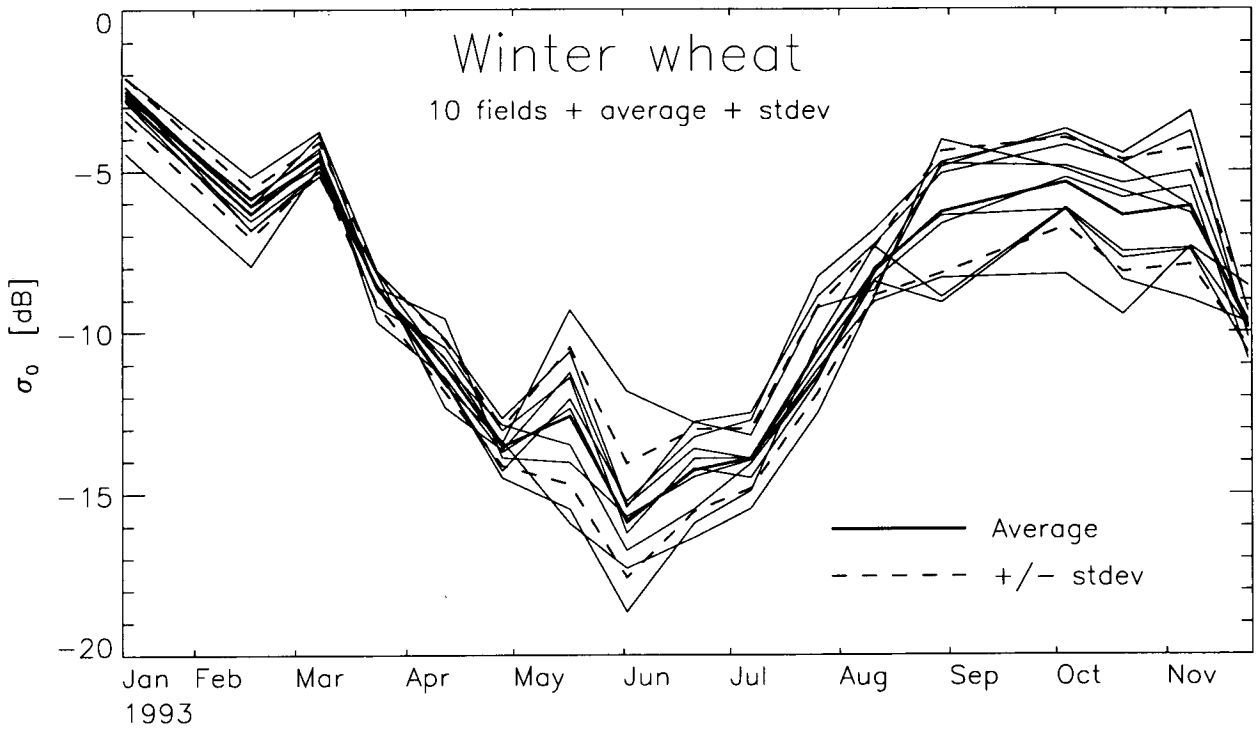

Figure 3.9. Between-field variability in winter wheat backscatter, The Netherlands 1993. (Courtesy of M. Borgeaud, ESA/ESTEC).

Other cereal crops
The UK, German and Dutch studies have also examined barley fields. Barley was seen to exhibit patterns of change similar to those of wheat with the notable exception that the backscatter minimum associated with the attainment of the heading stage occurs earlier than for winter wheat. *Figure 3.10* shows comparisons of wheat and barley signatures from the UK and Dutch test sites. The period of maximum separation occurs during days 150 to 190. During this period wheat is at maximum productivity (heading and anthesis) while barley crops are maturing (grain filling stage). Backscatter is at a minimum for wheat and is increasing as a function of time for barley. Therefore critical time windows appear to exist during which different cereal crops can be separated on the basis of their backscatter temporal signatures.

3.3.2 Other arable crops
A composite of temporal profiles for a mixture of arable crops studied with ERS-1 at the German, Dutch and UK test site is shown in *Figure 3.11*. The curves illustrate clearly the varying potential for inter-crop discrimination which ERS-1 may provide as a function of time in the growing season. Below, we pick out certain important crops and summarise briefly their backscatter characteristics and their perceived potential for identification.

Sugar beet
Temporal profiles of sugar beet *(Figure 3.12)* tend not to show the large changes through the season which are characteristic of cereals. Rather, it appears that after canopy closure, backscatter remains at a uniformly high level. Variations in backscatter between different fields

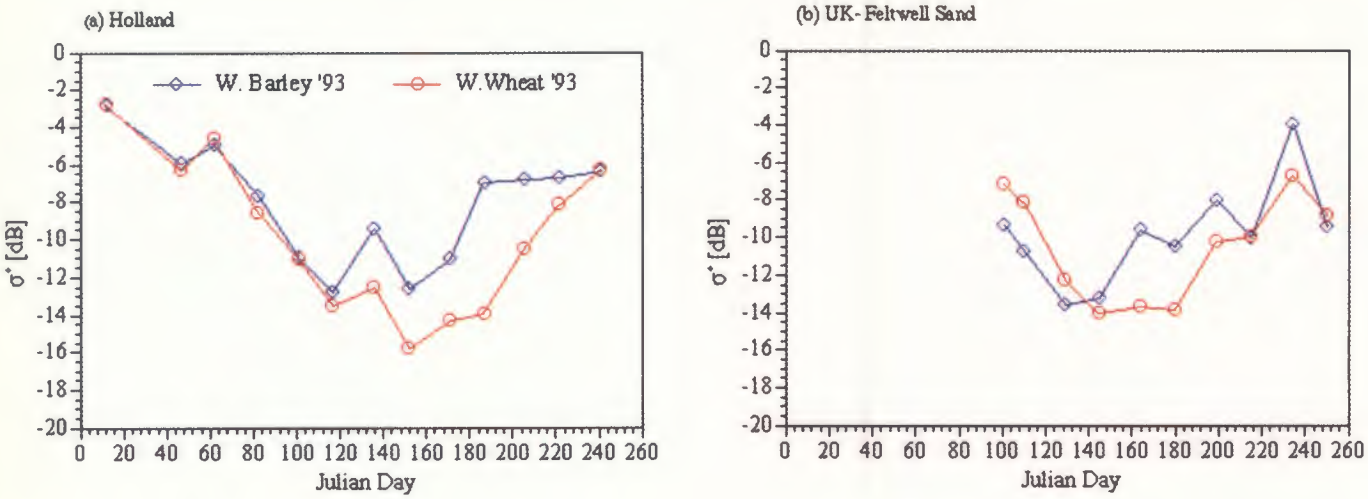

Figure 3.10. Changes in mean winter barley and wheat backscatter as a function of time (a) 1993 growing season, The Netherlands (Courtesy of M. Borgeaud, ESA/ESTEC); *(b) 1993 growing season, Feltwell, UK.* (Source: Zmuda et al. 1994).

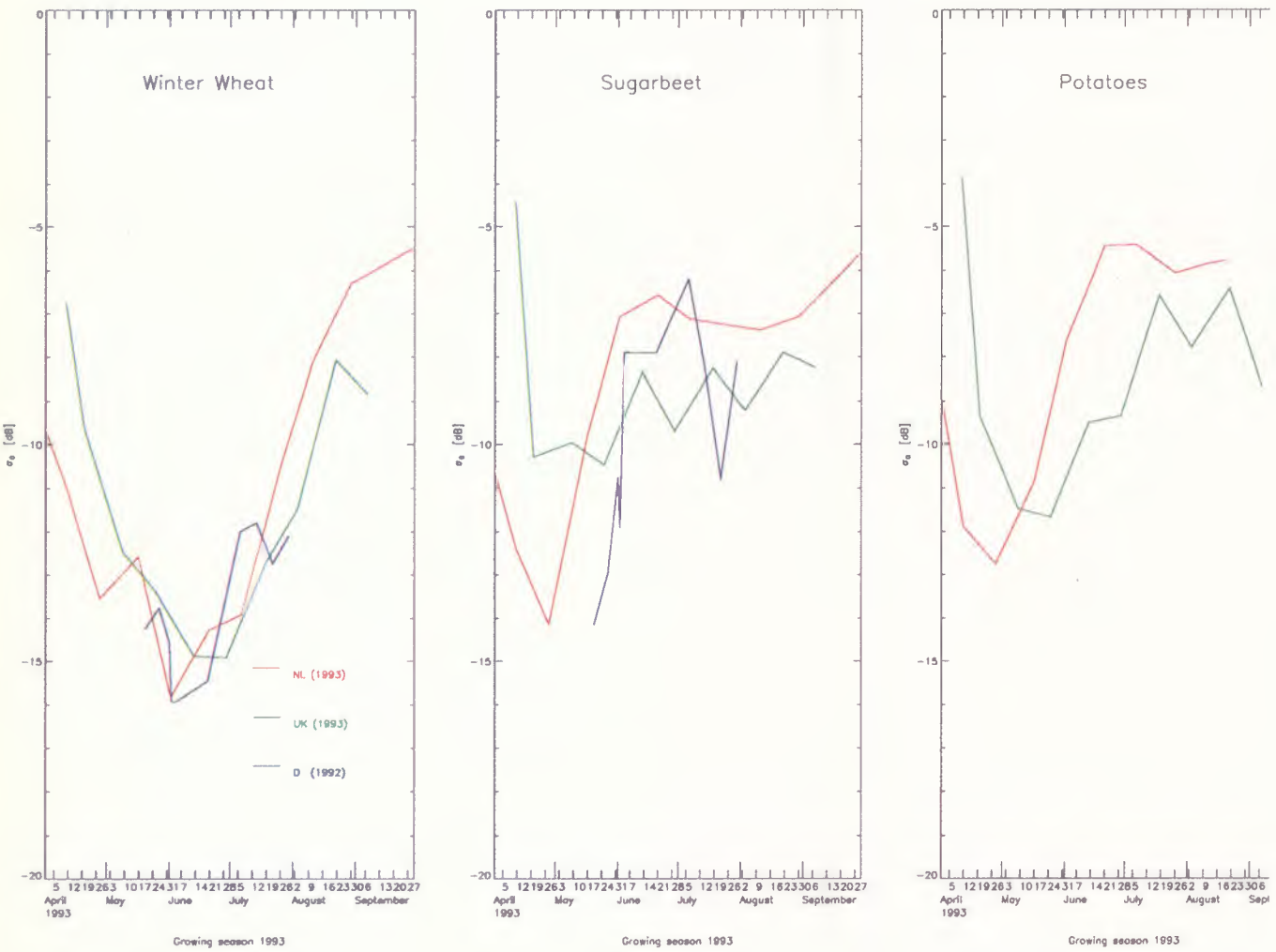

Figure 3.11. Changes in wheat, sugar beet and potato backscatter with time for the European test sites. (Source: M. Borgeaud, ESA/ESTEC, C. Schmullius, DLR and M. Wooding, RSAC).

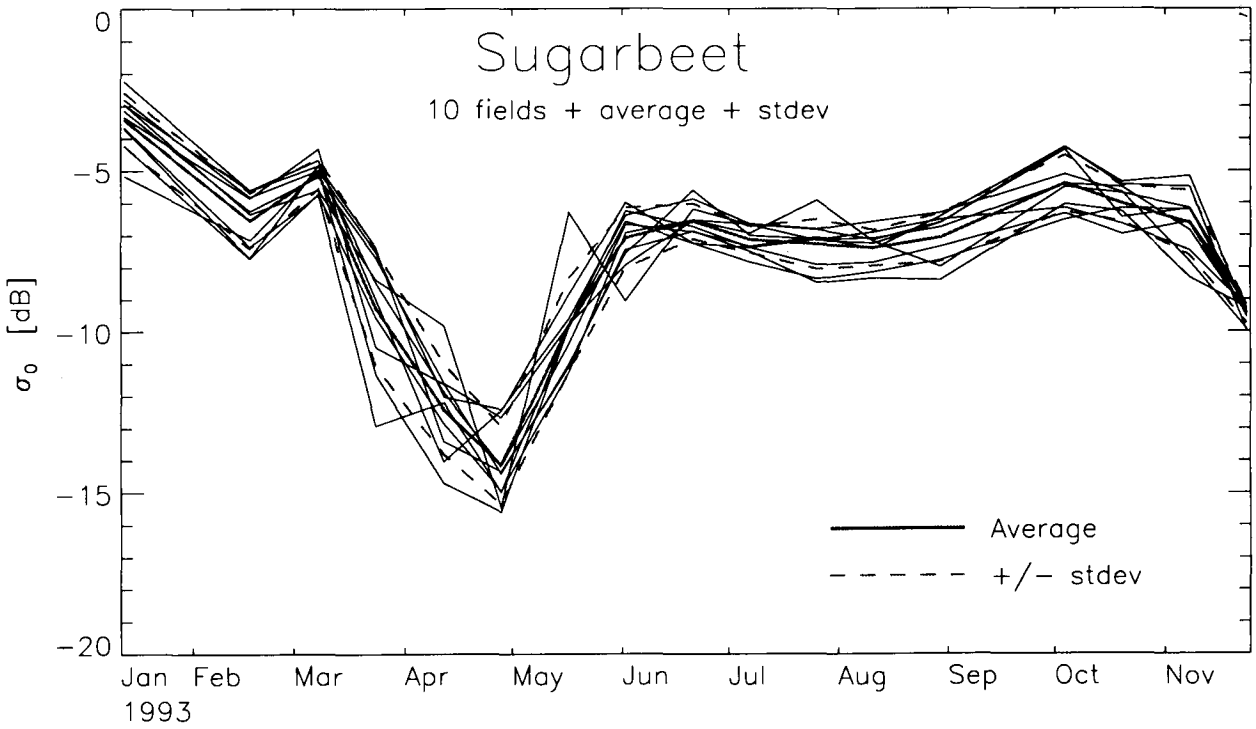

Figure 3.12. Between-field variability in sugarbeet backscatter, Flevoland, The Netherlands 1993. (Source: M. Borgeaud, ESA/ESTEC).

is greatest during the early part of the season at some sites while others show greater consistency; possibly reflecting differences in management practices in the different countries. In particular, sites in the Netherlands have exhibited a deep dip in backscatter before the emergence of the crop.

Oilseed rape

Oilseed rape does show significant features in its temporal profiles although, again, not nearly as pronounced as for cereals *(Figure 3.13)*. During and after anthesis (May and June), backscatter increases followed by a decline during senescence and seed ripening until harvest in mid August. The backscatter of the rough bare soil after harvest may be several dB brighter than pre-harvest levels. Compared to winter wheat, oilseed rape profiles display higher backscatter at all stages of development up to late July. Maximum backscatter for rape seed occurs at the seed development stage in June. At this time winter wheat backscatter is at a minimum. Following ploughing at the end of the growing season, similarly high backscatter values are associated with rough bare soil fields which had previously held either rape or wheat.

Potatoes

Potatoes, and indeed other root crops which have been investigated, tend to show less variations in backscatter through the season than either winter sown cereals or oilseed rape. Some differences between different sites are seen, especially in terms of the variation in backscatter about the mean. Scatter is greatest during the early part of the season which may be attributable to differences in the height and orientation of soil ridges, and to variability in above ground vegetation cover in different fields.

3.3.3 Rice

ERS-1 radar backscatter from rice fields exhibits a very characteristic and pronounced temporal signature during the growing season. This is associated with very significant changes in the nature of the crop, and of the growing medium during each growth cycle, which are more dramatic than those previously described for temperate arable crops.

Rice fields are flooded during the early growing stage with the soil surface almost completely covered by water. Plants emerge above the water surface, and increase in height up to a maximum level after which the ripening phase starts. Plant moisture content is high at the early growing stage, and drastically decreases during ripening. In most cases water is drained out from the field at the beginning of the ripening phase, leaving the soil surface moist. Before harvest the soil becomes drier and rougher due to cracks in the surface. It is these

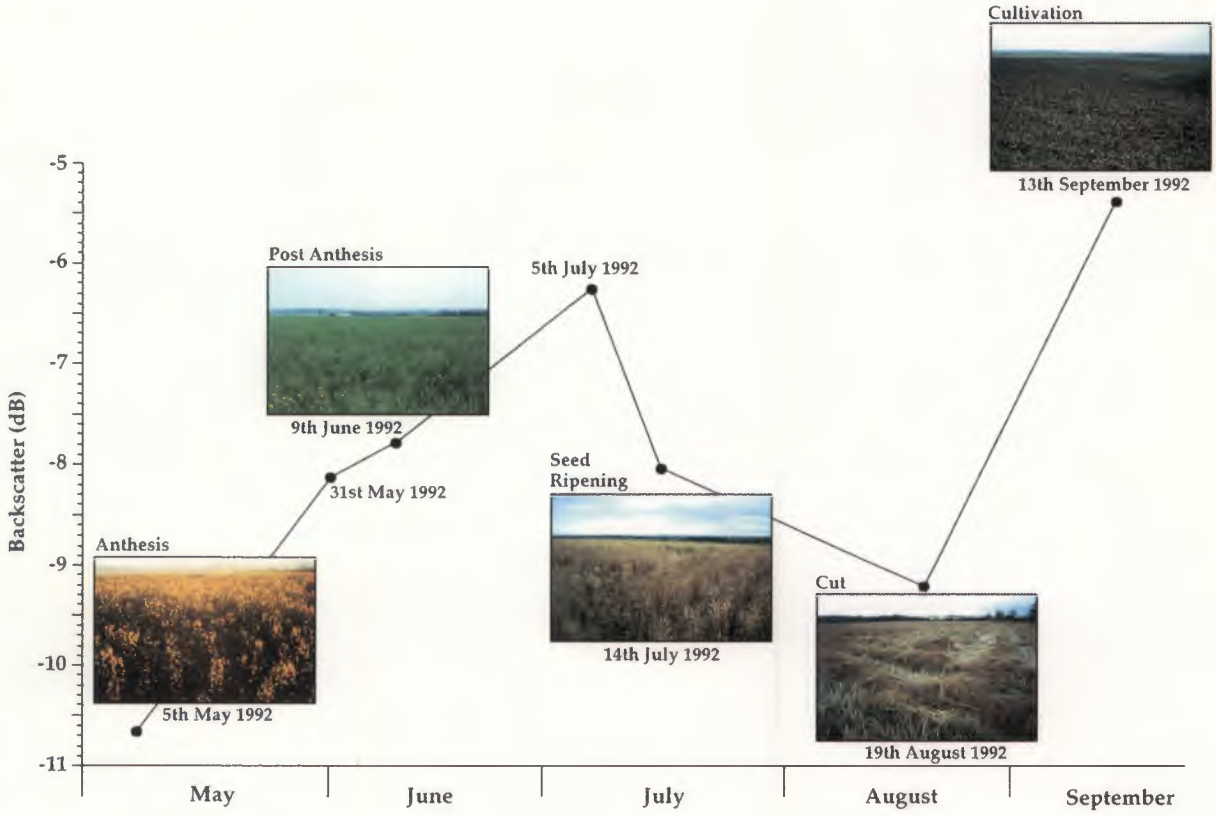

*Figure 3.13. Changes in oilseed rape backscatter with time, development stages also shown, UK 1992. (*Source: Wooding et al. 1993*).*

structural and moisture changes which are believed to be the main cause of changes in the nature of the radar interaction and consequently of the ERS image brightness.

In ERS-1 images, rice fields appear dark during the flooded and early growing stage and turn brighter during the later growing stage *(Figure 3.14)*. Radar backscattering reaches a maximum before the ripening phase. This maximum may plausibly be attributed to multiple radar reflections between vertical plant structures and the horizontal water surface at a growth stage when penetration of the microwaves to the water surface is still possible. Later, during the ripening phase, the scattering from the volume of the canopy increases, but penetration to the water decreases, leading to an overall darkening of the radar image. After rice is harvested, radar backscatter decreases to that of either water or bare soil, depending on the surface condition remaining after harvest (*Aschbacher & Paudyal, 1993*).

In Chapter 6, there are examples using the distinctive temporal signature of rice for the classification of growing areas.

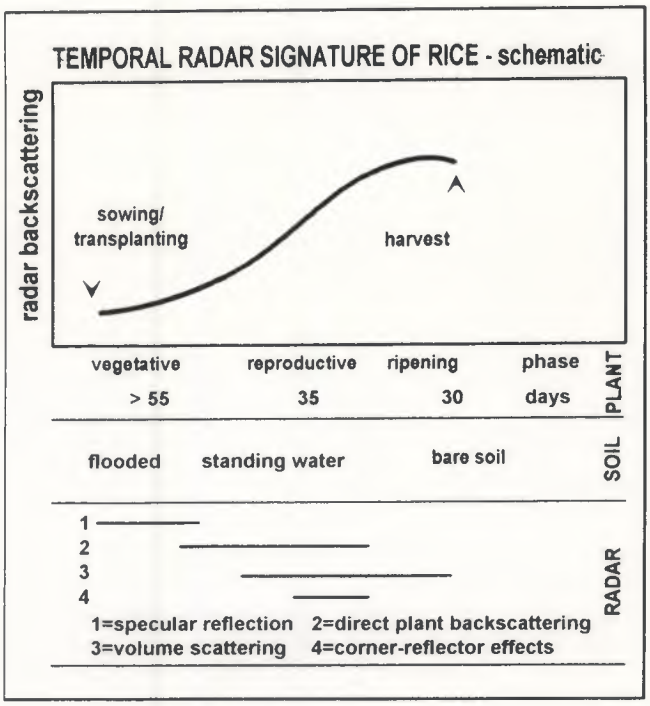

*Figure 3.14. ERS-1 temporal backscatter signature of rice. (*Source: J. Aschbacher, JRC*).*

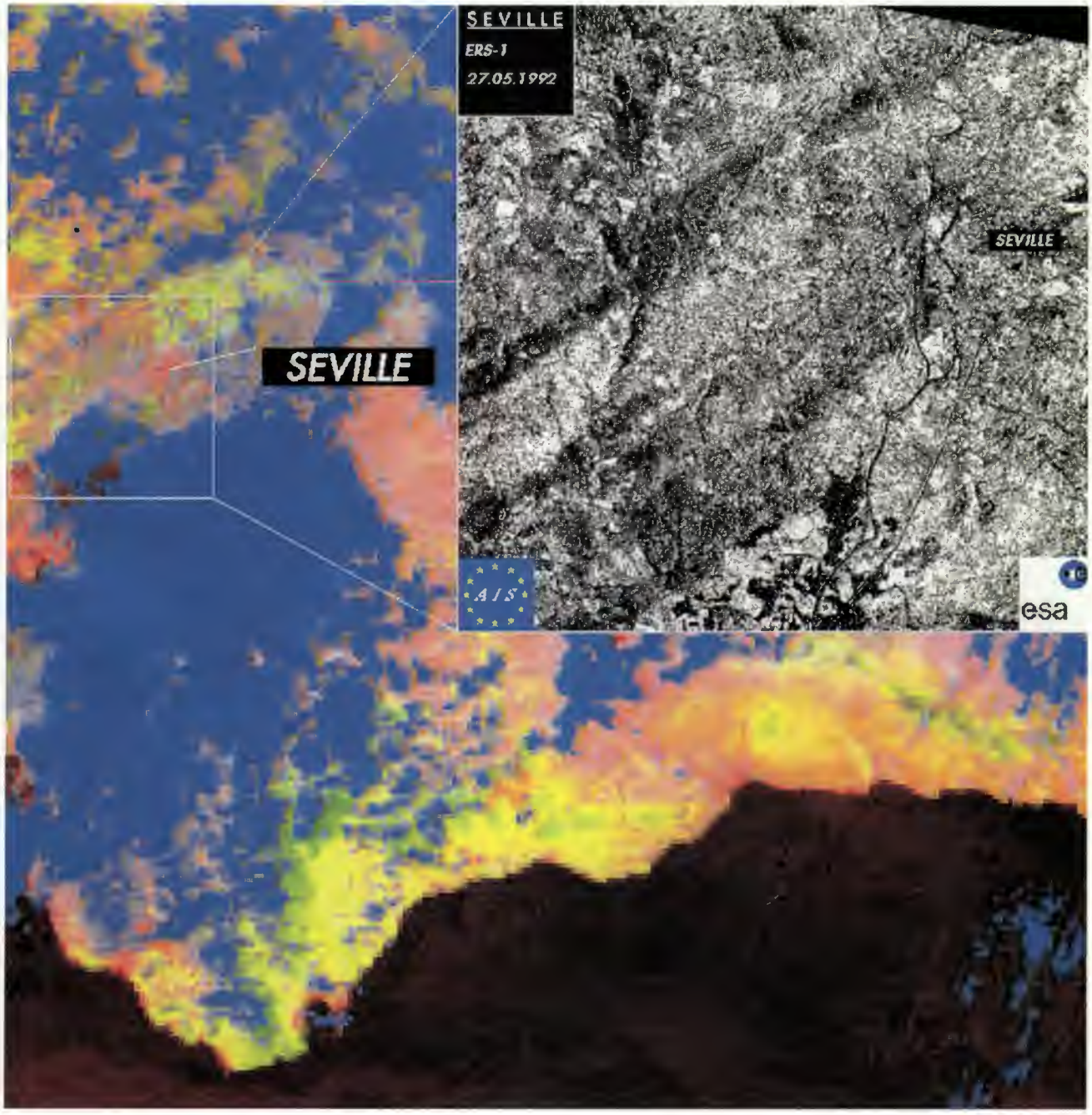

Figure 3.15. Moisture pattern in AVHRR and ERS-1 images of 27 May 1992. (Source: H. De Groof, JRC).

3.4 Environmental Effects

In addition to steady changes in crop structures during a season, there exist other influences on ERS temporal radar signatures which have been observed in experimental datasets and which may impact on the ability to discriminate different crops. Here, we discuss those associated with meteorological effects through their temporary or permanent influence on crop structure or moisture.

3.4.1 Influence of wind

To the casual observer the wind can often be seen to exert a very significant effect on the geometry of a plant canopy; particularly for smaller plants or those with thin stalks. In circumstances where the radar backscatter is influenced significantly by the vertical geometry of cereal crops, we may expect that temporary disruption or randomisation of that geometry will act to change the amount of backscattered energy. Wind is therefore seen to provide a contribution to regional 'noise' effects

on the temporal backscatter signatures of crops. As identified in temporal signatures of wheat in § 3.3.1, extreme wind disruption of the canopy late in the season (i.e. crop flattening or 'lodging') does lead to significant and irrecoverable changes in backscatter levels, leading to populations of outliers in distributions of crop signatures.

In the case of rice, the wind also influences the surface conditions; in this case the water surface present for at least part of the growing cycle. Wind during the early growing stage increases the roughness of the water surface, resulting in enhanced radar backscattering. Such effects are, indeed, seen in ERS-1 imagery of rice fields, and an example will be presented as part of the case study of Chapter 6.

3.4.2 The effect of rainfall events

ERS images are potentially sensitive to moisture, both within crops and, under some circumstances, within the upper layers of the soil. Rainfall, therefore, may constitute an additional 'noise' source affecting temporal radar profiles otherwise related to crop development. Significant enhancements to ERS-1 image brightness are, indeed, seen to be associated with rainfall events over agricultural areas. Evidence comes from a small subset of temporal radar profiles, including some of those obtained in 1993 from the UK test sites. *Figure 3.15* provides an illustration of rainfall effects on radar backscatter across an ERS-1 scene of the Seville area. In this example alternate light and dark zoning is seen in a part of the image where the similarly timed AVHRR image shows the presence of rain bearing cloud formations. In quantitative terms, rain events in the UK were observed to result in enhanced backscatter on particular days of up to 4 dB (i.e. a factor of 2.5 increase in reflected energy).

The effect of rainfall may have a significant effect on the comparison of radar observations both between different sites and different seasons. As a result, crop classifications to the highest potential accuracies achievable with ERS or other future satellite radars may need to be based primarily on local training of algorithms. However, with a sufficient number of measurements over a number of seasons, it may be possible to isolate accurate meaningful profiles characteristic solely of crop development.

4. Analysis Techniques

4.1 Pixel-based Approach

Computer-based crop classification using radar imagery is complicated by image speckle, which is a noise phenomenon of the radar imaging process (see § 3.3). There is a linear increase of noise level (expressed as the standard deviation of pixel values within a uniform land-cover area) with the average grey value.

Image speckle hampers the application of standard pixel-based classification techniques normally used to classify optical imagery. If one adopts a pixel-based approach it is first necessary to apply some form of image filtering or segmentation to reduce image speckle before image classification. *Figure 4.1* illustrates the effect of the Gamma-Gamma MAP filter (*Lopes et al., 1993*) applied on a multi-temporal ERS-1 composite of Zuid Flevoland in the Netherlands. Both unfiltered and filtered images are shown, and one can see how the within field variability has been reduced considerably in the filtered image, while edges of linear features have been preserved. Speckle reduction filters aim to reduce speckle while preserving spatial resolution and linear features.

Paudyal & Aschbacher (1993 a,b) have systematically investigated the performance of different filters, using a study area in Thailand. The speckle-specific filters tested included the Lee Local Statistics, Lee Sigma, Frost, Li, MAP and Gamma MAP filters (*Lee, 1986.; Frost et al. 1982.; Li, 1988.; Nezry et al., 1991*). The investigation included a number of non-speckle-specific filters, such as mean and median filters.

Filter performance has been assessed in terms of the improvement of the signal-to-noise ratio SNR (mean/standard deviation) for different land cover types (Table 4.1). These results demonstrate a significant improvement of SNR for both agricultural and non-agricultural cover types. Overall, the Lee and MAP filters show the highest SNR for agricultural land cover types.

The improvement in the SNR should not be the only means of judging the performance of a filter. SAR images also consist of heterogeneous areas, linear features and small scatters. These may need to be preserved and it is difficult to assess this quantitatively. Therefore a visual inspection often gives the best impression on a particular filter's performance.

Speckle filtering is a pre-requisite if pixel-based digital classification of SAR imagery is carried out. Speckle filtering also improves visual interpretation of SAR images. The choice of filter may depend on the image characteristics. For the work in Thailand, the best overall performance was observed using the Gamma MAP filter,

Table 4.1 The effect of speckle reduction filtering on signal to noise ratio for different land-cover categories (Source: Paudyal & Aschbacher, 1993a*)*

			Signal to Noise Ratio, SNR (μ/σ)							
Filter type	Window size	Passes	Water	Bush	Shrub	Urban	Paddy (l)	Paddy (h)	Sugar Cane (l)	Sugar Cane (h)
Original	–	–	3.3	3.2	3.5	1.5	3.3	3.3	3.3	3.4
Mean	3×3	1	6.8	5.3	6.3	2.3	5.7	5.3	5.6	6.1
Median	3×3	1	6.4	5.0	5.8	2.2	5.1	4.9	5.3	5.5
EPS	5×5	1	5.3	4.5	4.9	2.0	4.6	4.3	4.6	4.6
Lee	5×5	1	9.5	6.6	8.0	1.9	7.5	6.9	7.8	8.3
Sigma	5×5	1	6.6	5.3	6.3	2.0	5.7	5.7	5.9	6.4
Frost	5×5	1	5.2	4.4	5.1	1.7	4.7	4.4	4.8	4.8
Li	3×3	1	6.7	5.2	6.2	2.6	5.6	5.2	5.7	5.8
MAP(M)	11×11	1	5.4	5.2	7.7	1.5	7.0	10.2	7.5	8.1

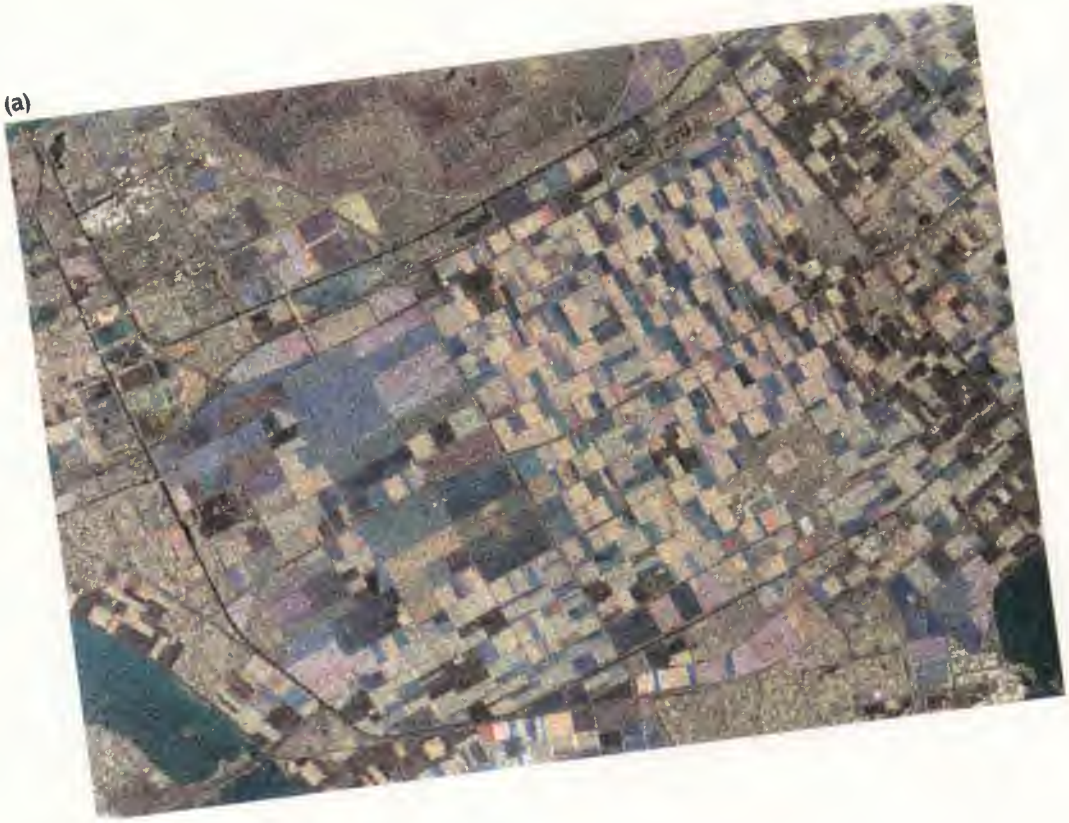

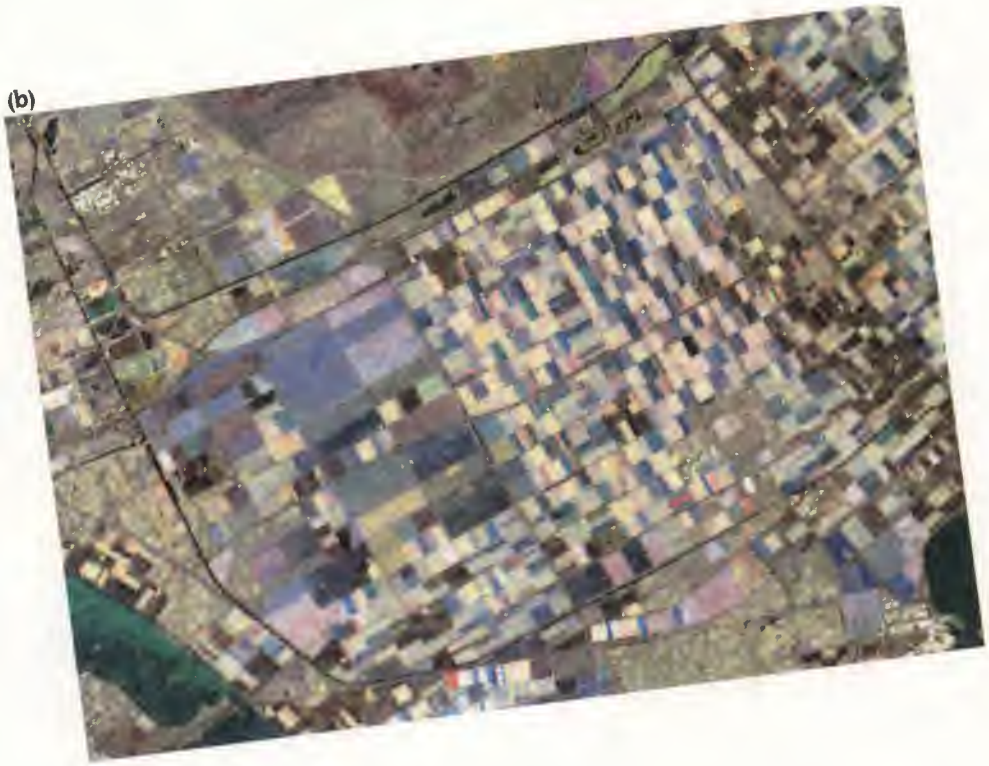

Figure 4.1. ERS-1 multitemporal composite, Zuid Flevoland 1992; (a) unfiltered composite, (b) filtered composite: red 7 June, green 12 July, blue 16 August. (Source: G. Nieuwenhuis, Staring Centre).

which was found to give the best combination of smoothing image speckle within homogeneous areas and edge preservation. Application of the Gamma MAP filter also improved visual interpretation. The Lee filter performed well for digital analysis when class separation was critical. However, edges and linear features tended to be degraded.

The application of speckle filters in the Thailand agricultural study areas has shown that land cover discrimination can be significantly improved. Classification performance also shows improvement. This is further developed in Chapter 6.

4.2 Field-based Approach

A field-based approach involving the use of digital field boundaries to extract image statistics, such as the mean field backscatter, effectively overcomes the problem of speckle. Clearly such an approach assumes that fields can be treated as individual objects and one can disregard the within field spatial variability. In general, only the mean field values are used for classification, but within-field variance and texture can be used as additional information for crop classification. At the spatial resolution of satellite radar, agricultural fields are relatively smooth uniform surfaces, lacking the grainy texture which can be associated with urban or forest areas.

An example of a field-based classification methodology using ERS-1 images integrated with digital field boundaries derived from a SPOT XS image is presented as a flow chart in *Figure 4.2*. In this example, digital field boundary information is stored in a GIS. A selection of ERS-1 acquisition dates is made, and the mean backscatter value (gamma) per field is calculated using the digitized field boundaries. These mean values are used to create signatures for each crop type, and to carry out a maximum-likelihood classification. The classification result is then added to the GIS to produce a land cover map.

Field boundaries can be obtained from cadastral maps, and then adjusted over an image backdrop, or alternatively can be obtained directly from radar or optical satellite images using visual interpretation or automated techniques.

When only ERS images are used to extract field boundaries, multitemporal composites aid the interpretation of field boundaries. *Figure 4.3a* shows field boundaries mapped over a multitemporal ERS-1 image of Terrington

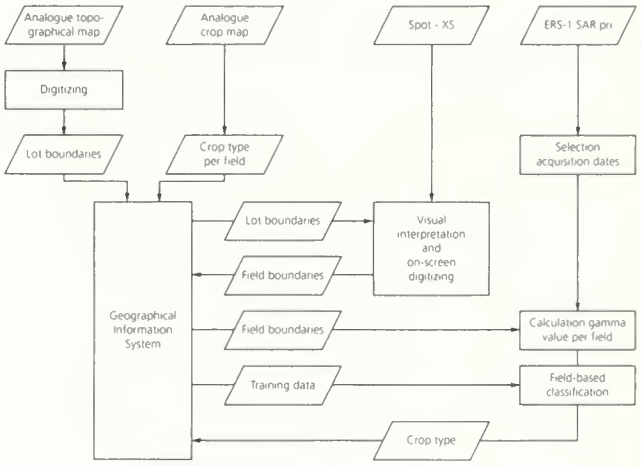

Figure 4.2. Flow chart of a field-based classification procedure of ERS-1 images using additional information from topographical maps, field work and optical data. (Source: Schotten et al. 1994).

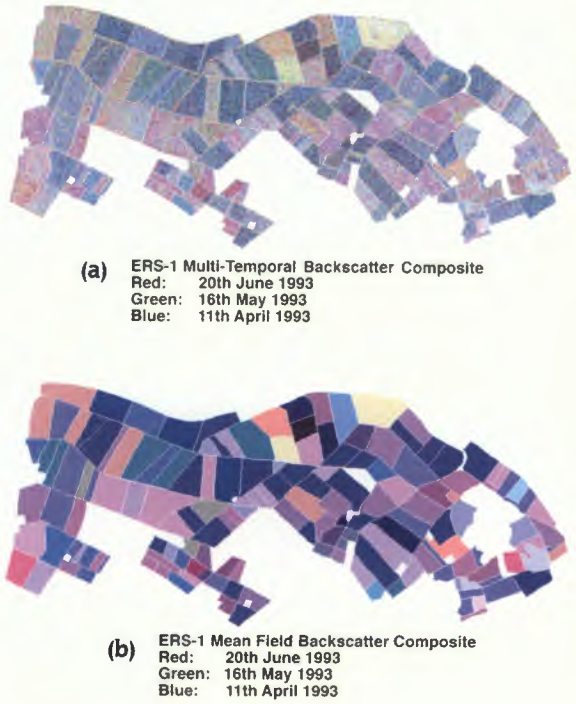

Figure 4.3. ERS-1 multitemporal backscatter composites, Terrington Marsh UK; (a) PRI imagery (b) mean field backscatter composite. Field boundaries are superimposed. (Source: M. Wooding, RSAC).

Marsh in the UK. The speckle effects are very evident in the backscatter composite as fields appear to contain

noise. A GIS has been used to capture field boundaries on screen using ERS-1 imagery as a 'backdrop'. As the ERS-1 imagery is georeferenced to the UK national grid, field boundaries can be linked to the radar image. However, edge effects have to be removed and this is achieved by creating a buffer zone around the boundaries. Field means can then be extracted and stored in the database of the GIS. Mean field backscatter colour composites can be produced by seed filling the fields with the mean values, as shown in *Figure 4.3b.*

Optical satellite images usually provide a better definition of linear features, and can be used as the source of field boundaries to be used for field-based analysis of satellite radar images. *Harms et al. (1993)* have performed an automated segmentation of a SPOT image as a basis for classifying multi-date ERS-1 imagery. The technique produced classification accuracies very close to those achieved by visual interpretation of field boundaries on optical images. Following georeferencing of the SPOT and ERS-1 imagery, segmentation of the SPOT image was performed using the principal of local contrasts. The segmentation performed over a large variety of agricultural crops has indicated the high quality and robustness of the algorithm. Comparisons with cadastral maps show over 95% accuracy for the segmentation. Having segmented the optical dataset, multitemporal ERS images were classified by a field-based algorithm using mean and standard deviation. The results obtained using this analysis process are shown in *Figure 4.4.*

A number of automated segmentation techniques are now being developed to identify parcel boundaries, and undertake field-based classification, directly using radar images. Techniques developed by *White (1994)* and *Quegan et al. (1993)* involve operations such as merging of an initial 'fine segmentation' based on calculated probability, edge detection and region growing, and the estimation of background radar cross section. Results obtained within different studies show the usefulness of such algorithms for segmenting imagery and classifying crops. Example images are shown in *Figure 4.5.*

4.3 Integration of Optical and Radar Data

One example of the integrated use of optical and radar data has been presented in the previous section, where a SPOT image has been used as the source of field boundaries for subsequent multi-temporal classification of ERS-1 images. Improving crop classification by combined analysis of the reflectance and backscatter data, respectively from optical and radar images, takes this one step further.

As yet, techniques for fully integrated analysis of optical and radar data are poorly developed. However, as far as visualisation of combined data sets are concerned, some interesting results have been obtained using the IHS technique (i.e. Intensity-Hue-Saturation). Normally, colour composites are produced using the red (R), green (G) and blue (B) colour guns to display different spectral or temporal channels. However an alternate colour space can be defined which uses Intensity, Hue and Saturation:

- Intensity is the overall brightness of a scene
- Saturation represents the purity of colour
- Hue represents the colour or dominant wavelength of the pixel.

The intensity, hue and saturation components can also be displayed as a colour composite or they can be contrast stretched before being transformed back into RGB space. One of the main advantage of the technique is that it enables the information content of more than 3 channels to be visualised. The steps involved in combining optical and radar imagery using this technique are as follows:

1. register SAR and optical images,
2. convert a 3-band optical image from RGB to IHS coordinates,
3. substitute the SAR image for the intensity coordinate, and
4. convert back to RGB space.

Figure 4.6 provides an example of this data integration technique, using Landsat TM and ERS-1 images for an area in Johor State, Malaysia. The resulting colour composite seems to provide enhanced discrimination of land cover types in comparison with what is possible using either just the Landsat or ERS-1 data. However, note that the mountains in the top of the composite contain terrain distortion from the ERS-1 image.

4.4 SAR Interferometry

A promising new technique is being developed using SAR interferometry. Interferometric processing of SAR data combines complex valued images for two passes to derive precise measurements of the difference in path lengths for the two sensor positions. Either airborne or spaceborne SAR can be used to create interferograms. ERS-1 operated during several phases with repeat orbits of 3 and 35 days. These repeat orbits are useful for performing SAR interferometry. Thanks to the excellent

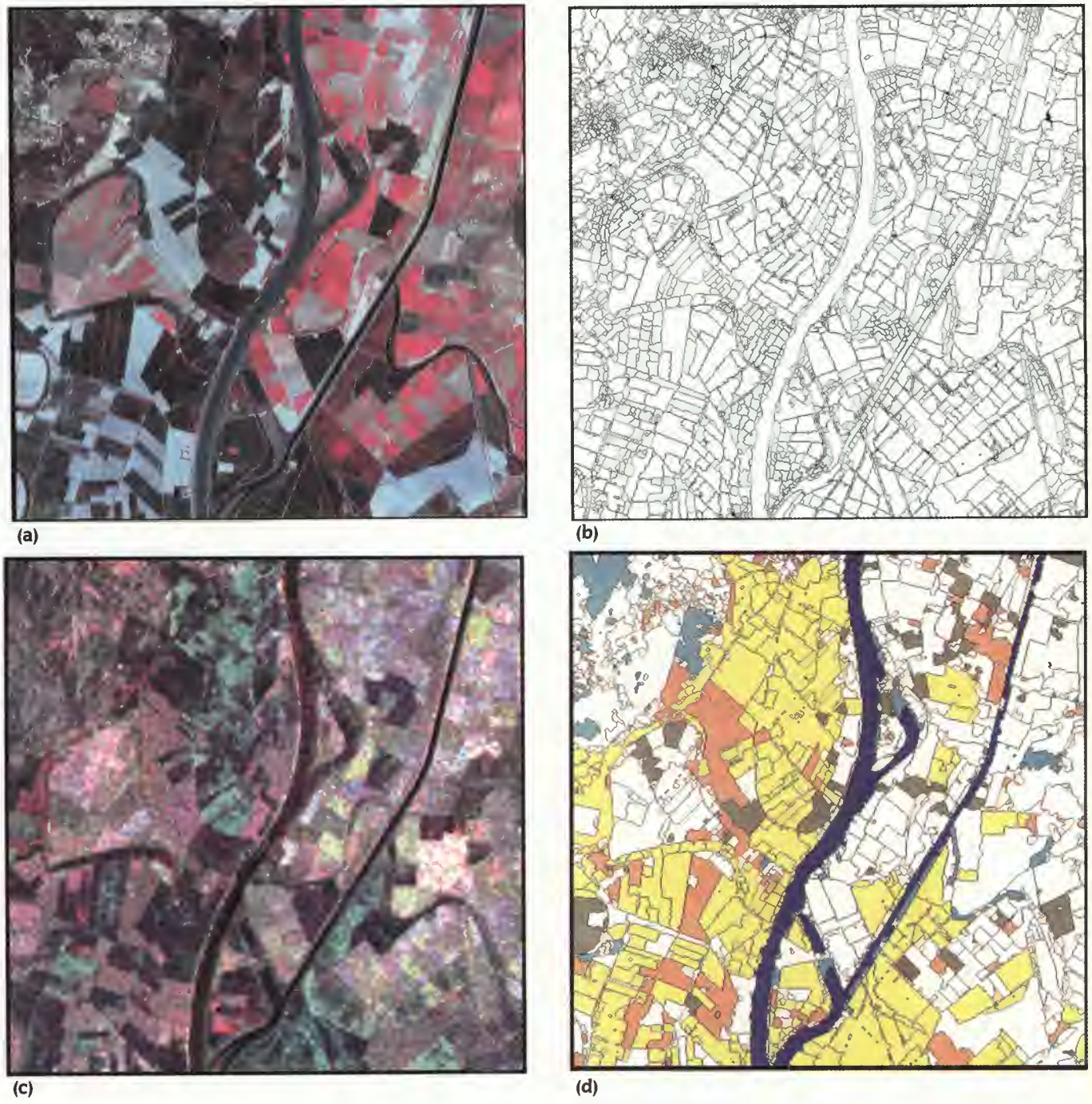

Figure 4.4. Field-based classification procedure by combining optical with ERS-1 imagery.
(a) SPOT image of July 1992
(b) Segmentation of SPOT image based on ARKEMIE software
(c) ERS-1 multitemporal composite (red: May; green: July; blue: August)
(d) Segmentation based per field classification of multitemporal ERS-1 imagery; classification results: yellow = rice, white = other crops, brown = misclassified.
(Courtesy of J. Harms, Scot Conseil).

(a) (b)

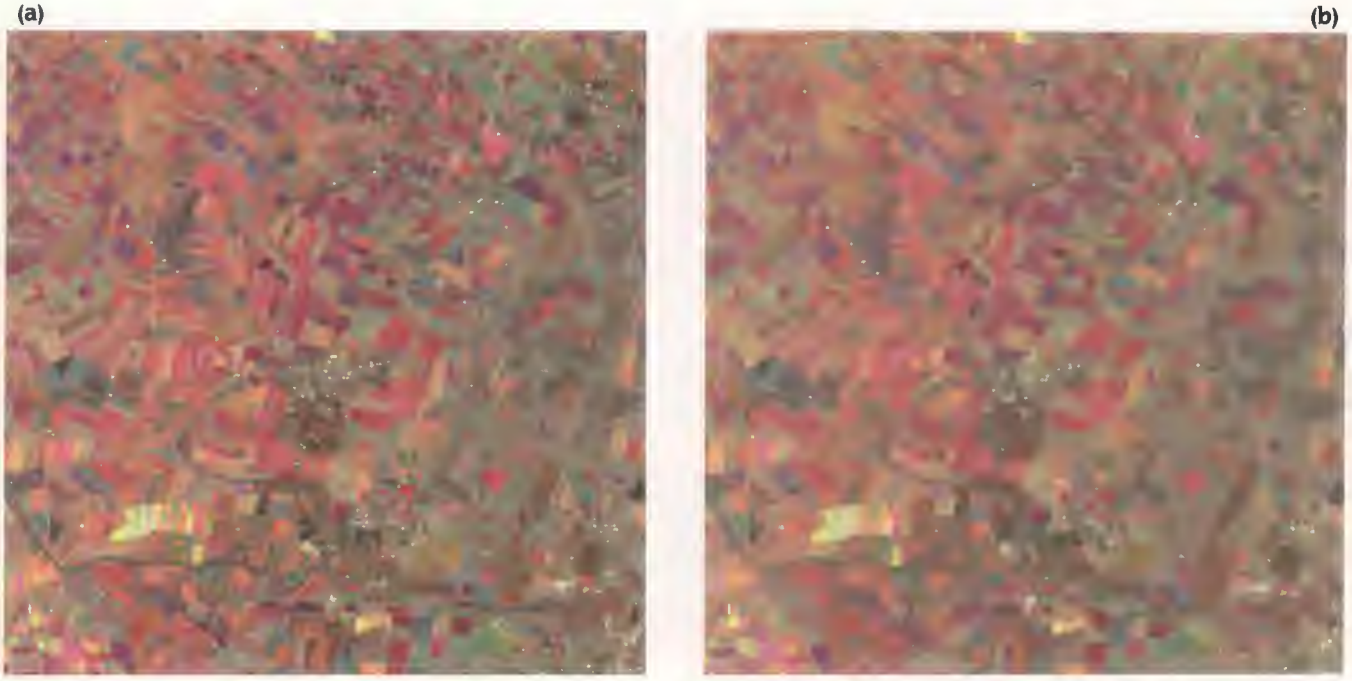

Figure 4.5. Multitemporal ERS-1 SAR composite of Feltwell UK. (a) before speckle reduction; (b) after speckle reduction using edge detection and region growing; red: 11 April 93, green: 20 June 93, blue: 29 August 93; (c) parcel boundaries derived from segmentation. (Courtesy of the Centre for Earth Observation, University of Sheffield, UK).

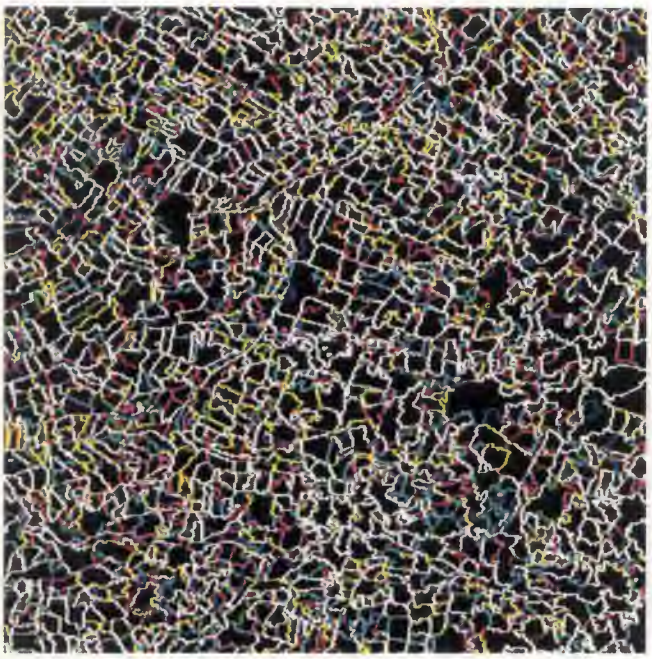

(c)

orbit and attitude control and the reliability of the SAR system, interferograms may be produced. Mainly as a result of high quality ERS-1 SAR data and extensive coverage, the development and application of repeat-pass SAR interferometry has become one of the prime research activities within the radar remote sensing community. The primary SAR interferometry applications are the preparation of height and differential displacement maps.

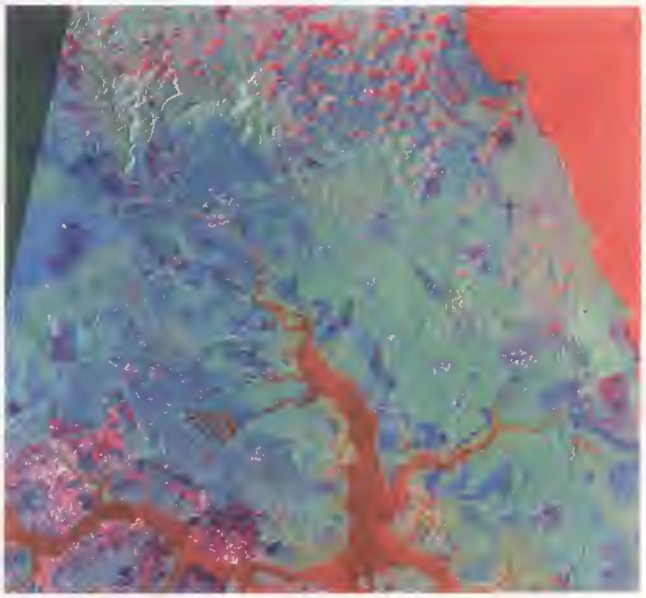

Figure 4.6. IHS combination of Landsat TM and ERS-1 images, Johor, Malaysia. (Source: M. Wooding, RSAC).

A significant amount of research is being undertaken to further refine the image processing steps required for the estimation of the interferometric phase, with the goal of an optimization of interferometrically derived height (*Zebker et al. 1994*) and displacement maps (*Massonet et al. 1993*). However, it has been shown recently that SAR interferometry has also a large potential for forest and agricultural applications (*Askne & Hagberg 1993, Werner & Wegmüller 1994, Wegmüller et al. 1995a*), particularly in providing a means for separating agricultural fields from forests in SAR images.

Using SAR interferometry, forest mapping with ERS-1 becomes almost straightforward (*Wegmüller et al. 1995b*). The interferometric correlation observed over forest is low due to the dominance of volume scattering and the geometric changes occurring between the repeat pass data acquisitions. The low interferometric correlation of forest can easily be distinguished from the much higher correlation shown by low vegetation canopies and bare soil surfaces.

In *Figure 4.7*, differences in land cover classes are shown by displaying the interferometric correlation, the backscatter intensity from one of the passes and the backscatter intensity change as a colour composite. This SAR interferogram was derived using ERS-1 SLC data measured on 24 and 27 November 1991. The region shown covers agricultural, urban, and forested areas, as well as a number of lakes near Bern in central Switzerland. The image covers an area of approximately 45 × 45 km.

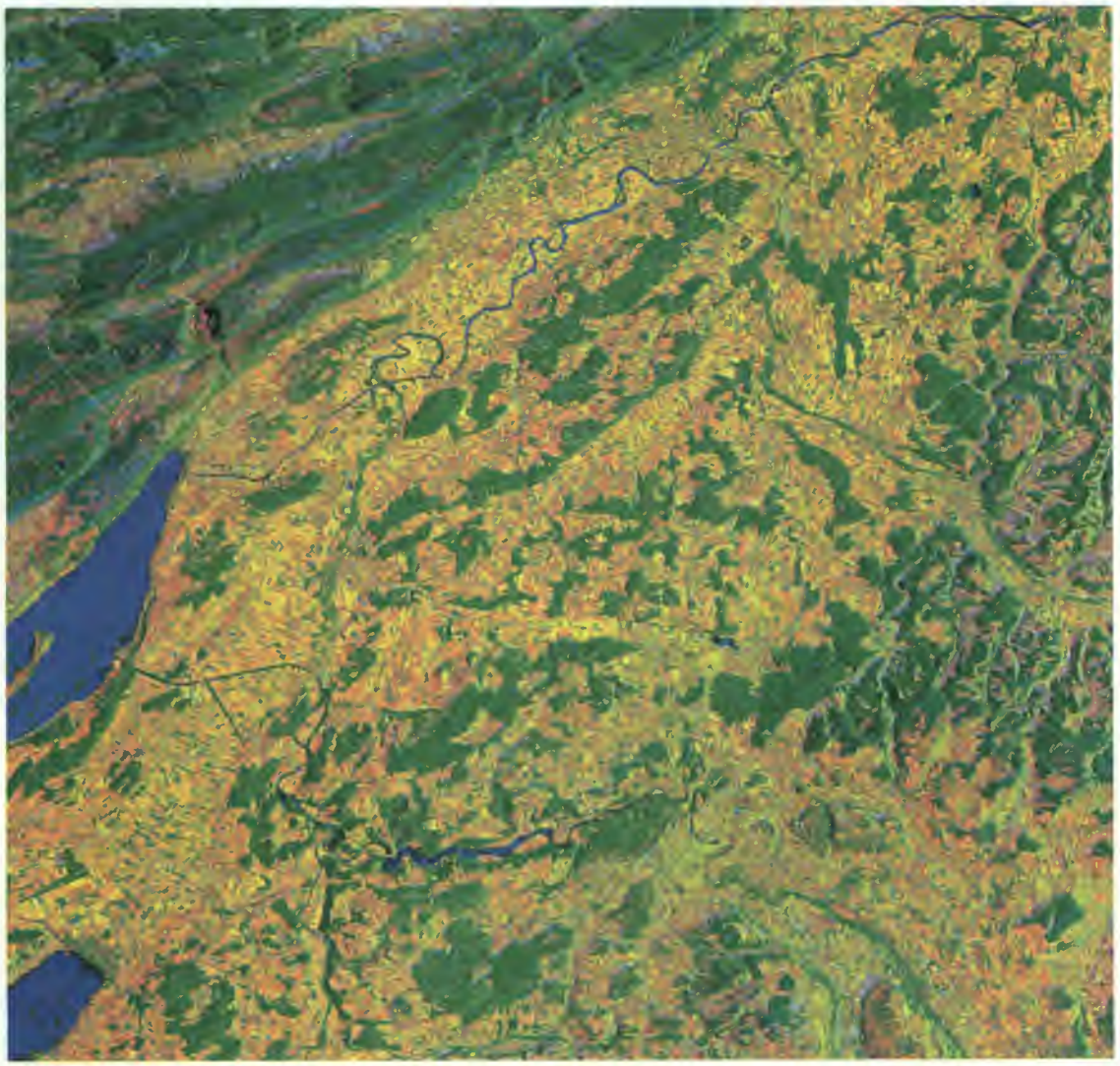

Figure 4.7. Interferometric signatures derived from an ERS-1 SAR image pair over Bern, Switzerland (red: interferometric correlation; green: backscatter intensity on 24 Nov.; blue: backscatter intensity change between 24 and 27 November). Water (blue), forest (green), sparse vegetation (orange/yellow), and urban areas (yellow/green), as well as certain farming activities (green/blue) and frost (magenta) can be identified. (Source: RSL, Zurich, Switzerland).

5. Temperate Crops

5.1 Classification of Arable Crops

UK example

Examination of backscatter time series (§ 3.3, UK sites) reveals that there are critical periods or windows in the crop calendar, in which certain crops can be separated on the basis of their backscatter profiles. By selecting different date images and combining them as colour composites, one is able to show this discrimination over an agricultural area. Research studies carried out in the UK have shown that images acquired from late May to late July can be used to discriminate wheat, barley, oilseed rape, sugar beet and grass.

Figure 5.1 shows a multi-date colour composite of ERS-1 images acquired in late May and June 1993. This colour combination has been chosen to highlight discrimination of winter wheat and oilseed rape. In this composite, winter wheat fields have the darkest signatures in contrast to oilseed rape fields which have the brightest signatures. This is because wheat backscatter is at a minimum, and rape backscatter is at a maximum for all three dates (compare also the temporal profiles in § 3.3). Two large winter barley fields in the top right hand of the composite have purple signatures, others show some purple colour. This is because winter barley backscatter has increased on the 13 and 29 June relative to wheat fields, which have low backscatter on all three dates. Other crops exhibit similar signatures at this time, because these fields contain bare soil undergoing management operations for the establishment of root crops (sugar beet and potatoes) and peas. Colour composites such as that described reveal that across the UK test sites:

- winter wheat has the darkest signatures because of low backscatter during this time period, and can be easily discriminated from all other crops;
- oil seed rape has the brightest signatures associated with very high backscatter in this period, and is therefore well discriminated from all other agricultural crops;
- winter and spring barley have purple signatures associated with increases in backscatter due to relatively early crop senescence;
- root crops have different colour signatures compared to rape and cereals, which is associated with bare soil conditions early in the crop growing season.

In the UK study, backscatter response for fields is represented by the field averages calculated by integration with digital field boundary information held in a GIS. Therefore the use of mean field backscatter for crop classification is investigated. Using mean backscatter on critical dates and differences in backscatter between dates, threshold values are explored as a way of classifying crops using discriminant analysis within the GIS database.

The 1993 UK database includes the cropping information for a total of 783 fields spread across 4 test sites. This dataset was divided into two, after assigning a random number to each field and sorting the database on that number. Backscatter differences were taken from 11 April to 29 June, and from 29 June to 3 August. One half of the dataset was used to generate training statistics for thresholds. The rest of the data were used to test the thresholds for crop classification.

Patterns of change were found to be unique for oilseed rape, compared to other agricultural crops. The April/June backscatter difference shows a negative change compared to other crops, whilst the June/August difference is positive. This was used to threshold fields not included in the training set. A threshold for backscatter on a single date (13 June) was also included in the classification. Oilseed rape fields can be discriminated with 100% accuracy using such a classification strategy.

The use of the methodology for classifying winter wheat was then investigated. Again, backscatter differences and single date backscatter thresholds were applied to the data not included in the training data. The backscatter difference thresholds were obtained from the training set. It was found that very high orders of classification accuracy could be obtained by using backscatter on two dates instead of one. The two dates corresponded with the period of minimum wheat backscatter (late May and late June). Table 5.1 shows the breakdown in classification performance by test site, with accuracy being at least 90% in all three cases. This change detection thresholding approach is seen to have considerable potential for classifying crops using multi-temporal ERS-1 SAR data.

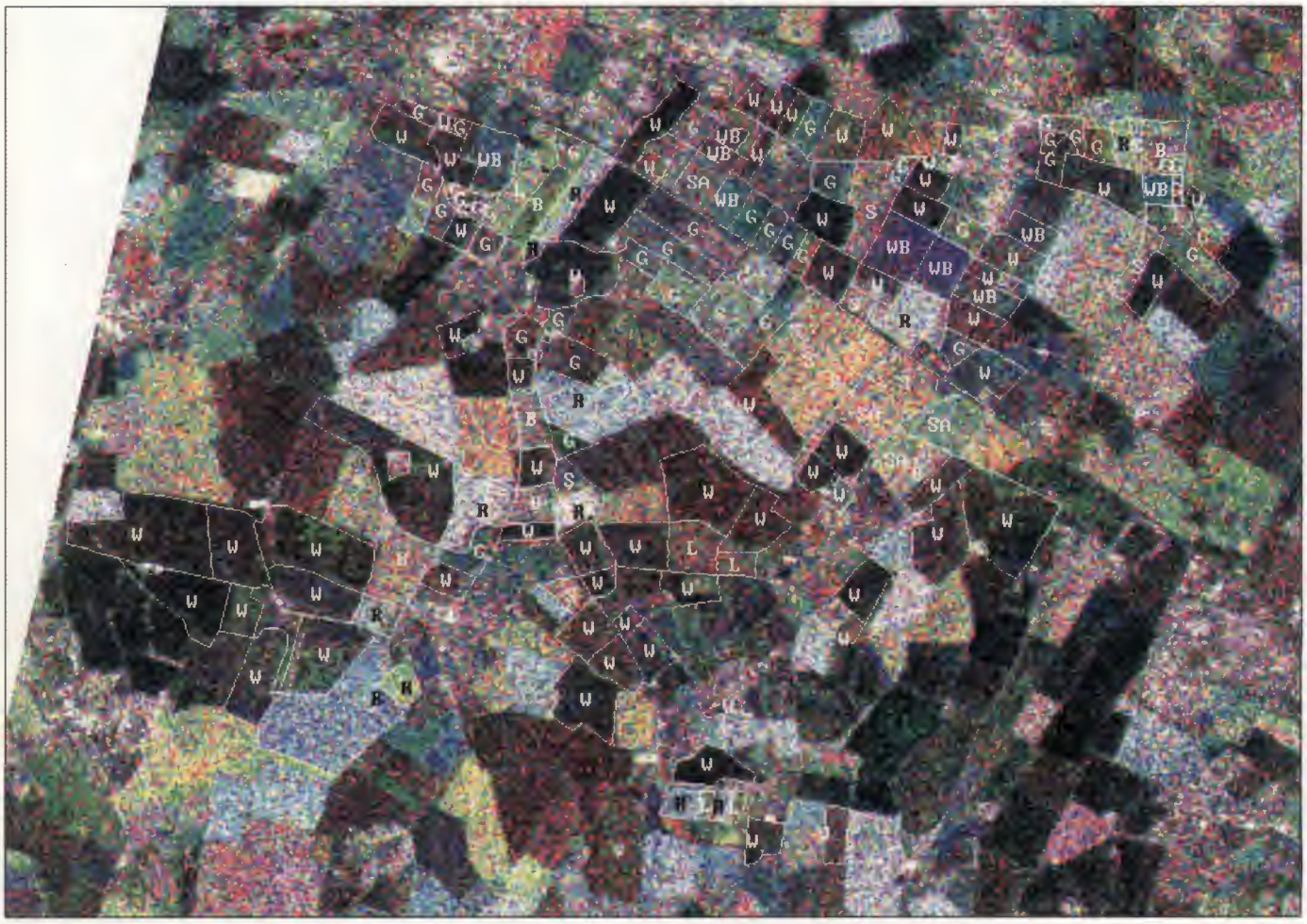

Figure 5.1. ERS-1 multitemporal composite, Boxworth UK (red: 25 May, green: 13 June, blue: 29 June 1993). Field boundaries and cropping are superimposed. W: wheat; R: oilseed rape; L: linseed; G: grass. (Source: Zmuda et al. 1994).

Table 5.1 Classification accuracy assessment for wheat by site, UK (Source: Zmuda et al. 1994*)*

Site	No. Classified	Total No.	% Correct	Omission	Commission	Fields Commissioned
Boxworth	38	40	95	2	7	grass (7)
Terrington	40	41	97.5	1	2	linseed (1) potatoes (1)
Feltwell	61	69	90	8	4	grass (2) oats (1) spring barley (1)

Classifications for winter barley using the threshold approach have been attempted. However, initial results indicate that barley is confused with other crops. Therefore the use of multivariate statistical analysis may be more appropriate for separating the cereals. The use of backscatter profile models and first and second order turning moments is under investigation for the UK data.

German examples

Three ERS-1 SAR images have been used together with airborne E-SAR images of the Lechfeld testsite, located 70 km west of Munich, *Schmullius et al. (1994). Figure 5.2* is a multitemporal colour composite of the three ERS-1 images acquired in June and July 1992. The colours indicate the radar backscatter variations over time. The brightest fields on the multitemporal image are sugar beet fields. This crop had the highest backscatter throughout the six-week period. The darkest fields are cereals. Colour variations are indicative of crops undergoing significant changes in backscatter between 1 June and 6 July.

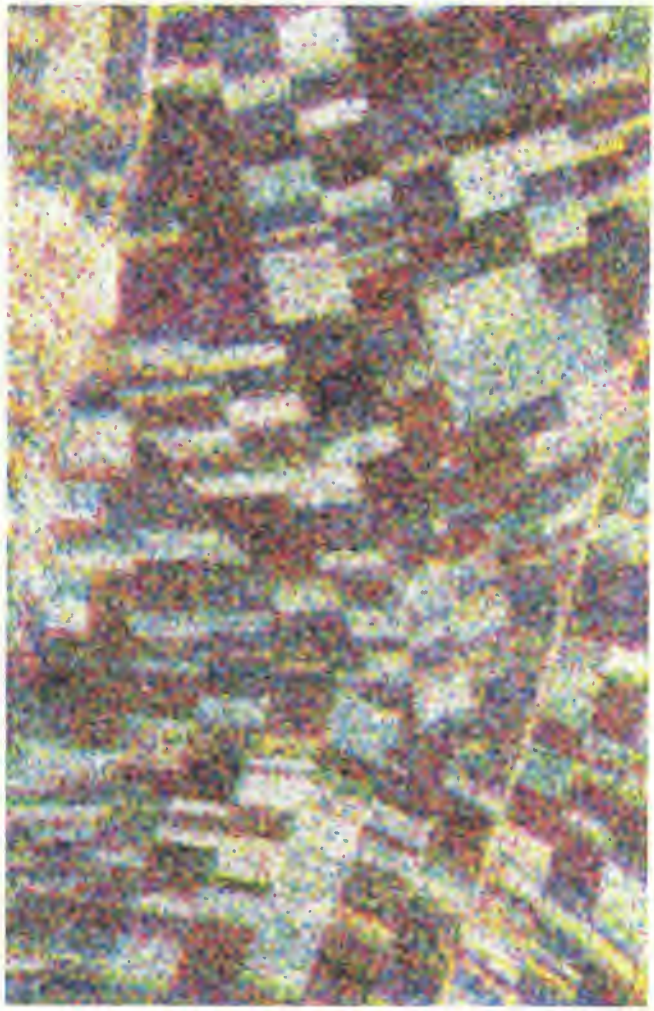

Figure 5.2. ERS-1 multitemporal composite, Lechfeld Germany, 1992 (red: 1 June, green: 20 June, blue: 6 July). (Source: C. Schmullius, DLR).

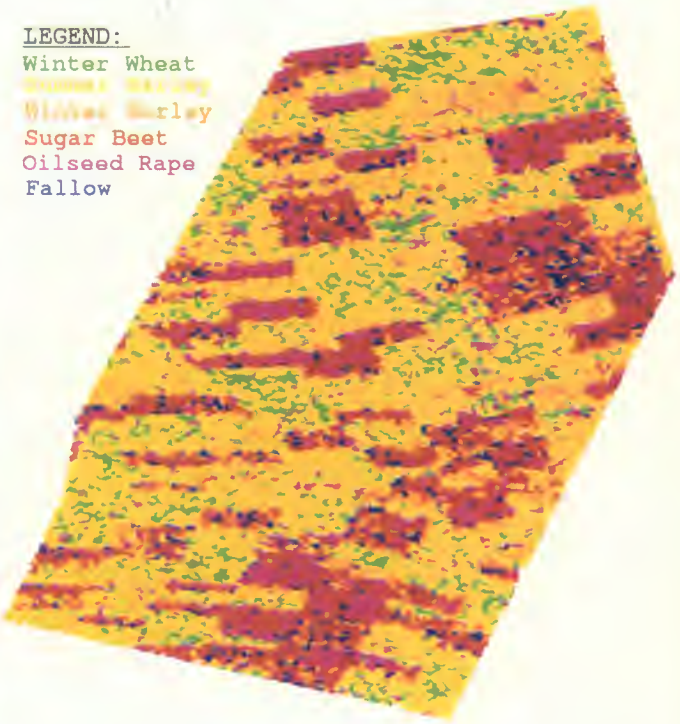

Figure 5.3. Pixel-based ERS-1 maximum likelihood classification of Lechfeld, Germany (Source: C. Schmullius, DLR).

The use of a Maximum Likelihood Classifier was investigated. *Figure 5.3* shows the resulting classification for six crop classes (winter wheat, summer barley, winter barley, sugar beet, oilseed rape and fallow). The confusion matrix of the training site pixels which were correctly classified, was calculated after a 5 × 5 median filter and a sieving window were applied to the classified image to reduce the effect of speckle. In this case the average (unweighted) overall classification accuracy is only 57%. However, there is little doubt that this could be improved significantly by better choice of imaging dates and by using segmentation techniques.

Table 5.2 illustrates the misclassification (due to statistical ambiguity of the covariance matrix) between fallow, sugar beet, cereals and oilseed rape. These results from the German test site are in accord with the UK findings presented above; in that cereals are easily discriminated from high biomass crops such as oilseed rape and sugar beet, as shown here. A better separation of grain crops or between rape and sugar beet might be possible with more multitemporal information. For large area applications, such as mesoscale climate models, a

Table 5.2 Confusion matrix (percent of training site pixels) in percent. Lechfeld testsite, Germany (Source: C. Schmullius, DLR)

Class	Fallow	S. Barley	W. Barley	W. Wheat	Sugar beet	Oilseed Rape
Fallow	40.1	1.1	16.1	0	37.9	4.8
S. Barley	0.4	75.5	5.4	14.6	1.4	2.5
W. Barley	0	27.6	58.6	0	7.3	6.9
W. Wheat	1.1	56	3.5	32.2	2.4	4.8
Sugar beet	8.9	1.2	9.2	0	66	14.7
Oilseed R.	1.9	1	0	0	25.3	71.7

mere separation into only three classes (cereal, large leaf canopies and fallow/grassland) could be feasible in terms of biomass estimation for evaporation calculations. In this case, a 3-class confusion table would show the following values along its diagonal: fallow 40%, cereals, 91%, and large leaf canopies 83%. The average accuracy then reaches 71%.

Dutch example

ERS-1 SAR images acquired from the beginning of May until the end of October 1992 have been used to map agricultural crops for the Flevoland test site in The Netherlands. *Figure 5.4a* is a multitemporal colour composite of the test site with field boundaries derived from a SPOT multispectral image. *Figure 5.4b* shows the ground reference data for each field, and *Figures 5.4c & d* the crop classification results, obtained using pixel-based and field-based approaches, respectively. A visual inspection of these classification results in conjuction with the ground data map shows that crops like grassland and winter wheat are accurately classified, but the sugar beets are mixed with the potato crop.

Schotten et al. (1995) have studied the effect of the number of images used in a field-based crop classification of Flevoland (Table 5.3). In general, classification performance improves with the number of images used. With one image, only a restricted number of crops could be classified with reasonable accuracy. With an optimal data set of eight images (selected using separability indices) good results were obtained for several crops. For several crops the accuracy is over 90%. Overall classification accuracy was 80% expressed as a percentage of the total number of fields, or 88% expressed as percentage of the total area (in hectares).

Figure 5.4. ERS-1 SAR imagery and crop classification results using field-based and pixel-based approaches, Zuid Flevoland, 1992. Source: G. Nieuwenhuis, Staring Centre.
(a) ERS-1 multitemporal colour composite (red: 7 June, green: 12 July, blue: 16 August).

(c) Field-based multitemporal classification (8 dates)

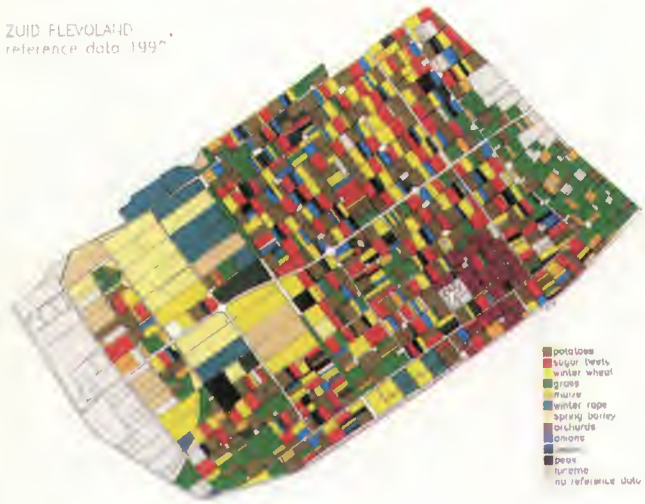

(b) Reference data

(d) Pixel-based multitemporal classification (10 dates) 5x5 majority filtered.

Table 5.3 Crop classification accuracy using multitemporal ERS-1 SAR imagery (set A: 1 date; set B: 3 dates; set C: 5 dates; set D: 8 dates). Accuracy is percentage of the total number of fields. Training statistics for this classification are based on a random selection of 25 fields per crop type (Source: Schotten et al. 1995*).*

	Crop Type												
Image set	Pots	S. Beet	W. Wheat	Grass	Maize	Rape	S. Barley	Fr. trees	Onions	Beans	Peas	Lucerne	Overall
A	92	0	37	0	0	92	87	76	60	0	38	0	37
B	91	27	81	57	44	92	87	76	59	58	42	67	64
C	65	44	86	73	50	100	91	74	68	68	63	75	73
D	88	70	85	85	62	100	91	88	64	74	81	100	80

Taking into account the large number of crops this is an encouraging result. Only for maize are the results very disappointing.

5.2 Early Estimates

For agricultural applications there is a need to provide information at the earliest possible stage in the growing season. For agricultural control applications it is important to distinguish crops early, so that fieldchecks can be performed before harvest. The main objective of the MARS project is to provide early estimates of crop production for economical planning purposes.

The systems presently being used for both agricultural control and crop production forecasting, rely on crop types and areas being derived from time series of optical imagery. For instance, the optimum requirement for classifying a full range of arable crops in northern/central Europe is a time series of three optical images including an optical image taken in early/mid July. Besides potential acquisition problems related to persistent cloudy weather conditions, the fact that an image taken relatively late in the growing season is needed for accurate classification of some crops is a limitation. The potential role of ERS-1 in providing early estimates is therefore a topic of some interest.

Part of the Dutch crop classification study reported above in § 5.1 has specifically addressed the issue of early detection of crops. Crop classification has been carried out starting with just the first ERS-1 image dated 12 May 1992, and then progressively adding images one by one as they are acquired through the crop growing season (Table 5.4). Early classification results are best for cereal crops; with just two images taken by the end of May, both winter wheat and spring barley have classification accuracies of around 80%. By mid-June results for potatoes and winter rape are also around 80%. Classification accuracies for crops such as onions, beans, peas and lucerne improve significantly when images taken from August are included in the analysis.

Examples presented above *(Figures 5.1 and 5.3)*, have shown that a multitemporal composite of ERS-1 images acquired before the end of June provide good discrimination of cereals, oilseed rape and grass fields.

Monitoring autumn cultivations

One approach being investigated to improve early season crop classification, involves ERS-1 monitoring of land cultivation practices in the autumn and winter months (*Lemoine & De Groof, 1994*). Different crops often require different field preparations, and as the ERS SAR is sensitive to the soil surface roughness and moisture content, it may be possible to identify tillage classes relating to particular crops. If tillage classes can be classified and mapped, this could provide very early determination of some crop types.

The ERS-1 backcattering coefficient of bare soil is known to be sensitive to soil moisture variation and changes in surface roughness. Many research efforts have been directed to the determination of soil moisture, while the backscattering variation due to surface roughness has often been treated as an undesired disturbance. For agricultural mapping and monitoring purposes, though, valuable information is contained in surface roughness parameters. Especially in the period between the crop seasons, the surface roughness state reflects the on-going tillage preparations, which can directly be linked with previous and subsequent cropping practices. Backscattering models can be used in combination with a priori knowledge on various ancillary resources, such as meteorological recordings, soil data and crop rotation practices, in a contextual classification scheme to detect tillage sequences and relate these to future crop types.

Table 5.4 Crop classification accuracy (%) using increasing numbers of ERS-1 images (Source: Groot et al., 1994*)*

No. images	Last Date	Potatoes	S Beet	W. Wheat	Grass	Maize	W Rape	S. Barley	F. Trees	Onions	Beans	Peas	Lucerne	Overall
1	12 May	4	5	58	6	17	38	78	17	29	0	4	0	19
2	31 May	45	7	80	42	33	69	87	60	44	4	10	58	42
3	7 June	60	26	77	45	31	77	91	60	46	23	23	75	50
4	16 June	91	29	81	57	56	100	91	69	45	53	40	75	63
5	5 July	89	42	83	65	56	100	96	71	48	72	54	92	69
6	12 July	90	50	86	74	56	92	96	74	52	70	67	92	73
7	9 Aug.	89	53	87	77	65	92	96	76	61	81	79	100	77
8	16 Aug.	88	67	85	80	67	92	87	74	75	85	85	100	80

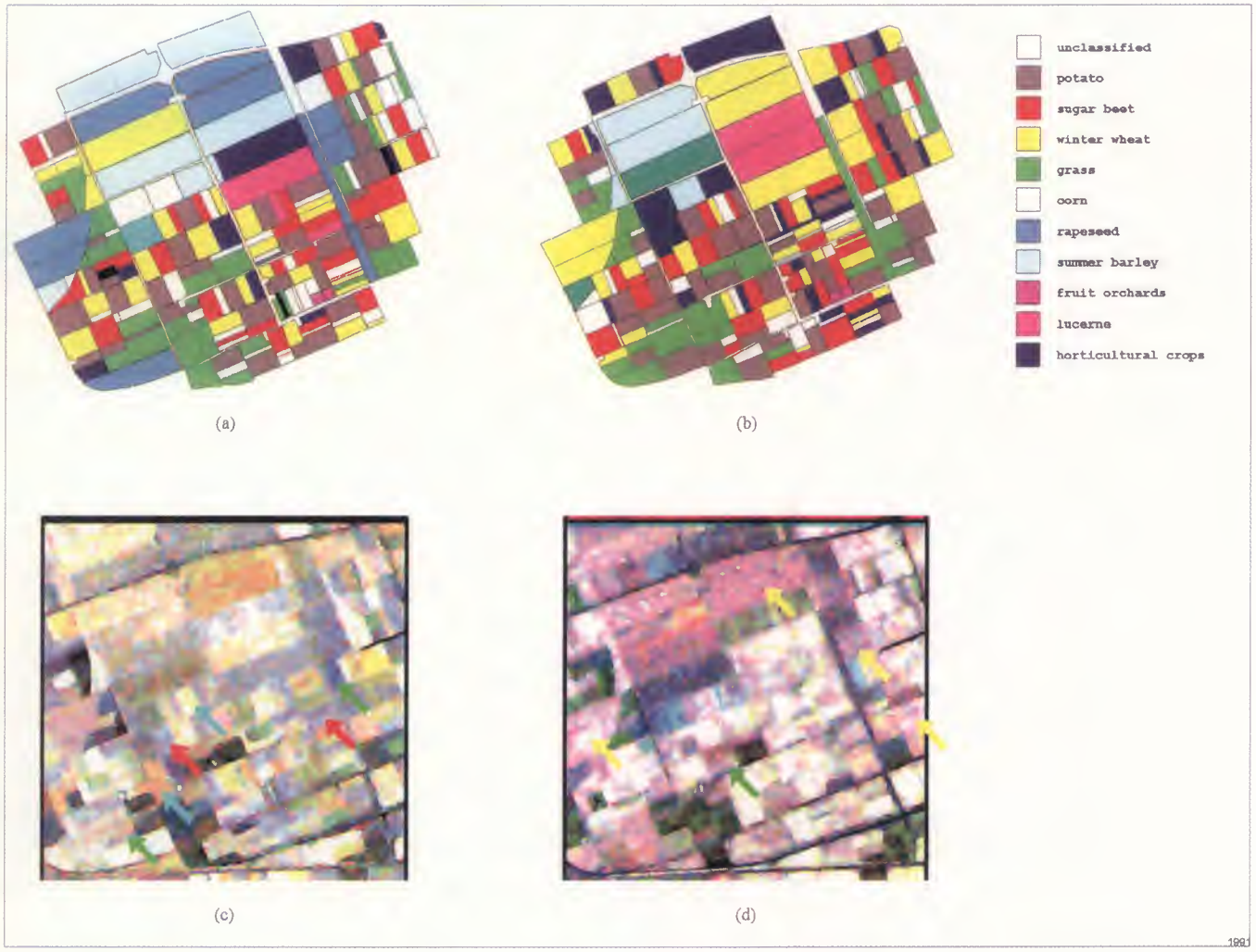

*Figure 5.5. Crop maps of the 1991 (a) and 1992 (b) growing seasons for the test area in the Dutch Flevoland polder. The RGB composite in (c) shows the filtered ERS-1 PRI images for the dates 19, 25 and 31 October 1991, the one in (d) that for the dates 24, 30 November and 6 December 1991. Colour variation reflects harvesting and tillage activities. (*Source: G. Lemoine, Synoptics*).*

This methodology has been tested on a multitemporal ERS-1 PRI series of the Dutch Flevoland polder acquired in the autumn of 1991 (19 October – 6 December). A total of seven images were available. *Figure 5.5* shows colour composites of two multi-date combinations, together with the crop maps of the area for 1991 and

1992 (i.e. the previous and subsequent growing seasons). The first colour composite, for the dates 19, 25 and 31 October, clearly shows variation that is related to harvesting (sugar beet: red arrows) and tillage (breaking up of grass fields: green arrows; ploughing of former potato fields: blue arrows). Note that the colour combinations do not only reflect the sequence of various tillages, but also its approximate timing. In the second composite (24, 30 Nov. and 6 Dec.), there is much less variation in colour. This is due to the fact that most fields are already in their winter condition (mostly ploughed: the light coloured fields), and also that the preceding period was very wet, so that little tillage was applied. Fields with winter cereals can already be identified at this stage, due to their typical, moderately rough, seedbed structure, and corresponding lower backscattering signatures after preparation (yellow arrows). With the use of a selection of all dates, the delineation of various conditions can be further refined (for instance, group potato fields by row direction, determine the timing of sugar beet harvesting, etc.).

Lemoine & De Groof are currently working on methodological aspects within the framework of the JRC's MARS Action IV Agricultural Monitoring programme. This work includes pre-operational testing and validation for the Great Driffield (UK) sampling site, for which a complete dataset, including ground observations on tillage types and cropping practices has been assembled. The aim of the work is to develop a complementary approach to the ongoing Action IV monitoring activities based on optical datasets.

5.3 Integrated Use of ERS-1 and Optical Imagery

Crop classification

Kohl et al. (1993) showed in a study that the combination of ERS-1 and SPOT imagery improved the classification accuracy of agricultural crops significantly, if compared to a single SPOT-XS scene. *Kohl et al. (1994)*, combined two ERS-1 SAR images with one SPOT image for land-use mapping of the Olsztyn (Poland) area. Results showed a better discrimination between built-up areas and natural vegetated surfaces, than was possible with a single SPOT image. *Schotten et al. (1993)*, carried out crop classifications of the Zuid Flevoland test site with one SPOT and one TM image, and with a set of eight ERS-1 images, and demonstrated that potatoes, winter wheat and grass could be classified more accurately using multitemporal ERS-1 data.

The PASTA project (Pilot Porject for the Application of SAR Techniques to Agricultural Statistics and Inspection of Land Use in Baden-Württemberg, Germany), is a practical example of the combined use of ERS-1 and optical imagery to provide reliable agricultural statistics on a year-by-year basis for the main crop types. During 1993, more than 560 test fields were analysed containing six crop types (winter wheat, winter barley, summer barley, oats, rape and corn). Six ERS-1 and three multispectral SPOT scenes were acquired during the main part of the growing season. The ERS-1 scenes were geocoded to remove the effects of terrain distortion, so allowing the ERS-1 and optical imagery to be combined. *Figure 5.6a* shows a combination of multitemporal ERS-1 imagery with a SPOT panchromatic image. The IHS transform is seen to improve the spatial information content as the inclusion of the optical image clearly improves the definition of field boundaries. Colours within the IHS composite are essentially derived from the ERS data.

The classification potential of the combined ERS-1 and optical dataset has been compared to that of optical data alone. After integration of the data into a GIS, classification was performed using training samples provided by the GIS. Using one SPOT scene, crops could be classified with 66% accuracy. However, classification performance increased by 8% when the optical image was combined with three geocoded ERS-1 scenes.

Monitoring grassland

A combined approach using ERS-1 SAR and Landsat TM images, has been used for a landcover classification and grassland monitoring study in Bavaria (*Schadt et al. 1994*). Often, the separation of grassland from cereal crops can be difficult using Landsat TM or SPOT images during the main part of the crop growing season, and crop classification accuracy depends strongly on the ability to separate grassland from other crops. Analysis of grassland on multitemporal ERS-1 SAR images has shown that grassland has a very similar backscatter across the year, although it is possible to separate managed grassland from degenerated grassland with bushes, on the basis of the second type having slightly higher backscatter. Using the temporal consistency, ERS-1 images can be used easily in a first stage to separate grassland from other land cover types. Landsat TM images have then been used in a second stage to classify the other crops. *Figure 5.7* shows the final classification, together with a ground truth map of the area. Classification accuracy for the two grassland classes is better than 90%.

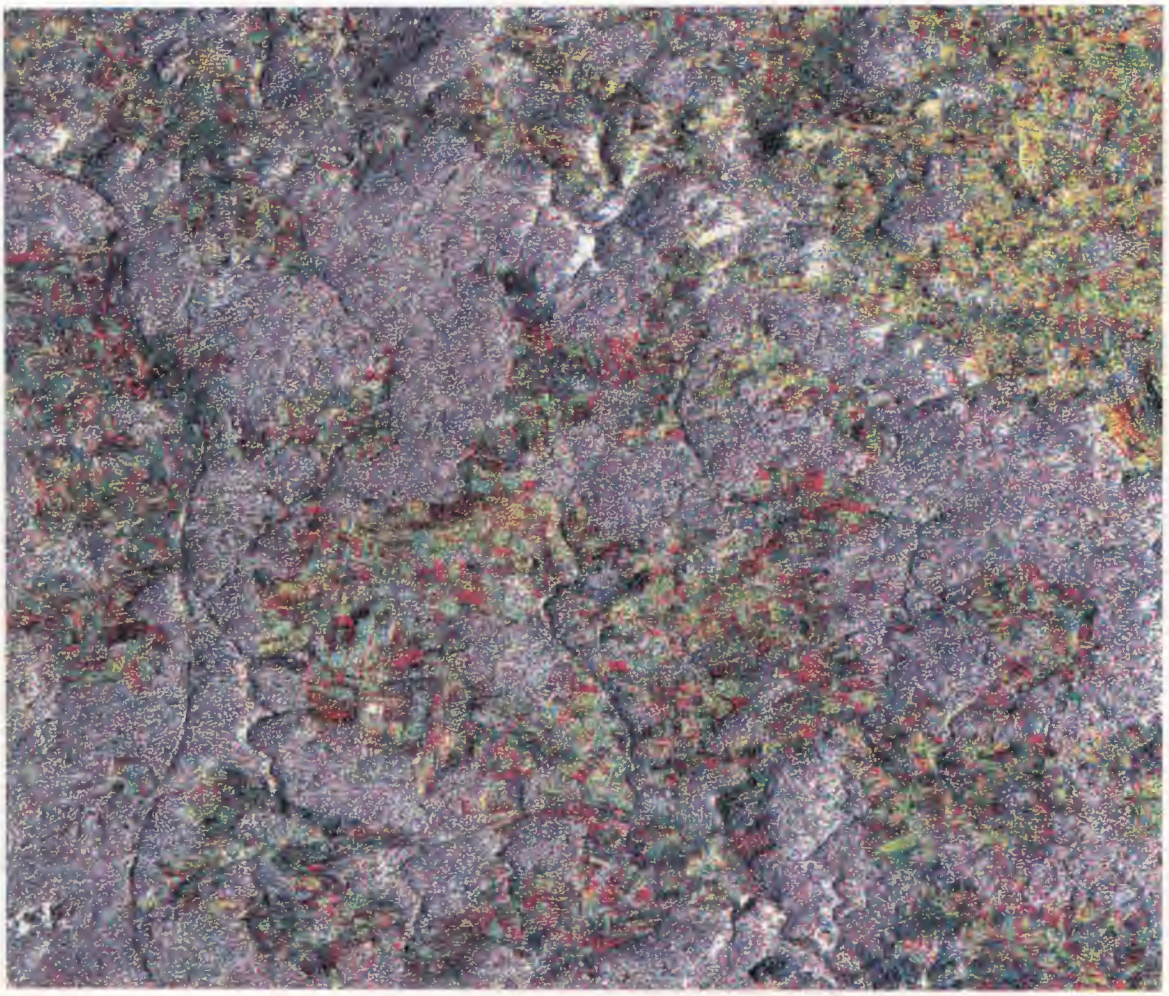

Figure 5.6a. ERS-1 multitemporal colour composite, Baden-Württemberg test site, Germany, 1993. Red: 20 May, green: 24 June, blue: 29 September. (Source: Hartl & Klaedtke 1994).

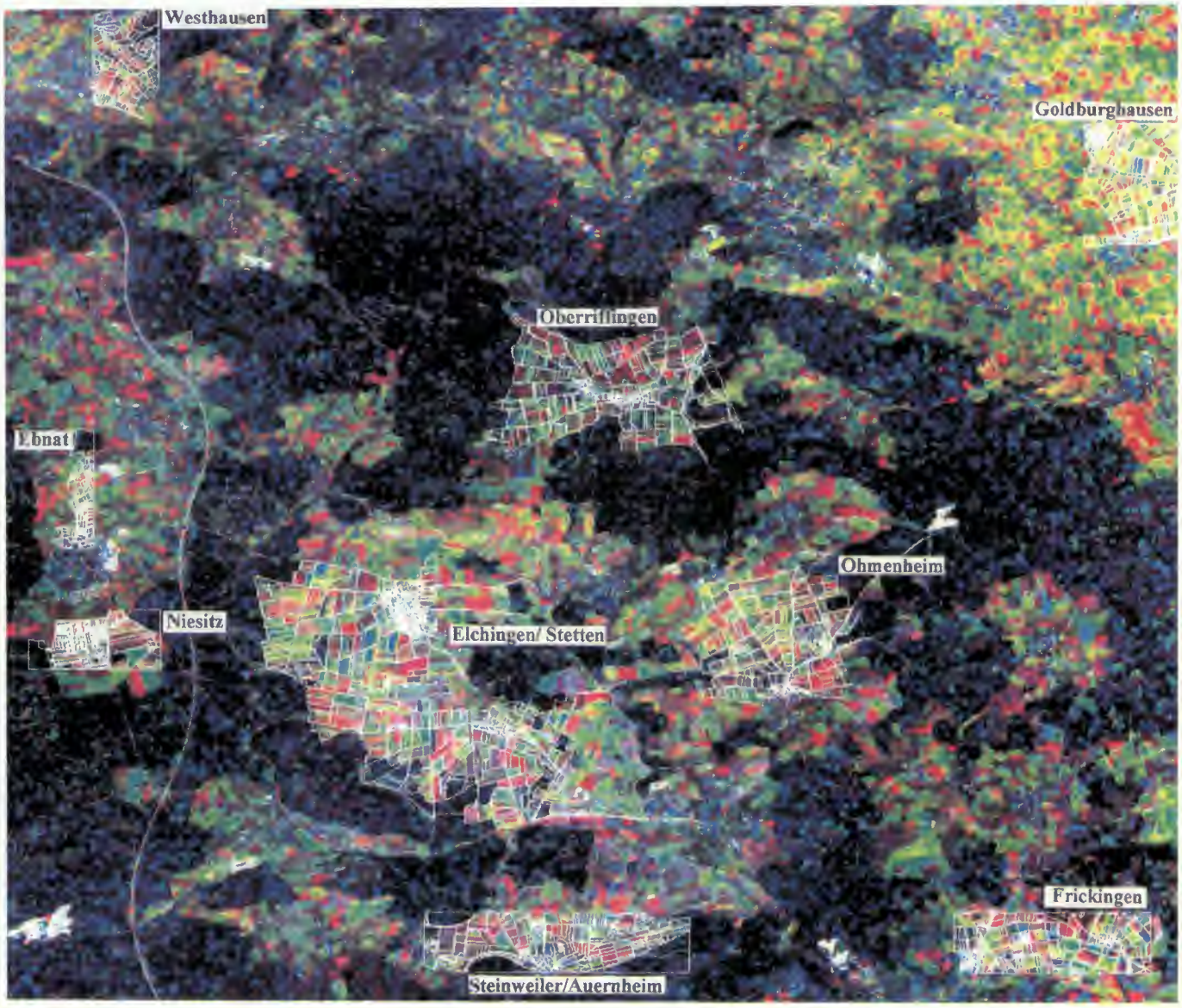

Figure 5.6b. IHS colour composite produced by combining ERS-1 imagery acquired on 20 May, 24 June and 29 July 1993 with a panchromatic image acquired on 1 April 1993, Baden-Württemberg test site. (Source: Hartl & Klaedtke 1994).

The Result of a Combined Landuse Classification of Multitemporal ERS-1 SLC Data of the Year 1992 and a LANDSAT TM Image of May,28th 1992 in Comparison to the Digital Ground Truth Map

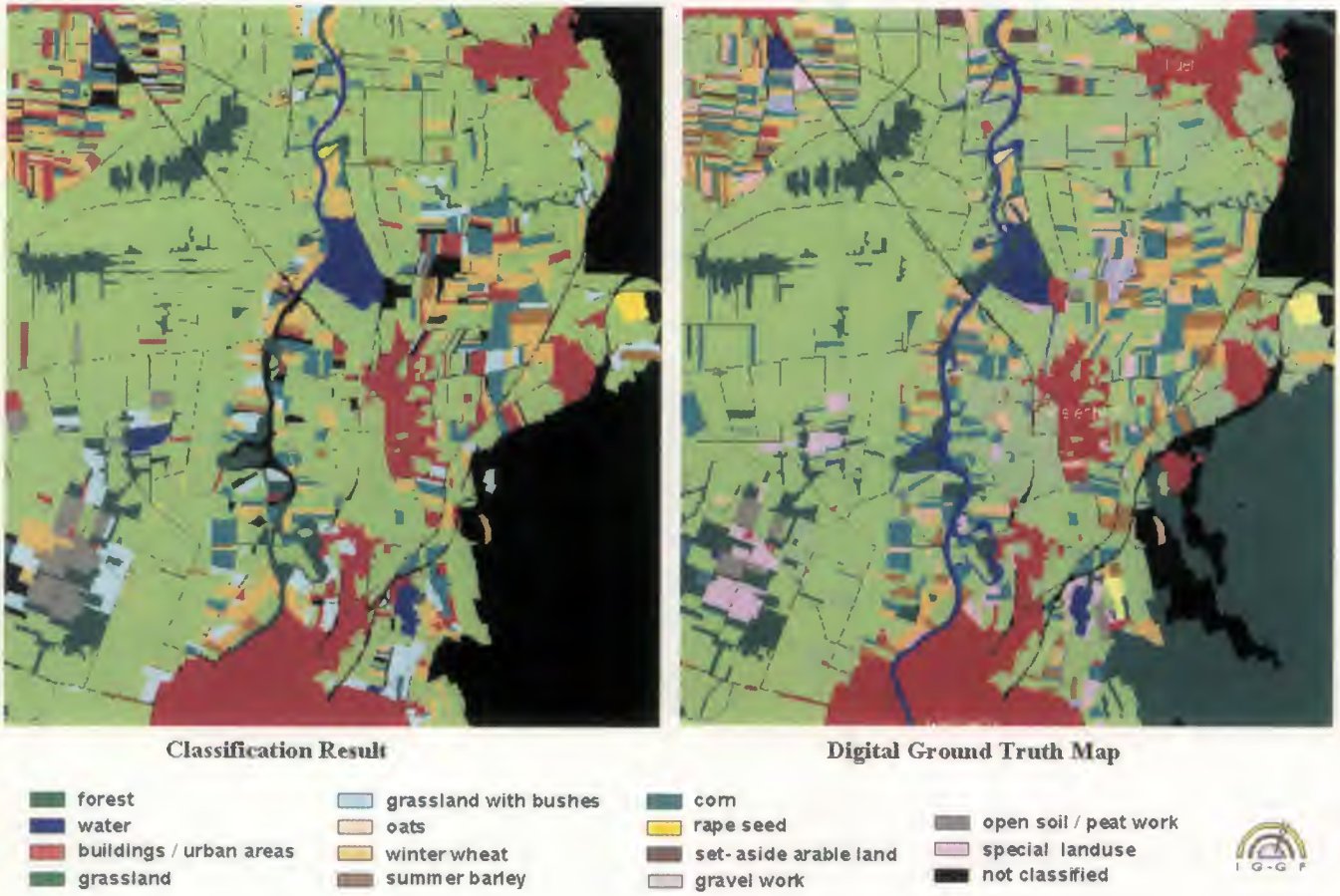

Figure 5.7. The result of a combined landuse classification using multitemporal ERS-1 SLC imagery and a Landsat-TM image 1992. The digital ground truth map is shown for comparison.

6. Tropical Crops

6.1 Rice

6.1.1 General

Socio-economic importance of rice
Rice is the prime source of daily food for those two thirds of the world's population living in Asia. Table 6.1 shows the major rice producing countries, including selected European countries. For some countries rice export is an important source of income. Thailand, for example, exports about one third of its annual production, which makes it the main supplier on the world rice market. The production of rice contributes to social and political stability within the country. Consequently, decision makers have placed the collection of information about the actual and predicted state of rice crops on the top of their political agendas.

The most interesting parameters to know are rice acreage and potential yield. Currently, the collection of this information is mostly based on interviews of the farmers or village level. The information gathering process is cumbersome, and sometimes unreliable information is given to Government authorities by the local farmers. An objective method of data collection – such as based on the use of satellite imagery – is therefore of high interest for the national authorities dealing with agricultural economics and planning. Since rice grows mostly in tropical countries, permanent cloud coverage during the growth period – which naturally coincides with the rainy season – is a major drawback for the use of optical satellite imagery. As an alternative, the use of radar remote sensing was demonstrated to be an excellent means for repetitive collection of information related to rice acreage and, even one step further, parameters related to rice yield (*Aschbacher et al., 1995a*).

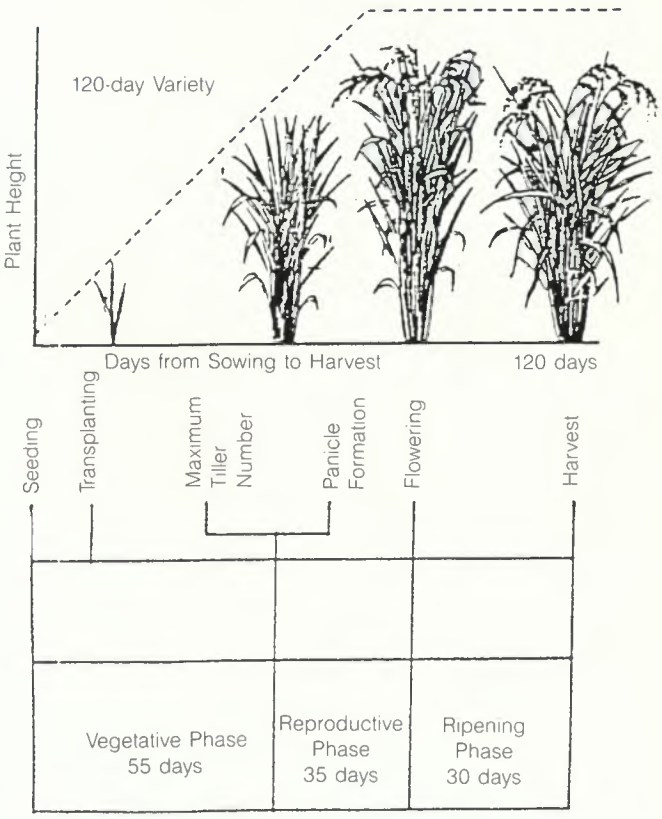

Figure 6.1. Phenological stages of rice plant growth for a typical period of 120 days.

Table 6.1 Rice production of the leading rice producing countries and selected European countries (numbers in 1000s of metric tons; source: Electromap Inc., 1989-93*).*

Country (Top 12)	Rice production (×1000 t)	Country (Top 12)	Rice production (×1000 t)	Country (Europe)	Rice production (×1000 t)
1. China	187,450	7. Myanmar	13,201	Italy	1,236
2. India	110,945	8. Japan	12,005	Spain	582
3. Indonesia	44,321	9. Brazil	9,503	Portugal	153
4. Bangladesh	28,575	10. Philippines	9,670	Greece	127
5. Thailand	20,040	11. S-Korea	7,478	France	109
6. Vietnam	19,428	12. USA	7,006	Hungary	38

Phenological stages of rice plant growth
A typical rice growth cycle lasts between 120-180 days from planting to harvest, depending on crop variety. There are three major plant growth phases: the vegetative, reproductive and ripening phase. After soil preparation rice fields are flooded. The *vegetative phase* starts either with direct sowing or transplanting of nursery plants. During this phase young plants emerge from the water surface.

During the *reproductive* phase, plants continue to grow until they reach a maximum height of about one metre. During the *ripening phase*, the grains develop. Water is normally drained out and the plants become drier and turn yellow. The *reproductive* and *ripening phases* are constant for most varieties and last about 35 and 30 days, respectively. The length of the *vegetative phase* differs with variety. After harvest a bare soil condition remains, sometimes with patches of standing water left. A typical phenological development of the rice plant during its growth cycle is shown in *Figure 6.1*.

There are glutinous and non-glutinous, photo sensitive and non-photo sensitive, as well as resistant and less resistant crop varieties. In recent years short-cycled varieties are favoured, which allow an increased production through more frequent harvests. In intensive rice producing areas such as in Thailand the typical growth cycle lasts 120 days. Crop yield depends on crop variety and water availability. A typical crop yield for a well irrigated field is approx. 5 tons/ha. The availability of water during the early growth stage is crucial, which has led to the development of sophisticated irrigation networks in most of the intense rice growing areas (*Aschbacher & Paudyal, 1993*).

Radar remote sensing studies for rice crop mapping and monitoring
From an agro-economic point of view there are two main parameters of interest, namely (i) rice acreage, and (ii) rice yield. Rice production of a given area can be obtained as the product of acreage and yield (per unit area). As will be shown later in this Chapter, it is easier to retrieve acreage from radar imagery than yield.

The investigations of ERS-1 SAR data for rice monitoring include studies carried out in Thailand (*Aschbacher & Paudyal, 1993*; *Paudyal, 1994*), in Indonesia (*Aschbacher et al., 1995*; *Harms, 1993*), in Spain (*Kohl et al., 1993*) and in Japan (*Kurosu et al., 1993*). Earlier studies carried out before the launch of ERS-1 are from *Le Toan (1989)* based on X-band scatterometer measurements, and *Aschbacher & Lichtenegger (1990)* based on SIR-A L-band data.

The Thailand and Indonesia studies are described in detail in this Chapter, while the studies carried out in Spain and Japan are also included for comparison with those of the tropical countries.

Multitemporal radar backscattering signatures
With reference to § 3.3, the radar backscattering coefficient σ^0 [dB] of rice fields undergoes a very characteristic temporal signature during the growing season. Compared to other agricultural crops, the temporal signature of rice fields is probably the most significant one showing the largest changes in radar backscattering values during the growing period. This is caused by the changing influence of macroscopic radar backscattering interactions between standing water and plant canopy. A schematic temporal backscattering profile has previously been shown (§ 3.3.), and real values as observed with ERS-1 SAR data are shown in § 6.1.2 and 6.1.4, respectively.

6.1.2 Case studies in Thailand
Some of the most detailed case studies on the use of ERS-1 SAR data were carried out in Thailand (*Paudyal, 1994*; *Aschbacher et al., 1994, 1995a*). Two main study areas were used, both of which are located east of the town of Kanchanaburi, Thailand. Although both areas are only about 30 km apart the characteristics of the rice fields are quite different. The northern area shows slightly undulating terrain, with small individual rice fields and a heterogeneous growing pattern between neighbouring fields, The southern study area is flat with large individual fields and a generally homogeneous growing pattern. In both areas a well developed irrigation network provides sufficient water for rice growth. The southern site is part of the EC-ASEAN ERS-1 project, described in *Aschbacher (1992)*.

For both studies, multitemporal ERS-1 SAR data were available from nine acquisition dates, namely 22 Nov 91, 7 Oct 92, 11 Nov 92, 24 Feb 93, 7 May 93, 11 Jun 93, 20 Aug 93, 29 Oct 93 and 3 Dec 93. The 1991/92 dates are mostly used for the northern study area, while all dates are used for the southern study area.

Detailed ground measurements were carried out for both study areas. During the rice growth period (June – December 1993), the ground measurements described in Table 6.2 were taken in parallel with ERS-1 acquisitions. Ten different sample areas were selected for detailed investigations, each of them approximately 1 – 2 hectares in size.

Table 6.2 Ground measurements taken in parallel with ERS-1 SAR data acquisitions during June-December 1993 at the southern study area in Kanchanaburi, Thailand (Aschbacher et al, 1995).

Parameter	Details	Method
Location	deg lat/long	GPS and topographic map
Site photograph	state & geometry of rice plants and surface	square grid behind plant
General information	Site acreage, planting method (seeding/transplanting), variety name, date of planting, date of harvest, yield, irrigation (rainfed/irrigated)	measurements and farmer interviews
Weather at acquisition time	wind (heavy/medium/light/no), plant orientation (vertical/bended-in which direction), rainfall (heavy/light/no), surface & plant condition	measured, visual inspection
State of plant growth	soil preparation/vegetative stage/tillering/booting/flowering/panicle/harvesting stage	visual inspection
Plant parameters	plant density, plant height, plant moisture content (weight before & after drying), no. of leaves, leaf width, leaf length, stalk diameter	measured, average of 10 samples within 50 x 50 cm frame
Field information	height of standing water, general state of surface, general state of plants, etc.	measurements, visual inspection

Estimate of rice acreage

Rice acreage can be retrieved from multitemporal radar imagery, making use of the characteristic backscattering signature of rice fields. The temporal σ^0 [dB] profile of rice is unique, and thus quite easily distinguishable from that of other crops. The fact that rice fields are flooded during a certain period of time creates a clear signature, namely that of a water surface during the early growth period. Later, when plants are increasing in height, backscatter increases to values which are typically higher than those of other agricultural crops. The large dynamic range of σ^0 [dB] between the early (flooded) and late (pre-harvest) growing period is an important factor for rice mapping. It is, however, crucial to select optimum dates within this cycle. These are during the early growing period when the surface is flooded, during the flowering phase and shortly before harvest. This corresponds to the minimum (approx. −16 dB), maximum (approx. −8 dB) and (slightly decreased) pre-harvest values of σ^0.

The growing cycle for the main rice harvest in the Kanchanaburi study area lasts from August to December, and for a secondary harvest from April to July. A three-date multitemporal image combination is displayed in *Figure 6.2*, in which rice fields (in green/bluish colours) can easily be discriminated by visual interpretation from other land-use categories. A digital classification was carried out based on four acquisition dates in order to produce a 'rice map'. All images were co-registered and Gamma MAP filtered (*Nezry et al., 1995*) before a simple clustering algorithm was applied.

The result is shown in *Figure 6.3* for the three classes: 'rice fields', 'non-rice fields', and 'water'. This clearly indicates that the rice growing area is generally well classified. There is, however, some confusion with water areas and the backslopes of mountains. Both effects can be removed if GIS-type information is included in the final classification process (*Aschbacher et al., 1995a*).

Rice growth parameters

The ultimate goal in the use of radar imagery for rice studies is to retrieve yield figures from satellite imagery. Currently, there are only two studies known which point in this direction, one carried out in Japan (*Kurosu et al., 1993*) and one in Thailand (*Aschbacher et al., 1995a*). Both aim at yield-related parameters such as plant height rather than yield itself. An example from the Thai studies is shown in *Figure 6.4*, where measured plant height is compared with radar backscattering values. Because the timing of rice planting is almost identical for different years, two more dates from previous years have been included, namely 22 Nov 91 and 7 Oct 92, in order to complement some of the missing acquisitions during the 1993 growth cycle or the 'wind-disturbed' image of 20 Aug 93. As can be seen from *Figure 6.4a* there is a clear increase of radar backscattering values with increasing plant height. The mean σ^0 values is −10.6 dB two months before harvest (with a spread

Figure 6.2. ERS-1 multitemporal composite of Kanchanaburi study area in Western Thailand, 1993; red: 11 June; green: 29 October; blue: 3 December. All images are Gamma MAP speckle filtered. (Source: J. Aschbacher, JRC).

from −12.6 to −9.0 dB), and increases to −8.5 dB (−9.5 to −6.8 dB) shortly before harvest. This corresponds to mean plant heights (above water surface) of approx. 45 and 85 cm, respectively, as evident from *Figure 6.4b*. Similar observations were also made by *Kurosu et al. (1993)* for the Japanese study area (see § 6.1.4).

6.1.3 Case studies in Indonesia

A feasibility study for a MARS-type project, but based on ERS-1 SAR data instead of optical imagery and focusing on rice only, was carried out by a team of European investigators in cooperation with the Indonesian Government (Scot Conseil, CESR). The overall project goal, was to define a rice monitoring system based on satellite data, in-situ data and modelling for the retrieval of statistical information about rice growth. Two test sites were selected, one in West Java and one in Central Java. Over both sites field information and satellite data were combined in a Geographic Information System. Data interpretation was performed by computer-aided visual interpretation and automatic classification using segmentation based field classifiers *(Harms, 1993)*. An overview of the rice planting area and a rice classification based on one ERS-1 image from the area are shown in *Figures 6.5 and 6.6*, respectively.

The area shown in *Figure 6.5* was also investigated by *Aschbacher et al. (1995b)*, who distinguished different growth stages of rice plants based on the information content of multitemporal images. The image is an excellent example, showing the ability of radar to monitor

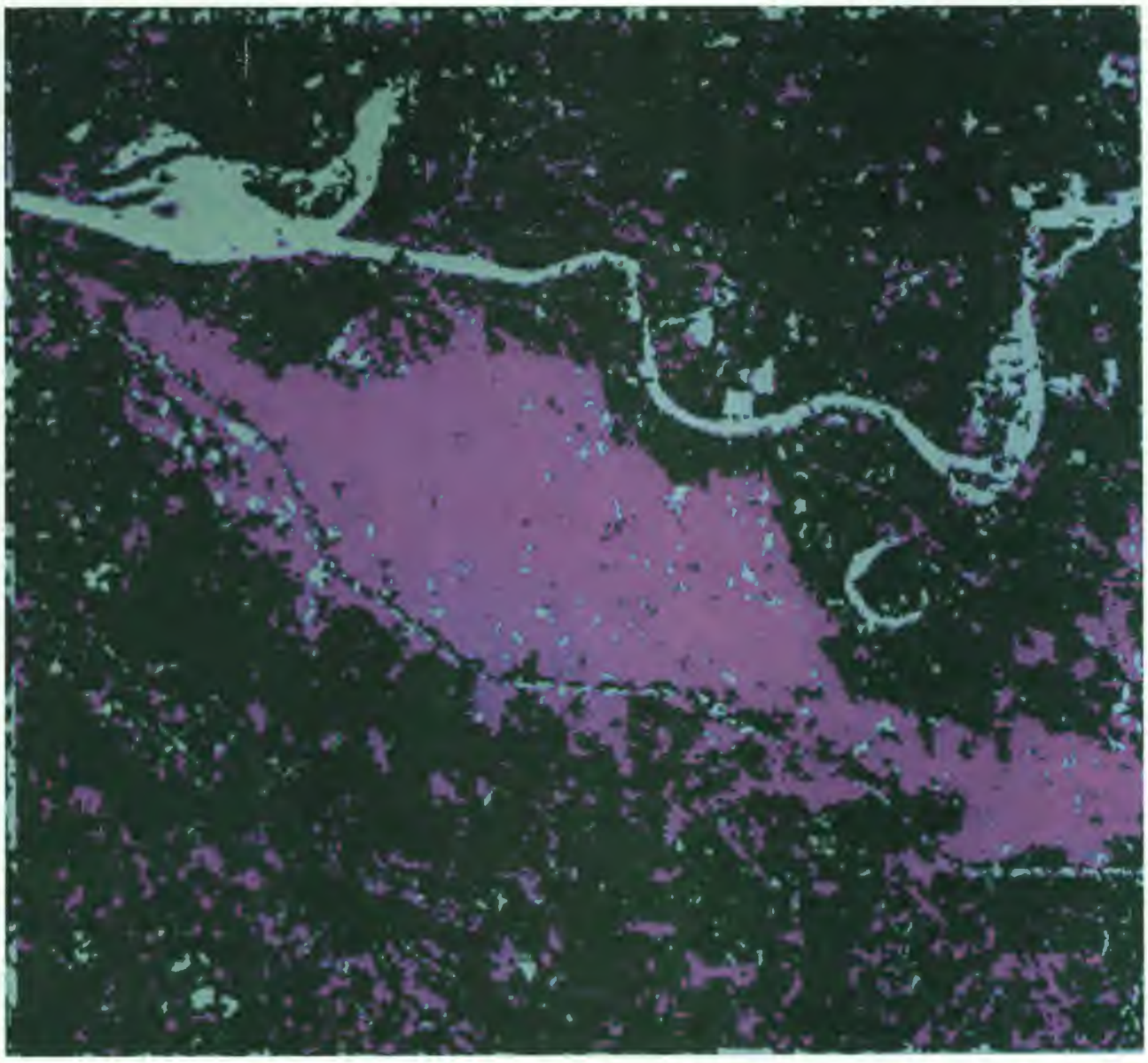

Figure 6.3. Classified 'rice map' based on four ERS-1 acquisitions (6 Jun., 20 Aug., 29 Oct. and 3 Dec. 1993). Rice is shown in mauve, non-rice areas in dark green and water in light blue. (Source: Aschbacher et al., 1995).

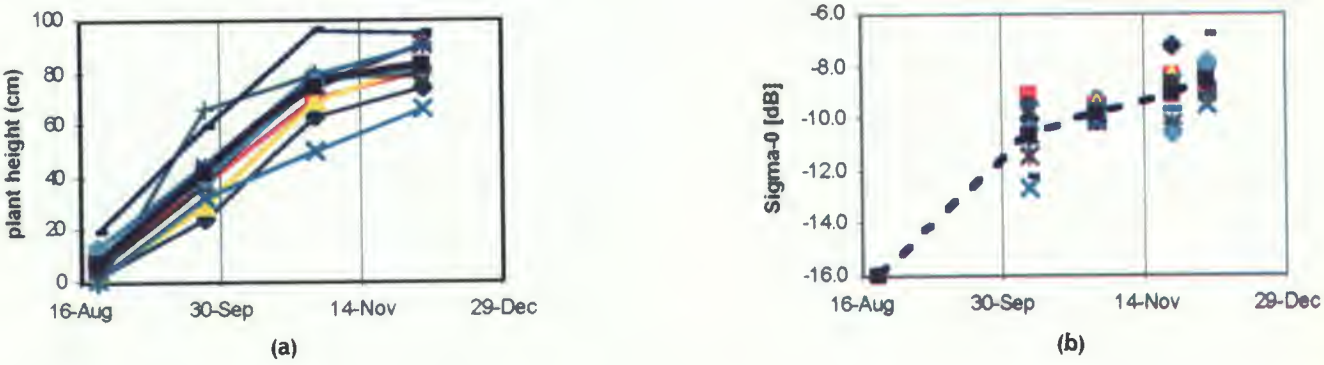

Figure 6.4. Comparison of (a) changes in rice backscatter with time of rice fields in Kanchanaburi, Thailand (the rice growing period lasts from August to December); (b) rice plant height (above water) measured at the same sample fields. (Source: Aschbacher et al. 1995a).

the status of growing, and rice field management practices with multitemporal SAR data. Individual rice fields, or groups of rice fields, are shown in greenish and bluish colours, with some smaller fields in red. According to ground truth information, most of the fields in the area were harvested either in early or late February, and a very few in early January 1994. After harvest bare soil was left, which has a relatively high radar backscattering value (approx. −7 to −5 dB), and is thus higher than that of pre-harvest rice fields (approx. −8 to −7 dB). Taking these two considerations into account and assuming a temporal signature of rice fields as shown in § 3.3.3, one can easily attribute greenish fields to fields harvested in early February (with bare soil in the 16 Feb and flooded fields in the 6 Mar images), and bluish fields to rice fields harvested in late February (bare soil in 6 Mar image). The few red fields are harvested in early January, and show flooded to early growth stages in the February and March images (*Aschbacher et al., 1995a*).

6.1.4 Case studies in Spain & Japan

Geographically, the growth of rice is not only limited to the tropical belt, as it is evident from Table 6.1. In Japan and Spain, for example, rice is also grown and mainly used for local consumption. However, if compared to tropical countries, the management of rice fields is generally more homogeneous over larger areas, and the individual field sizes are larger. Therefore, the results are expected to be less disturbed by within-field variations of growth stage or by vegetation along the field boundaries (e.g. banana trees, palm trees).

An example of a digital classification of an agricultural area in temperate zones was carried out by *Kohl et al.*

Figure 6.5. ERS-1 multitemporal composite of Semerang, Central Java, Indonesia (red: 23 January, green: 16 February, blue: 6 March 1994). Depending on the status of the plant growth cycle, rice fields appear in different colours. (Source: J. Harms, Scot Conseil and LAPAN).

(1993), based on a comparative analysis of multitemporal SPOT and ERS-1 SAR data. It is interesting to note that the classification result based on SPOT is quite similar to the ERS-1 based classification (compare *Figure 6.7* SPOT – AIS with ERS-1 – AIS). There is, however, some

Figure 6.6. Rice classification using a single ERS-1 image of the Semerang area, Indonesia, acquired during the field flooding stage; (a) extract of rice growing area, (b) pixel-based classification, rice fields are black. (Source: J. Harms, Scot Conseil).

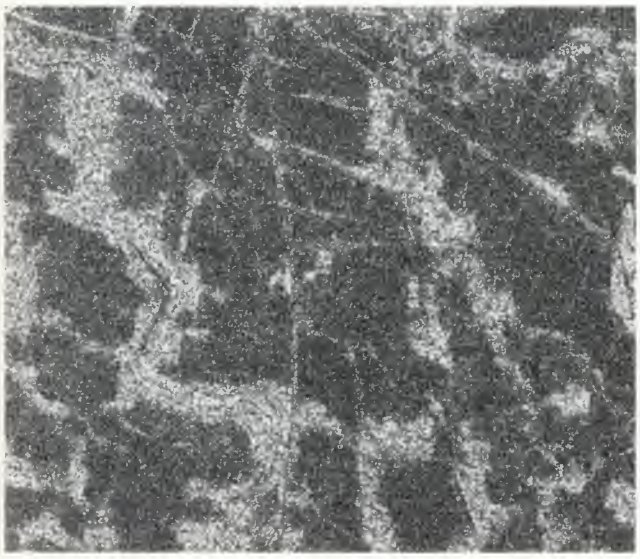

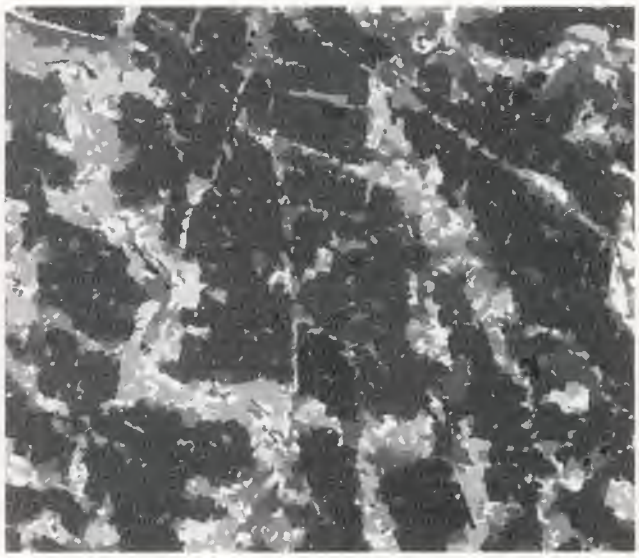

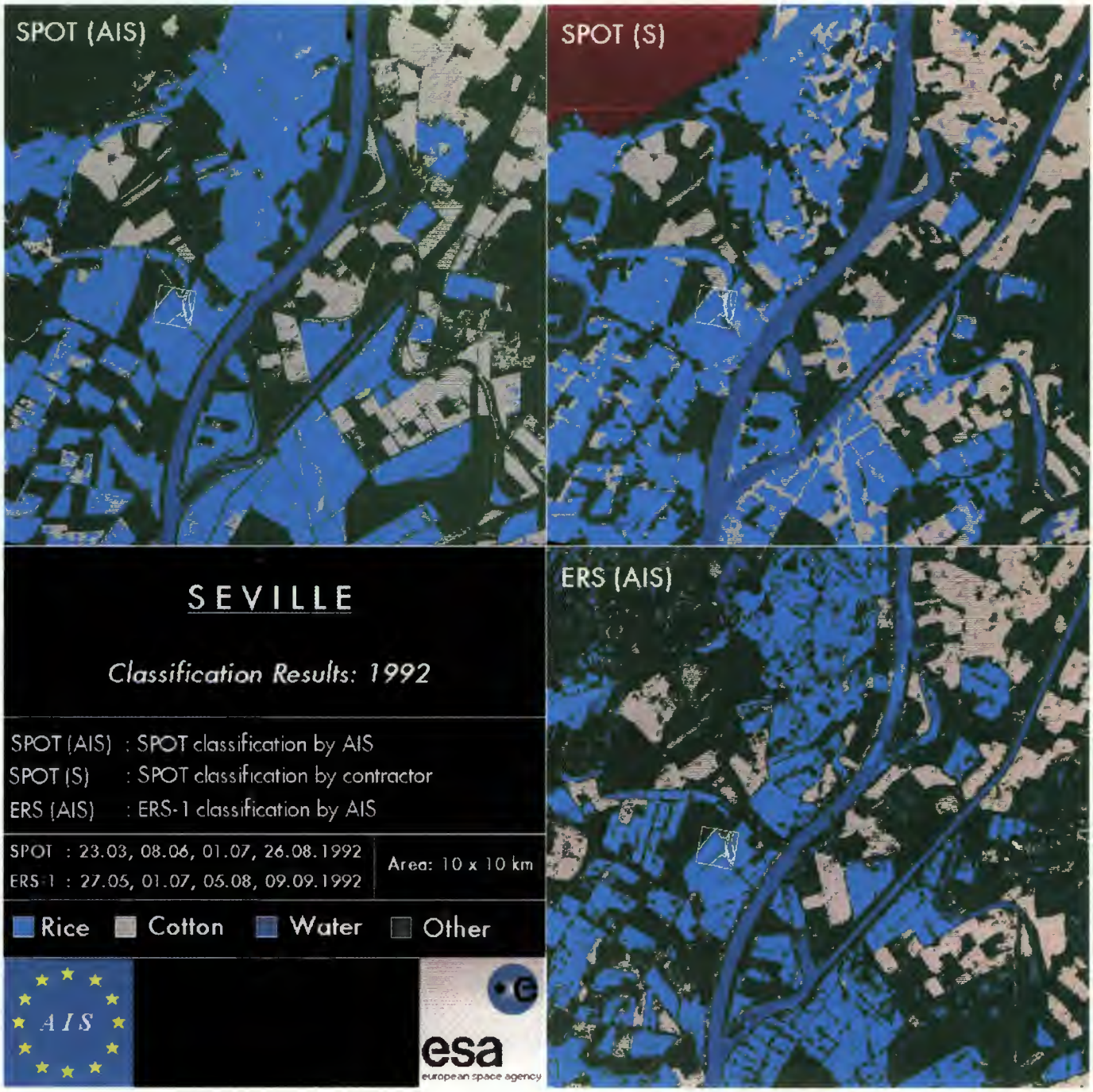

Figure 6.7. Comparison of rice and cotton classification for Seville, Spain, using SPOT and ERS-1 imagery. (Source: Kohl et al. 1994).

confusion between classes where the land use is less homogeneous, such as in the top left corner of the image.

Kurosu et al. (1993) relate rice plant height [cm] with ERS-1 radar backscatter values σ^0 [dB] at a study area in Japan, where eight consecutive ERS-1 SAR observations were available. The correlation coefficient obtained using just six values of different dates during the growth cycle is remarkably high ($r = 0.98$). The fields included in this study are part of an Agricultural College and thus very homogeneous in terms of field management and plant growth stage.

6.1.5 Conclusions

Among all the agricultural crops, the use of radar remote sensing is probably most promising for rice crops due to its significant temporal backscattering signature. The dynamic range of σ^0 [dB] is the largest

among all agricultural crops, ranging from approx. −16 dB during the flooded and early growing stage, to approx. −8 dB during the pre-harvest stage. The selection of appropriate acquisition times is crucial for mapping purposes. As regards yield estimates or parameters that lead to yield estimates, there is a clear correlation between radar backscattering signals and plant height. This allows the approximate age of rice plants to be determined, and thus a prediction of the approximate harvesting time.

The results available from several case studies allow the following conclusions to be drawn on the use of ERS-1 SAR data for rice mapping and monitoring (*Aschbacher et al., 1995a,b*):

1. Multitemporal ERS-1 SAR data can be used in an operational or quasi-operational mode for mapping of rice fields, both for irrigated and rain-fed fields.
2. Multitemporal ERS-1 SAR data can be used in a pre-operational manner for the retrieval of yield-related parameters.
3. A priori knowledge about the rice crop calendar and growing practices as well as parallel in-situ measurements largely facilitate the interpretation of radar images. However, reliable results can be obtained without or with a very limited set of in-situ measurements. This is of particular interest in view of large-scale operational rice monitoring systems.
4. For mapping purposes, at least three dates should be available during the growing cycle. The optimum acquisition times are during the early flooded stage, the flowering stage and shortly before harvest. An additional post-harvest image is useful if the time of rice harvest is different from that of other agricultural crops on the same scene.
5. For the retrieval of yield-related parameters the use of 4 – 8 acquisitions during the growth cycle is recommended. The image dates should be equally spread throughout the growth period. An acquisition shortly before harvest is mandatory.
6. Multi-temporal ERS-1 SAR data can be used to determine field management practices; such as the timing of irrigation, time of harvest, method of water supply (irrigated or rain-fed), and the length of the growth cycle. This information can be retrieved largely without in-situ measurements.
7. As regards the optimum analysis technique applied to radar imagery for rice mapping, it is recommended to speckle filter the images and apply texture and/or segmentation based algorithms, before classifying the images. Depending on the scene characteristics, special measures may have to be applied if field management differs within one scene.
8. If an operational rice monitoring system is developed, it is strongly recommended to include multitemporal radar imagery as a prime data source.

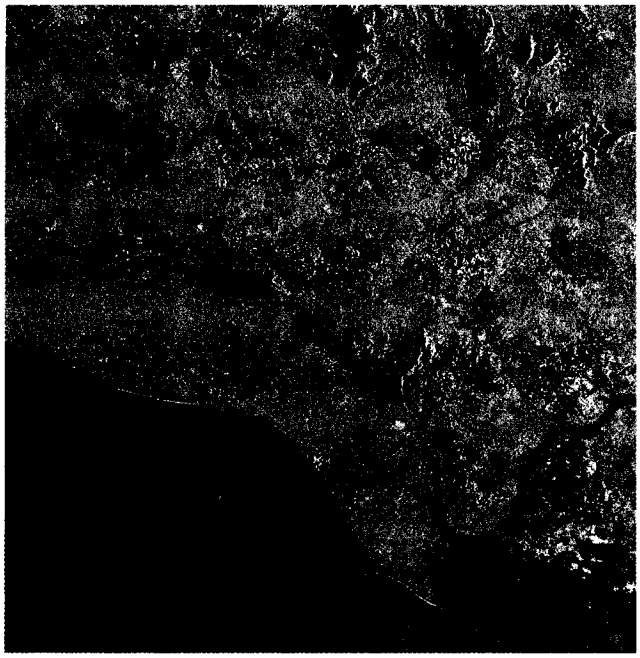

Figure 6.8. ERS-1 image of part of Johor state, Malaysia, 24 August 1993, coverage 100x100 km. (Source: M. Wooding, RSAC).

Figure 6.9. ERS-1 PRI extract of Costa Rican coast, 18 May 1992; banana plantations show the brightest returns, Gamma MAP filtered. (Source: M. Wooding, RSAC).

6.2 Plantations

ERS-1 images are potentially valuable for mapping some types of plantation crops, which form an important part of the economy of many tropical countries. Oil palm and bananas, in particular, tend to have very bright image tones in comparison with other types of tropical vegetation because of the large leaf sizes and the overall structure of the vegetation.

Figure 6.8 is an ERS-1 image covering parts of southern Malaysia and Singapore Island. Large oil palm plantations are seen as the lighter toned patches in the zone between the coastal plain and the mountains to the north-east. The coastal plain itself is an area of mixed smallholder agriculture without clear field patterns, which has darker image tones. Besides the potential for mapping new areas of oil palm, there is also some interest for monitoring the replanting of oil palm, which happens approximately every 30 years. Replanted oil palm appears dark on ERS-1 images because the signal is dominated by the low herbaceous ground cover between young trees.

Banana plantations are readily seen on ERS-1 images, *Beaulieu et al. (1994). Figure 6.9* shows large plantations in Costa Rica located on flat land near the coast and on large alluvial fans within the mountains. Banana plantations are identified both by their brightness and geometric shape. Although the extent of areas cultivated with banana are relatively well known in Costa Rica, there is potential for monitoring changes in the extent of plantations, which can be quite rapid in some areas.

6.3 Other Crops

There is a great variety of tropical agricultural crops, examples of which are rice, sugarcane, maize, tapioca, coffee, tea, rubber and fruit tree plantations. Rice and tree plantations have been discussed in § 6.1 and 6.2, respectively. *Paudyal (1994)* has investigated also other land cover categories at the Thailand study area (described in § 6.1), where, apart from rice fields, large plots of sugarcane are present, intermixed with bushes, shrubs, water and urban areas.

Various classification methods were compared such as maximum likelihood with knowledge-based classification methods, or unfiltered versus speckle filtered and/or texture analysed images. The latter method was developed making use of pre-assumptions about the rice growth cycle based on temporal profiles of σ° [dB]. These results were compared with a Landsat TM image and ground measurements for accuracy assessment. An overview of the classification results is given in Table 6.3.

The results of the supervised classification based on five dates (MAP-filtered) has given an overall classification accuracy of 70%, while the knowledge-based method gave 80%, which is a clear improvement. The same accuracy was obtained when combining speckle and texture analysed images as input for a maximum likelihood classification. As an example, the classification accuracy matrix was extracted for the agricultural crops, rice and sugarcane only, and compared with the overall accuracy including all six land cover categories. It is worth noting that the accuracy of rice alone has increased from 72% for the MAP-filtered classification to 92% for the knowledge-based segmentation method.

*Table 6.3 Classification accuracy for different classification methods based on five radar image dates. The observed land cover categories in the Thailand study area (Kanchanaburi, site 1) are rice, sugarcane, bush, shrubs, water and urban areas (*from Paudyal, 1994*).*

No.	Classification method	Input data	Overall Accuracy (%)	Rice Accuracy (%)	Sugarcane Accuracy (%)
1	Max. likelihood	unfiltered	65	58	71
2	Max. likelihood	MAP-speckle filtered	70	72	73
3	Max. likelihood	Lee-speckle filtered (2 iterat.)	75	78	88
4	Max. likelihood	texture (angular 2nd moment + contrast)	70	64	73
5	Max. likelihood	texture (ASM + IDM) + Lee-speckle filter	80	78	88
6	Knowledge-based segmentation	MAP filtered	80	92	71

For sugarcane, however, the combined speckle filtered and texture analysed images are the best input source for further classification. The accuracy reaches 88% in this case.

As can be seen from Table 6.3, there is no general method superior to another if all land-use categories are considered. However, the more sophisticated methods which combine speckle filtered and texture analysed data are clearly superior to a classification using only unfiltered or speckle filtered images. The knowledge-based method was adapted to discriminate rice fields from other categories and performs best for the category of rice. A further description of the methodology can be obtained from *Paudyal et al. (1994)*.

7. Future Developments

7.1 Data Continuity

Since its launch in 1991, ERS-1 is the first radar satellite to have provided a long period of continuous data acquisition. ERS-1 data have been used by the international science community since then to extract environmentally important parameters. Despite the restriction to a single frequency and polarization, the guaranteed high-repetition frequency and the sensor's quality and stability make it a very important monitoring tool. ERS-1 has acquired more than half a million images, which will be exploited for years to come. With the launch of ERS-2 in 1995 and Envisat in 1998, there is the prospect of data continuity well into the next century using ESA satellites. Other radar satellites including JERS-1 and Radarsat will further extend the amount of data. Brief technical specifications for these satellite radar systems are given in Table 7.1.

Built like ERS-1, ERS-2 carries the same active radar instruments to continue the data flow started in 1991. For a period of time, it is planned to operate both spacecraft 'in tandem' to collect interferometric data pairs (see § 4.5 and 7.3). One of the main applications of interferometry is to develop three-dimensional digital maps of the Earth's surface. The C-band data continuity will be guaranteed with the ASAR (advanced SAR) system on-board the Envisat platform. The Envisat mission will be ESA's third major remote sensing effort. As ERS-1/2, it will use a polar orbit at 800 km altitude and 98.5° inclination. Based on the Polar Platform concept, Envisat carries ten active instruments to cover a wide range of remote sensing tasks from Earth's surface monitoring to atmospheric research.

The Japanese spaceborne SAR programme started with a SAR on JERS-1 (Japanese Earth Resources Satellite). Application objectives focused on Earth resources and environmental protection, disaster prevention and coastal monitoring. In contrast to the other systems, JERS-1 allows observation at L-band (23 cm wavelength), supplying additional information about the Earth's surface. *Figure 7.1* illustrates a comparison of ERS-1 and JERS-1 SAR images over the Dutch Flevoland agricultural site (*Borgeaud et al., 1994*).

The Canadian Radarsat adds, by using HH-polarization, an additional feature to the available radar parameters. It is also capable of beam steering, allowing varying incidence angles and geometric resolutions (fine resolution vs. wide swath). The SAR data will be distributed to commercial, government and scientific organizations for applications in resource management, ice mapping and reconnaissance and environmental monitoring.

7.2 Multi-parameter Radar

The useful information which a satellite radar can provide on an agricultural field depends on the kinds of structures within the crop canopy or the soil with which it interacts. The natures of those structures and the strengths of interaction are influenced by the parameters of the radar, including its frequency and polarisation (*Schmullius & Nithack, 1992*). A multi-channel radar exploits these differing responses to provide a more complete instantaneous picture of the structure or density of a crop.

Table 7.1 Continuously operating and planned spaceborne SAR systems

Sensor	ERS-1	ERS-2	Envisat	JERS-1	Radarsat
Agency	ESA	ESA	ESA	NASDA	CSA
Launch	1991	1995	1999	1992	1995
Expected lifetime	3 years	3 years	5 years	2 years	5 years
Frequency (GHz)	5.3	5.3	5.3	1.3	5.3
Polarisation	VV	VV	VV, HH, VH	HH	HH
Incidence angle	23	23	15 to 55	38	10 to 60
Range resolution	26	26	30	18	9 to 100
Azimuth resolution	28	28	30	18	9 to 100

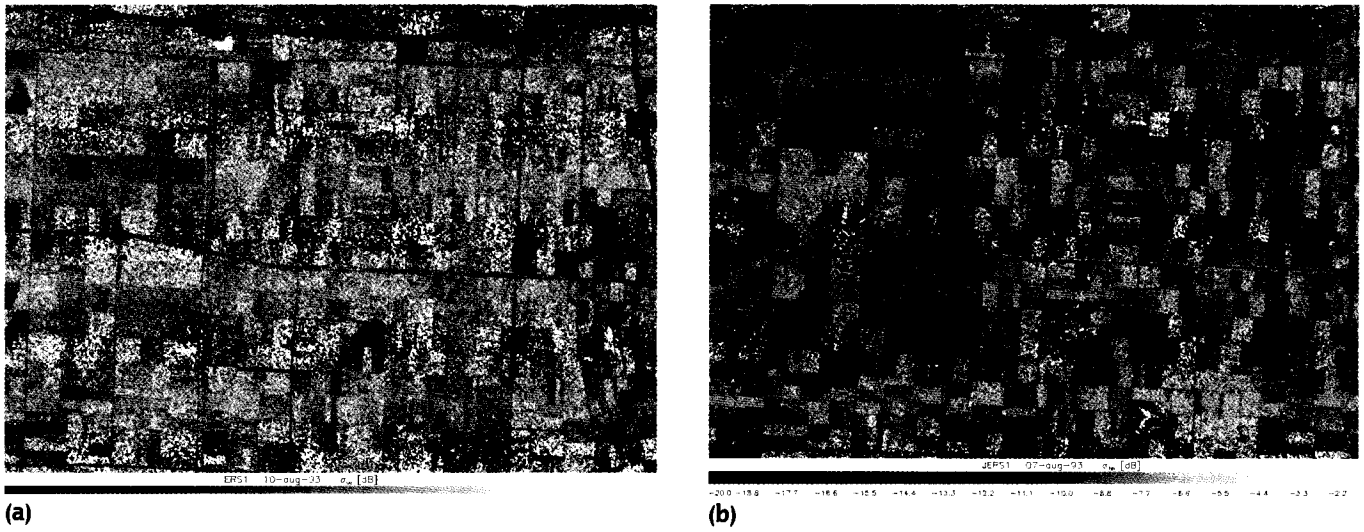

Figure 7.1 Comparison of (a) ERS-1 and (b) JERS-1/SAR images over the Dutch test site, Flevoland. (Source: M. Borgeaud, ESA/ESTEC).

Radar frequency is a tool for varying the penetration of microwaves into the canopy of a crop. While, in some circumstances, the C-band radiation of ERS-1 can penetrate completely through a canopy, it is not generally as penetrative as longer wavelengths such as L- band. Longer wavelengths react with structures through a greater volume of a canopy, and more regularly interact with the soil below. Higher frequencies, such as X-band radars, are more sensitive to the small-scale properties of the upper layers of vegetation or the canopy boundary layer.

The selection of horizontal and vertical polarisation varies the response of a radar to different shapes or scattering elements within a canopy. Selecting crossed polarisations between the radar transmitter and receiver, tends to detect backscatter from within the volume of a crop canopy rather than from the soil, and as such may be an indication of the amount of biomass. We might conceivably select different single radar channels or particular frequency and polarisation combination to optimise the discrimination of certain crops at some point in the growing season. Of far greater potential, however, is the use of multiple frequencies and/or polarisations simultaneously to provide a multi-dimensional set of measurements, akin to moving from monochrome optical imagery to colour.

Airborne radar experiments over the last two decades have supplied the remote sensing user community with high-quality multi-frequency and/or multi-polarization data (e.g. AGRISTARS, ROVE, AGRISCATT, AGRISAR, MAESTRO 1, Mac Europe 91, EMAC-1994). The recent SIR-C/X-SAR 1 and 2 experiments during April and October 1994 offered, for the first time, an opportunity to acquire multi-parameter SAR data from space within the 10-day mission time frame.

The application of multi-frequency SAR data for crop identification is demonstrated in *Figure 7.2*, which is a colour composite of X-band, C-band and L-band images covering the same 2.5 × 6 km area as the multitemporal ERS-1 composite shown in *Figure 5.2*. On the imaging date in July, all crops are fully developed and cause characteristic backscatter intensities, which simplifies the digital landuse classification. The brightest fields belong to oilseed rape (yellow-white) and sugar beet (light orange), since they have the highest backscatter in all three wavelengths. Dark blue fields are winter wheat (higher L-band returns), green fields are summer barley (higher C-band returns), making discrimination between cereals possible (compare the C- VV temporal signatures in *Figure 3.10*).

Figure 7.3 shows a multi-frequency composite acquired from the space borne SIR-C/X-SAR. The image was acquired at 04:00 GMT at night, as a thick cloud layer covered Germany, and shortly after a heavy storm covered the area with 20 cm of snow. The quality of the image demonstrates the capabilities of radar remote

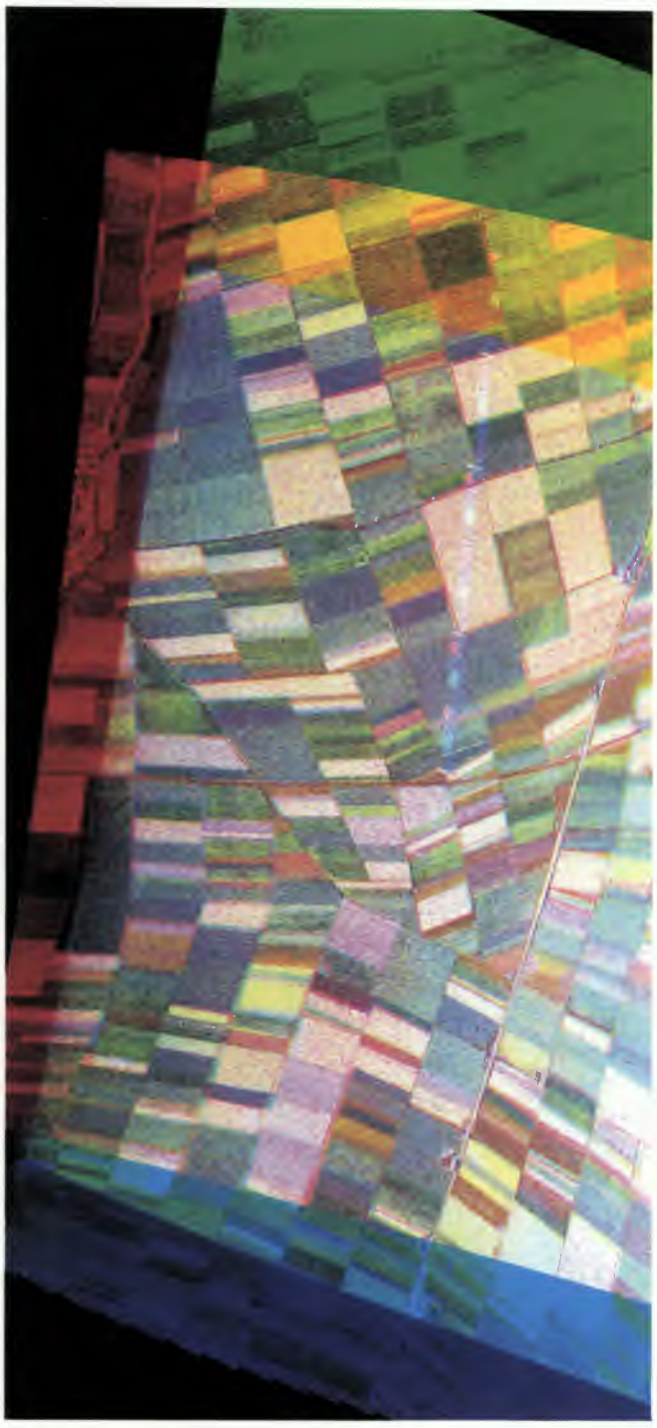

Figure 7.2. DLR ESAR multifrequency colour composite, CLEOPATRA test site Lechfeld, Germany, 14 July 1992; red: X-VV, green: C-VV, blue: L-HH. (Source: C. Schmullius, DLR).

sensing for environmental monitoring independent of weather conditions. Forested areas appear in red, because the long L-band wavelengths penetrate the vegetation canopy and are scattered by tree trunks and branches. Agricultural fields (mostly bare soil) appear blue in this April image, since the longer wavelengths are forward scattered, i.e. away from the sensor, but the X-band signals undergo diffuse scattering. Where the vegetation is taller, e.g. in the marshy areas at the northern tip of the large lake (Ammersee), L- and C-band returns add to the yellow colour.

Figure 7.4 provides an example of a C-band multi-polarisation composite. The airborne imagery was acquired by the EMISAR system developed by the Technical University of Denmark. It shows an agricultural area near Uppsala, Sweden, and is a composite of HH, VV and HV polarisation channels. The large range of colour associated with the agricultural fields provide a simple illustration of the extra information content of multi-polarisation radar, and is indicative of the future potential of Envisat with its dual-polarisation capability.

7.3 Analysis Techniques

Neural networks

Davison (1994) has investigated the potential of neural computing techniques, which are being increasingly applied to a wide variety of classification applications, and are recognised to cope particularly well with 'noisy' data. Pixel-based neural network classification of multi-temporal ERS-1 data of the Great Driffield site, UK, produced an accurate classification result for a small number of fields.

The work of *Melis & Lazzari (1994)* provides a further example of the use of neural network classification technique. *Figure 7.5a* is a multitemporal ERS-1/SAR image (April, May and July 1992) for a test site in the Tiber Valley, Rome. *Figure 7.5b* is an unsupervised classification obtained by a neural network (3-dimensional Kohonen's Map).

SAR interferometry

SAR interferometric data processing combines two complex valued images acquired with slightly different sensor positions. For ERS-1 imagery, random dislocation of the individual scatters between the two acquisitions reduces the interferometric correlation. As a consequence, this correlation contains thematic information which can be used to support land-use classification and change detection (*Wegmüller et al., 1995*).

A series of ERS-1/SAR SLC images of an area near Bonn, Germany, have been analysed using interferometric methods. The images were acquired in 3-day intervals giving good phase coherence between image pairs. Images acquired between 1 and 28 March were considered, and a total of nine coherence images from the different image pairs were generated.

Figure 7.3. SIR-C/X multifrequency colour composite, Germany, 13 April 1994; red: L-total power; green: C-total power; blue: X-VV. (Source: C. Schmullius, DLR).

Figure 7.6 shows the results of combining three of the coherence images. Forest areas and highways have low coherence so they show up as dark areas. For forests, this can be explained by the well-known de-correlation due to multiple scattering. For the 'smoother' highways, the amplitude of the reflected signal is too low for coherence detection.

All fields with no change in coherence over the period 7 – 16 March 1994 appear black and white. Ground observations at the time of image acquisition help to explain the apparent changes in coherence between fields. The coloured fields result from different grey values in at least one of the image planes. The red fields have low coherence in the green and blue image planes and, therefore, do not contribute to the perceived colour. This can be explained by cultivation activities. Red fields were ploughed in the period 13 – 19 March 1994 and therefore had low coherence compared to the start of cultivation. Yellow fields have no coherence in the blue image plane as farming activities occurred after 13 March. In the same manner, all other colours can be explained.

It should be noted that not only farmer activities cause de-correlation. Other factors such as rain, wind blow and irrigation can be involved. However, in the German study, growth-related loss of coherence can be ruled out

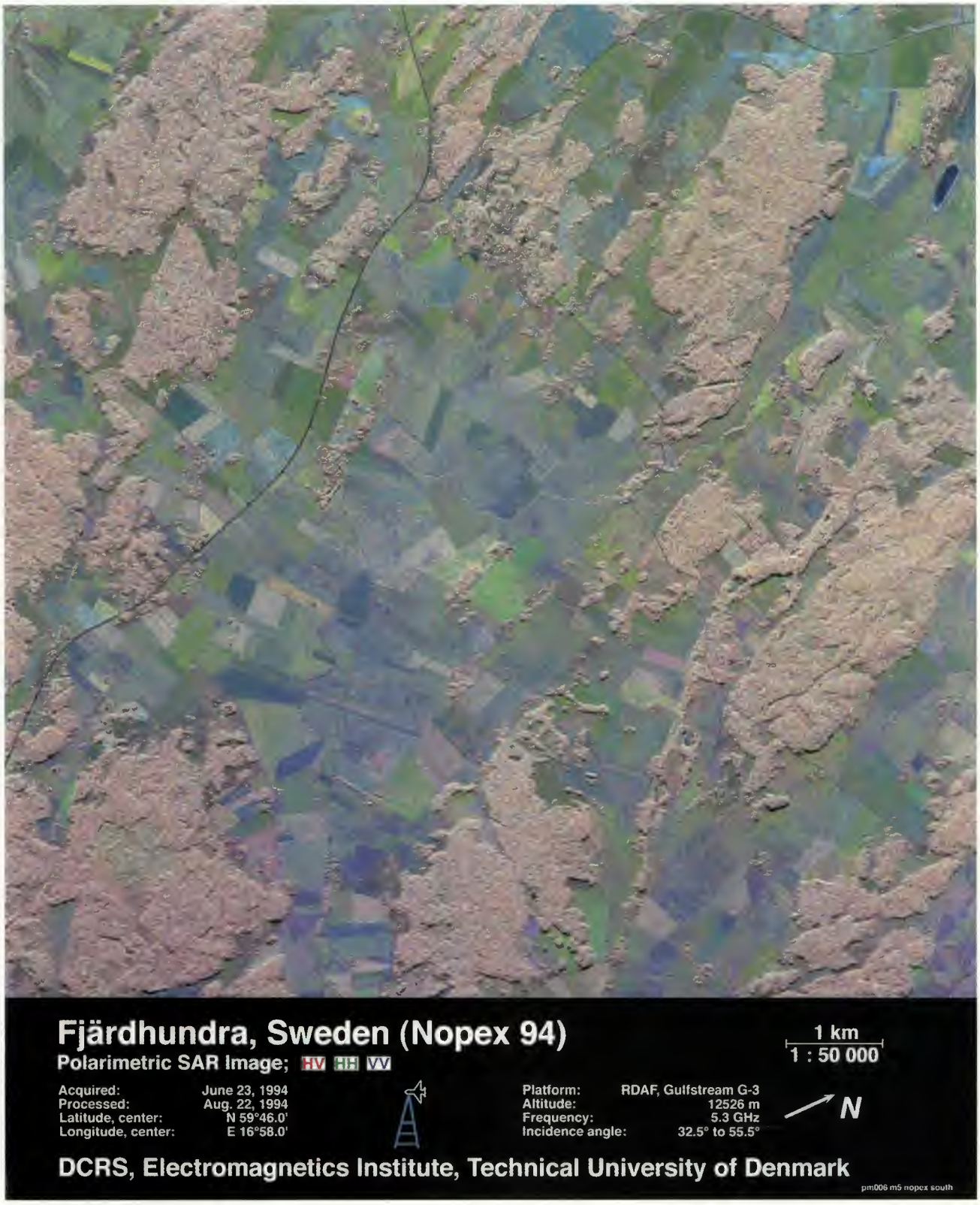

Figure 7.4. EMISAR C-band multi-polarimetric colour composite, Uppsala, Sweden, 23 June 1994; red: HV; green: HH; blue: VV. (Source: E. Attema, ESTEC).

as the crops were not experiencing rapid changes in productivity.

In a similar study of Baden-Württemberg, coherence images were generated from image pairs acquired

Figure 7.5a. Multitemporal ERS-1 FDC composite, Tiber Valley, Rome in 1992; red: April; green: May; blue: July. (Source: J. Lichtenegger, ESA/ESRIN).

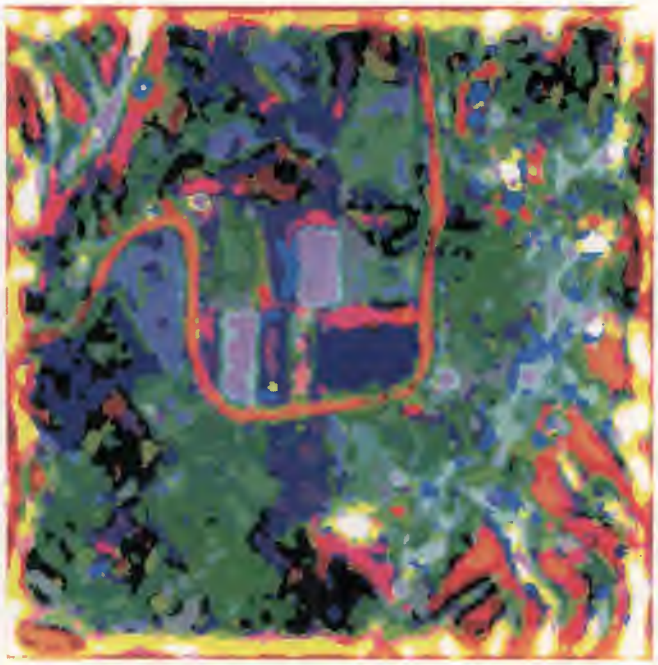

Figure 7.5b. Unsupervised classification obtained by a neural network (3-D Kohonen's Map) approach after feature extraction and statistics computation.

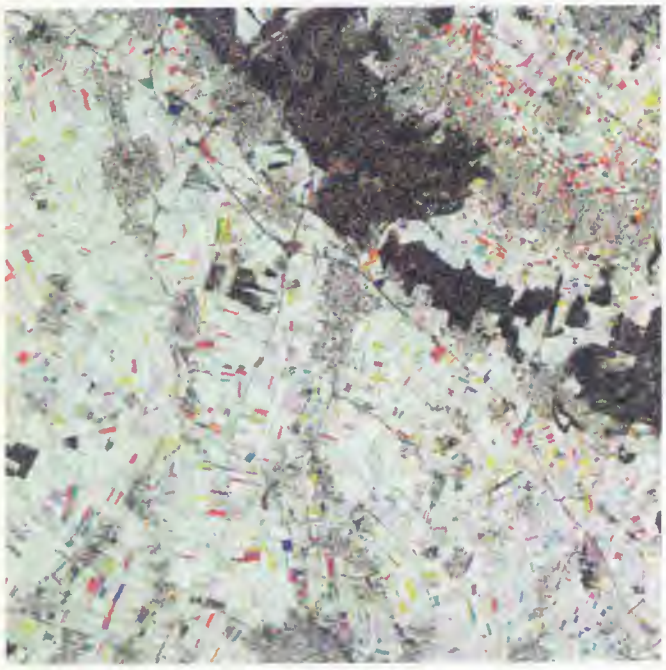

Figure 7.6. ERS-1 multitemporal colour composite showing repeat-pass interferometric correlation, near Bonn, Germany, 1994; red: 7-10; green: 10-13; blue: 13-16 March. Coloured fields indicate farming activities in the observed periods mostly attributed to the effects of ploughing.

during the period March to September. In all cases, no fringe images or coherence images could be generated due to the time interval of 35 days between consecutive passes. This period was too large and de-correlation occurred due to abundant changes in vegetation cover.

The potential of repeat-pass SAR interferometry for crop monitoring has been investigated using ERS-1 imagery acquired over Flevoland ,The Netherlands, in 1991. *Figure 7.7* shows a multitemporal composite of the interferometric correlation which occurred between three different time periods. The colours indicate differences in crop development and cultivation practice. Most potato fields appear blue due to the high correlation only between 19 October and 9 November. Prior to this period, interferometric correlation was low due to harvesting and spraying. However, for some potato fields, changes had already occurred between 19 September and 4 October as indicated by the turquoise colour (high green and high blue). The yellow fields (high red, high green) indicate that fields were mechanically cultivated between 19 October and 9 November for the establishment of winter crops. Corresponding explanations are valid for the other crops.

Figure 7.8 shows a multitemporal backscatter composite for the same site. It is much harder to interpret the colour changes. Only minimal differences are observed despite the fact that fields are undergoing cultivation and harvesting. For a more detailed appraisal of this work, see *Wegmüller & Werner (1995)*.

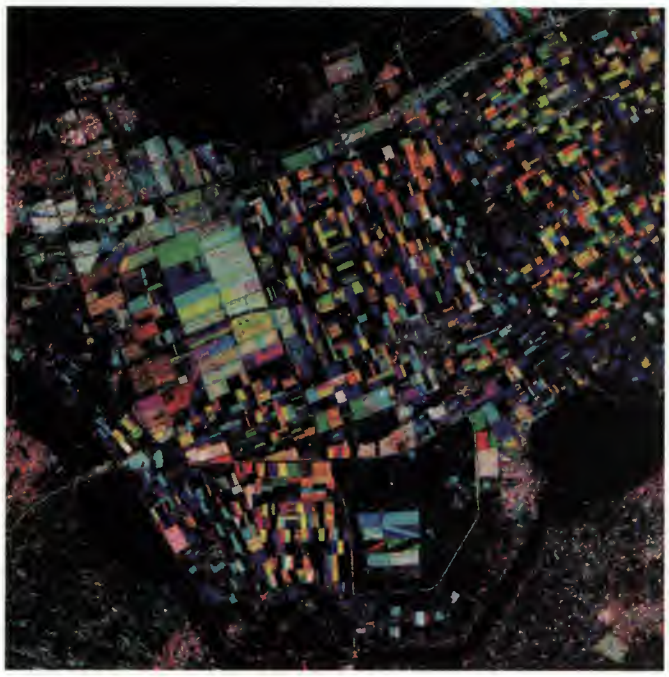

Figure 7.7. ERS-1 multitemporal colour composite showing repeat-pass interferometric correlation, Flevoland, 1991; red: 19 Sept.-4 Oct. pair, green: 4-19 Oct. pair, blue: 19 Oct.-4 Nov. pair.

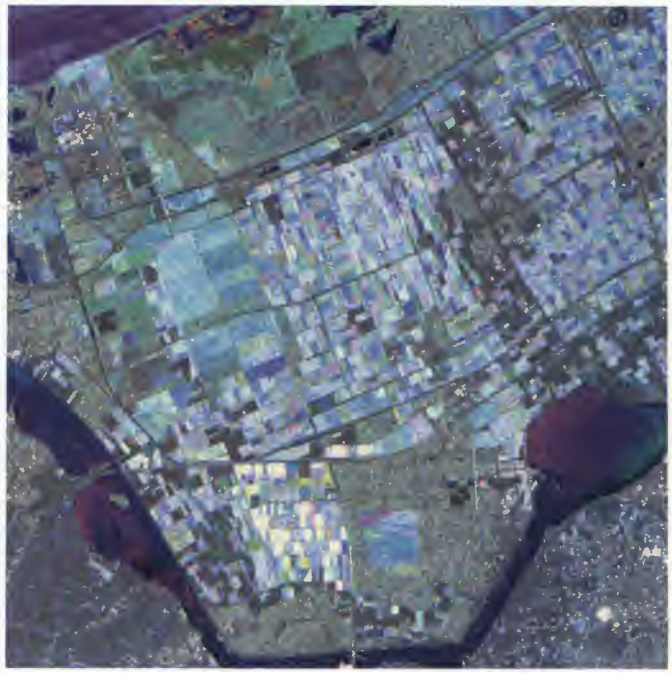

Figure 7.8. ERS-1 multitemporal backscatter colour composite, Flevoland 1991; red: 19 Sept.; green: 4 Oct.; blue: 9 Nov. (Courtesy of U. Wegmüller, RSL).

Crop growth models

Agricultural crop growth can be monitored by using crop growth models. However, often estimates of crop growth are inaccurate for non-optimal growing conditions. Remote sensing can provide information on the actual status of agricultural crops, thus calibrating the growth model for actual growing conditions. Encouraging results have already been obtained using optical remote sensing data in estimating the leaf area index (LAI) regularly during the growing season and subsequently calibrating the growth model on time-series of estimated LAIs.

By combining the SUCROS crop growth model for sugar beet (*Bouman, 1992*), with microwave and optical remote sensing data, it was possible to improve the predicted yield. As shown in Table 7.2, the average error on the crop yield is smallest when L-band SAR data together with an optical model are used to calibrate the SUCROS crop growth model.

Table 7.2 Average errors in yield estimation for sugar beet using a vegetation growth model calibrated either by microwave and/or optical data.

Techniques	Error (tons/ha)	Error (%)
SUCROS (vegetation growth model)	13.4	19.1
SUCROS with radar data (L-HH)	10.8	15.4
SUCROS with radar data (C-VV)	6.5	9.2
SUCROS with optical remote sensing data (3 dates)	4.0	5.7
SUCROS with radar data (C-VV) and optical model	3.7	5.3
SUCROS with radar data (L-HH) and optical model	3.3	4.7

8. Conclusions and Recommendations

8.1 ERS-1 Backscatter of Agricultural Crops

There have been significant developments in our understanding of the radar backscatter of agricultural crops over the lifetime of ERS-1. Prior to the launch of ERS-1 in July 1991, research experience had concentrated on experimental programmes using airborne radar systems, and involvement in space had been limited to brief duration Seasat and Shuttle Imaging Radar (SIR-A and SIR-B) missions. The availability of frequent and reliably timed satellite radar data from ERS-1 has provided new insights into the potential of multitemporal radar imaging for monitoring agricultural crops. The excellent stability of the ERS-1/SAR calibration has been another important factor, facilitating comparisons of crop backscatter measurements across different test sites and over different years.

Research work carried out within the ESA Announcement of Opportunity Programme has included studies in successive years at test sites in The Netherlands, UK and Germany. In general there is very good correspondence in the backscatter of crops across the different test sites. It has been found that cereal crops (wheat and barley) consistently show trends in backscatter as a function of time. The main features are:

(i) a decline in backscatter during the tillering to the flag leaf stage
(ii) a period in which backscatter is at a minimum at the time of heading and ear development
(iii) an increase in backscatter during grain fill until harvest.

The backscatter minima which occurs at the heading stage is a characteristic which shows up consistently. As barley matures before wheat, the backscatter profiles for barley appear to turn earlier and this provides a basis for separating these different cereal crops.

Rice also has been shown to have a characteristic temporal behaviour. In this case there is low backscatter at the early stage of development associated with the presence of standing water, backscatter increases to reach a maximum at the heading stage, and then declines slightly during senescence and harvest.

Environmental and meteorological effects have been found to have some influence on the crop backscatter. Wet crop conditions following rainfall seem to be the main factor, and this can result in an increase in backscatter by several dB's. This suggests the need for ancillary information on the timing of rainfall events.

Recommendation
The establishment of crop backscatter databases which include both field averaged backscatter measurements and details of crop growing conditions at the time of ERS-1 acquisitions. This is vital for improving our general understanding of causative relationships, and also the effects of specific environmental/meteorological factors (e.g. rainfall, disease, drought, wind blow). A better understanding of the interaction of electromagnetic waves with different crops is important for improving current backscatter models.

8.2 Crop Classification

The fact that particular crops have distinctive temporal backscatter profiles can be exploited for crop classification purposes. Rice, wheat, barley, oilseed rape and grass have been shown to have particularly distinctive behaviour. Time windows exist in which these crops are separable on the basis of their backscatter and difference in backscatter between dates, and this allows these crops to be classified with high orders of accuracy. Best results have been achieved using a field-based approach to classification. However, good results are also possible using a pixel-based approach, where this involves the use of special filtering or segmentation techniques.

Often there is an important requirement to distinguish crops at the earliest possible stage in the growing season so that field checks can be performed well before harvest. Results from Holland and the UK indicate that winter wheat can be accurately classified in early May and June (classification accuracies of $>80\%$). Oilseed rape can be mapped to accuracies approaching 100% using images from within the same time frame. However, more difficulties have been experienced with the separation of sugar beet and potato crops. Barley crops can be distinguished at the

end of June and early July. At this time barley ripens relative to wheat and this is reflected in the temporal profiles. Grass can only be distinguished using additional images acquired after the more seasonal crops are harvested.

Results from Holland indicate that surface roughness in autumn is an indicator of site specific tillage and cropping practices in the following growing season. Although crop development is insignificant in Autumn, experimental results have shown that information could be obtained which was relevant to crop type discrimination much later in the growing season. There seems to be potential to use a combination of autumn and spring images to map crops earlier than would be possible using optical imagery.

Mapping of rice fields is also possible at a very early stage when fields are flooded, which coincides with sowing or transplanting.

The potential for crop classification may be limited in areas where field sizes are very small. The accuracy of averaged field backscatter measurements is reduced for field sizes less than 1 ha, and it becomes difficult to resolve individual fields of this size. However, this has not been a significant problem for rice mapping because of the common management of groups of fields related to water availability. Another important consideration is the effect of geometric distortion in hilly areas. Much of the preliminary work has been carried out in areas where terrain distortion is not a problem (ie. East Anglia in the UK, Lechfeld in Germany, the Dutch Polders and Kanchanaburi in Thailand).

Recommendation
Further research studies are required to investigate crop classification accuracies for a wide range of crops in different environmental situations. New work is required to assess the effect of local incidence angle correction on crop classification performance in hilly terrain. There should be an emphasis on the potential for early crop forecasts.

8.3 Strategies for Operational Use of Satellite Radar Data

The main weakness of current crop monitoring systems based on the use of optical satellite data is the unreliability of image acquisitions in parts of the world with frequent cloud cover. However, even when optimally timed images are available, there still appears to be problems with the identification of some crops. The SPOT satellite for instance still lacks a spectral channel in the middle infrared which provides much approved crop discrimination (a situation that will change with the launch of SPOT-4).

Although it is attractive to contemplate the use of satellite radar data for operational crop monitoring simply on the basis of reliable cloud-free data acquisition, the major issue is the value of the data for crop classification in comparison, or used in conjunction with optical data. The research results on ERS-1 crop classification presented in this document are viewed as being highly encouraging in this respect, and two alternative approaches are suggested depending on the difficulties encountered in obtaining optical satellite images.

Firstly, in cloudy parts of the world, such as the humid tropics and northern Europe, multitemporal satellite radar data should increasingly fulfil a primary role, supplemented by occasional optical images. In this case, optical images would be used for field area measurement and to aid in the classification of crops which are poorly discriminated on radar images.

Secondly, in parts of the world with generally clear weather conditions, optical satellite images should continue to be the main data source, although supplemented by satellite radar images if these can be shown to be useful for early crop identification, or for dealing with particular crops which are difficult to classify using optical images. Examples have been presented which show that classification performance can be improved by the combined use of optical and ERS-1 imagery.

Experience with ERS-1 has established the potential of satellite radar for agricultural applications. With ERS-2, JERS-1, Radarsat (launch in 1995), and ASAR (launch in 1998) providing continuity of data into the next century, there are excellent opportunities for exploiting the potential of satellite radar for operational crop monitoring in Europe and the rest of the world. Operational multi-frequency, multi-polarisation radars now being planned for early next century will extend the capabilities even further. The potential for crop growth monitoring is likely to be improved both by the availability of multi-frequency and multi-polarisation data, and by the further development of interferometry techniques. For rice there are already very positive yield prediction results.

Recommendations

A programme of pilot projects should be initiated to develop methodologies and to evaluate crop classification accuracies using ERS-1/2 data in different agricultural situations. There is also a need for more detailed analyses of radar backscatter time series linked to crop growth models. These should be carried out within the framework of present remote sensing control and statistics projects within Europe and elsewhere.

Furthermore, the complementarity of optical and radar data should be studied in more detail as well as the possibility of combining ERS and JERS data.

Finally, after four years of research and encouraging results, operational users should be encouraged to integrate ERS-1 imagery into their programmes.

9. References

Aschbacher J, 1992. Can satellites help in the management of tropical ecosystems? *Proc. Intl. Space Year*, Regional Seminar on Remote Sensing Applications to Tropical Eco-System Management, Khao Yai, Thailand, 14-20 June 1992, ESCAP/UNDP, pp. 90-92.

Aschbacher J & Lichtenegger J, 1990. Complementary nature of SAR and optical data: a case study in the Tropics, *ESA Earth Obs. Quart.*, Sept. 1990, No. 31, pp. 4-8.

Aschbacher J & Paudyal D R, 1993. Studies of rice fields in Thailand using ERS-1 SAR data, *Proc. National Conf. ERS-1/Landsat/SPOT Applications: A Complementary Approach*, Jakarta, Indonesia, 23-25 November 1993, p. 9.3. 1-9.3.9.

Aschbacher J, Dipak R P, Pongsrihadulchai A, Karnchanasutham S & Rodprom C, 1994. Radar backscattering studies of rice fields using ERS-1 SAR data, *Proc. IGARSS 94*, Pasadena, California, 10-12 August 1994.

Aschbacher J, Pongsrihadulchai A, Karnchanasutham S, Rodprom C, Paudyal D R & Le Toan T, 1995a. Assessment of ERS-1 SAR data for rice crop mapping and monitoring, *Proc. IGARSS 95*, Florence, Italy, 10-14 August (Abstract submitted).

Aschbacher J, Poniman A. & Wismann V, 1995b. Assessment of ERS-1/SAR for tropical land-use mapping along coastal zones in Indonesia, *Proc. IGARSS 95*, Firenze, Italy, 10-14 Aug. (Abstract submitted).

Askne J & Hagberg J, 1993. Potential of interferometric SAR for classification of land surfaces, *Proc. IGARSS 93*, Tokyo, Japan, pp. 985-987.

Beaulieu N, Leclerc G, Velasquez S, Pigeonnat S, Gribius N, Escalant J-V & Bonn F, 1994. Investigations at CATIE on the potential of high-resolution radar images for monitoring of agriculture in Central America, *SAREX-92 Workshop Proc.*, Paris, 6-8 December 1993, ESA WPP-76, pp. 139-153.

Borgeaud M, Noll J & Bellini A, 1994. Multitemporal comparisons of ERS-1 and JERS-1/SAR data for land applications, *Proc. IGARSS 94*, Pasadena, CA, 10-12 Aug. 1994.

Bouman B A M, 1992. Linking physical remote sensing models with crop growth simulation models applied for sugar beets, *Intl. Jl. of Remote Sensing*, Vol. 13, No. 14, pp. 2565-2781.

Davison M, 1994. Development of neural network techniques for the classification of multitemporal ERS-1/SAR imagery with respect to agricultural applications. *Proc. 1st Workshop on ERS-1 Pilot Projects*, Toledo, Spain, June 1994, ESA SP-365, pp 469-473.

Frost V S, Stiles J A, Shanmugan K S & Holztman J C, 1982. A model for radar images and its application to adaptive digital filtering of multiplicative noise, *IEEE Trans. on Pattern Analysis and Machine Intelligence*, Vol. PAMI-4, No. 2, pp. 157-165.

Geudtner D, 1995. Die interferometrische Verarbeitung von SAR Daten des ERS-1, DLR Forschungsbericht (in press).

Groot J, Van der Broek B, Nieuwenhuis G, Schotten C, Van Rooij W & Jansen L, 1994. Crop classification using ERS-1/SAR data, Experts Meeting, JRC-IRSA Agricultural Project, 7-8 Feb. 1994.

Harms J, 1993. Integration of ERS-1 data into the European project of agriculture statistics, *Proc. 1st ERS-1 Symp.*, Cannes, France, 4-6 Nov. 1992, ESA SP-359, Vol. 2, pp. 629-630.

Harms J, Galaupe M, Rabaute T, Cailton J M, Roques J M & Demailly C, 1994. Integration of ERS-1 data into the European project of agricultural statistics, *Proc. 2nd ERS-1 Symp.*, Hamburg, 11-14 Oct. 1993, ESA SP-361, Vol. 1, pp. 85-86.

Hartl P & Klaedtke H G, 1994. Some results of the PASTA project concerning agricultural classification, *Proc. 1st Workshop on ERS-1 Pilot Projects*, Toledo, June 1994, ESA SP-365, pp. 481-491.

Hartl P, Klaedtke H-G, Reich M & Xia Y, 1994. Agricultural implications of ERS-1 data: Preliminary results of the PASTA project, *Proc. 2nd ERS-1 Symp.*, Hamburg, 11-14 Oct. 1993, ESA SP-361, Vol. 1, pp. 63-68.

Jutten C, Blayo F, Cabestany J, Cheneval Y, Cowmon P & Verleysen M, 1995. Eds. 'ELENA – Enhanced Learning for Evolution Neural Architects', ESPRIT III Basic Research Action (No. 6891), Project Results and Industrial Openings, Brussels.

Kohl H-G, 1994. An evaluation of ERS-1 PRI data in the context of the rapid estimation of crop acreages in Europe, *Proc. IGARSS 94*, Pasadena, CA, 10-12 Aug. 1994.

Kohl H-G, King C & De Groof H, 1994a. Agricultural statistics: Comparison of ERS-1 and SPOT for the crop acreage estimation of the MARS project, *Proc. 2nd ERS-1 Symp.*, Hamburg, Oct. 1993, ESA SP-361 (Jan. 94), Vol. 1, pp. 87-92.

Kohl H-G, Nezry E, De Groof H & Kattenborn G, 1994b. Monitoring agricultural surfaces using ERS-1 multitemporal SAR data, *Proc. IGARSS 94*, Pasadena, CA, 10-12 Aug. 1994.

Kohl H-G, Nezry E, Mroz M & De Groof H, 1994c. Towards the integration of ERS/SAR data in an operational system for the rapid estimate of crop acreage at the level of the European Union, *Proc. 1st ERS-1 Pilot Projects Workshop*, Toledo, Spain, ESA SP-365, pp. 433-441.

Kuroso T, Suitz T, Fujita M, Chiba K & Moriya T, 1994. Rice crop monitoring with ERS-1/SAR: a first year result, *Proc. 2nd ERS-1 Symp.*, Hamburg, ESA SP-361, Vol. 1, pp. 97-102.

Laur H, Sanchez J, Dwyer E & Meadows P, 1993. ERS-1/SAR radiometric calibration, *Proc. SAR Calibration Workshop*, ESA WPP-48, pp. 257-281.

Lee J S, 1986. Speckle suppression and analysis for synthetic aperture radar images, *Optical Engineering*, Vol. 25, No. 5, pp 636-643.

Lemoine G G & De Groof H, 1994. Personal communication.

Le Toan T, Laur H & Mougin E, 1989. Multitemporal and dual-polarisation observations of agricultural vegetation covers by X-band SAR images, *IEEE Trans. on Geoscience & Remote Sensing*, Vol. 27, No. 6, pp. 709-718.

Li Chang, 1988. Two adaptive filters for speckle reduction in SAR images using variance ratio, *Intl. Jl. of Remote Sensing*, Vol. 9, No. 4, pp. 641-653.

Lopez A, Nezry E, Touzi R & Laur H, 1993. Structure detection and statistical adaptive speckle filtering in SAR images, *Intl. Jl. of Remote Sensing*, Vol. 14, No. 9, pp. 1735-1758.

Massonnet D, Rossi M, Carmona C, Adragna F, Peltzer G, Feigl K & Rabaute T, 1993. The displacement field of the Landers earthquake mapped by SAR interferometry, *Nature*, No. 364 Vol. 6433, 8 July 1993, pp. 138-142.

Meadows P J & Wright P A, 1994. ERS-1 SAR analogue to digital convertor saturation, *Proc. SAR Calibration Workshop*, CEOS Calibration/Validation Working Group, Ann Arbor, MI, Sept. 1994.

Melis M & Lazzari A, 1994. Multitemporal and single-image features extraction from ERS-1 image data with wavelet transforms and unsupervised neural networks, *Proc. 1st ERS-1 Pilot Projects Workshop*, Toledo, June 1994, ESA SP-365.

Nezry E, Lopes A & Touzi R, 1991. Detection of structural and textural features for SAR image filtering. *Proc. IGARSS 91*, pp. 2169-2172.

Nezry E, Leysen M & De Grandi G, 1995. Speckle and scene spatial estimators for SAR image filtering application to ERS-1 over fragmented forest, *Proc. IGARSS 95*, Florence, Italy (in press).

Paudyal D R, 1994. An assessment of spaceborne radar remote sensing for monitoring of tropical agriculture, Doctoral thesis, Asian Institute of Technology, Bangkok, Thailand (unpublished).

Paudyal D R & Achbacher J, 1993a. Evaluation and performance tests of selected SAR speckle filters, *Proc. Intl. Symp. on Operationalization of Remote Sensing*, ITC, Enschede, The Netherlands, 19-23 April 1993, Vol. 5, pp. 89-96.

Paudyal D R & Aschbacher J, 1993b. Land cover separability studies of filtered ERS-1/SAR images in the tropics, *Proc. IGARSS 93*, Tokyo Japan, 18-23 Aug. 1993, pp. 1216-1218.

Paudyal D R, Eiumnoh A, Aschbacher J & Schumann R, 1994. A knowledge-based classification of multitemporal ERS-1 and JERS-1/SAR images over the tropics, *Proc. IGARSS 94*, Pasadena, CA, 10-12 August 1994.

Quegan S, Caves R G & White R G, 1993. The structural content of ERS-1 images and its implications, *Proc. 2nd ERS-1 Symp.*, Hamburg, ESA SP-361, Vol. 2, pp 623-628.

Schadt R, Kellndorfer J & Mauser W, 1994. Comparison of ERS-1 SLC and Landsat thematic mapper for monitoring grassland and detecting changes in agricultural use, *Proc. 2nd ERS-1 Symp.*, Hamburg, ESA SP-361, Vol. 1, pp. 75-78.

Schmullius C & Nithack J, 1992. High-resolution SAR frequency and polarization dependent backscatter variations from agricultural fields, *Proc. IGARSS 92*, Houston, Texas, 26-29 May 1992, pp. 930-932.

Schmullius C, Nithack J & Kern M, 1994. Comparison of multitemporal ERS-1 and airborne DLR E-SAR image data for crop monitoring, *Proc. 2nd ERS-1 Symp.*, Hamburg, ESA SP-361, Vol. 1, pp. 79-84.

Schotten C G J, Van Rooij W W L, Janssen L L F, 1995. Assessment of the capabilities of multitemporal ERS-1/SAR data to discriminate between agricultural crops (accepted by *Intl. Jl. of Remote Sensing*).

Wegmüller U, Werner C L, Nuesch D & Borgeaud M, 1995. Land surface analysis using ERS-1/SAR interferometry, *ESA Bulletin*, February 1995, No. 81, pp. 30-37.

Wegmüller U, Werner C L, Nuesch D & Borgeaud M M, 1995. Forest mapping using ERS-1/SAR interferometry, *ESA Earth Observation Quarterly*, No. 49, Sept. 1995.

Wegmüller U & Werner C L, 1995. Farmland monitoring with SAR interferometry, *Proc. IGARSS 95*, Florence, July 1995.

Werner C L & Wegmüller U, 1994. Extraction and characterization of interferometric parameters for agricultural and forest regions. *Progress in Electromagnetics Research Symp. PIERS '94*, 11-15 July 1994, Noordwijk, The Netherlands.

White R G, 1994. A simulated image annealing algorithm for radar cross-section estimation and segmentation, *SPIE Intl. Conf. on Applications of Artificial Neural Networks V*, 4-8 April, Orlando, Florida, Manuscript 2243-25, pp. 1-10.

Wooding M G, Zmuda A D & Griffiths G H, 1994. Crop discrimination using multitemporal ERS-/SAR data, *Proc. 2nd ERS-1 Symp.*, Hamburg, ESA SP-361, Vol. 1, pp. 51-56.

Wright P, Saich P & Cordey R, 1994. Crop monitoring with ERS-1/SAR in East Anglia, *Proc. 2nd ERS-1 Symp.*, Hamburg, ESA SP-361, Vol. 2, pp. 103-108.

Zebker H A, Werner C L, Rosen P A & Hensley S, 1994. Accuracy of topographic maps derived from ERS-1 interferometric SAR, *IEEE Trans. on Geoscience and Remote Sensing*, Vol. 32, No. 4, pp. 823-836.

Zmuda A D, Batts A J, Wooding M G & Fletcher P, 1994. Discrimination of agricultural crops using multitemporal ERS-1/SAR data. Results of the 1993 crop growing season. Unpublished report to the Defence Research Agency, UK.

APPENDIX
User Calibration of ERS Image Products

Users can generate accurately calibrated ERS/SAR images using information contained in the header files supplied by ESA's Processing and Archiving Facilities (PAFs) with the datasets.

For standard precision products (ERS.SAR.PRI), image values are supplied which are proportional to the amplitude of the normalised backscattered signal. The square of these numbers (I) is related to the normalised radar cross section σ_0 by the expression:

$$\sigma_0 = \frac{<I>}{K} \frac{\sin \alpha_D}{\sin \alpha_{ref}}$$

where σ_0 = normalised radar cross section of region
$<I>$ = average pixel intensity of region
K = calibration constant
α_D = radar incidence angle at the region
α_{ref} = reference incidence angle (23°)

The PAFs apply the necessary corrections for any variations of calibration associated with the antenna pattern of the radar before they are distributed to the user.

In a large proportion of cases where ERS-1 images agricultural regions, the calibration equation can be simplified to:

$$\sigma_0 = \frac{<I>}{K} \frac{\sin \alpha_D}{\sin \alpha_{ref}}$$

For work to the very highest levels of accuracy, and to achieve the calibration performance described in Chapter 5, additional corrections for 'replica pulse power' and 'ADC power loss' are recommended.

The replica pulses, which are copies of the pulses transmitted by the radar, are used in the generation of image products from the raw radar signals in the PAFs. The power of the replica pulses is not perfectly constant and for accurate measurements of radar backscatter this variation in power should be corrected (*Laur et al. 1993*). The replica pulse power for each product is stored in its header.

In cases were ERS-1 images bright areas of land or sea, extending over areas of a few tens of km^2, a loss of power can result from saturation of the analogue-to-digital converter (ADC) in the receiver on-board the satellite. When imaging regions darker than $\sigma_0 = -7$ dB, the power loss amounts to less than 0.5 dB. The details of how to calculate the ADC power loss are given in *Meadows & Wright (1994)*. For ERS-2, it is intended that the impact of ADC power loss will be considerably reduced by a reduction in the gain setting of the on-board radar receiver.

Members of the Specialist Panel

Dr. Josef Aschbacher
Joint Research Centre
IRSA/MTV, TP 440
I-21020 Ispra (Varese)
ITALY
T +39 332 78 5968
F +39 332 78 5461
E josef.aschbacher@jrc.it

Evert Attema
ESTEC
NWA
Keplerlaan 1
Noordwijk 2200 AG
THE NETHERLANDS
T +31 1719 84461
F +31 1719 85675
E eattema@jw.estec.esa.nl

Dr. Maurice Borgeaud
ESTEC-XEP
ESA
P.O. Box 299
NL-2200 AG Noordwijk
THE NETHERLANDS
T +31 1719 84830
F +31 1719 84999
E maurice@xe.estec.esa.nl

Dr. Ralph Cordey
GEC - Marconi Research Centre
West Hanningfield Road,
Great Baddow
Chelmsford, Essex CM2 8HN
UNITED KINGDOM
T +44 1245 473331
F +44 1245 475244
E cordey@gec-mrc.co.uk

Dr. Hugo de Groof
Joint Research Centre
IRSA/MTV, TP 440
I-21020 Ispra (Varese)
ITALY
T +39 332 785048
F +39 332 789074
E hugo.de-groof@cen.jrc.it

Jochen Harms
Scot Conseil
1 rue Hermes
Parc Technologique du Canal
Ramonville Cedex 31526
FRANCE
T +33 6139 4600
F +33 6139 4610
E jh@scot.cnes.fr

Jurg Lichtenegger
ESA/ESRIN
Via Galileo Galilei - C.P. 64
00044 Frascati
ITALY
T +39 6 94180419
F +39 6 94180361
E jlichten@esrin.bitnet

Gerard Nieuwenhuis
DLO-Winand Staring Centre
Postbus 125
Wageningen 6700 AC
THE NETHERLANDS
T +31 8370 74319
F +31 8370 24812
E nieuwenhuis@sc.agr.nl

Christiana Schmullius
DLR
Inst. of Radio-Frequency
Technology
P.O. Box 1116
D-82230 Wessling
GERMANY
T +49 8153 28 2337
F +49 8153 28 1135
E schmullius@ohf015.hf.op.dlr.d
e

Mike Wooding
Remote Sensing Applications
Consultants
4b, Mansfield Park, Medstead
Alton, Hampshire GU34 5PZ
UNITED KINGDOM
T +44 1420 561377
F +44 1420 561388
E mikew@rsac.demon.co.uk

Andrew Zmuda
Remote Sensing Applications
Consultants
4b, Mansfield Park
Medstead
Alton, Hampshire GU34 5PZ
UNITED KINGDOM
T +44 1420 561377
F +44 1420 561388
E andyz@rsac.demon.co.uk